Universität Rostock

Traditio et Innovatio

Master Thesis

Infrared spectroscopy via path integral techniques

by Sven Karsten

Matr.-Nr. 209204089

April 27, 2016

Rostock University

Institute of Physics

Molecular Quantum Dynamics Group

1st referee: Prof. Dr. Oliver Kühn

2nd referee: Dr. Sergei Ivanov

Contents

1. Introduction

Understanding the dynamics of complex many-body systems is one of the most important and challenging issues in molecular physics. Investigation of the (non-)linear spectra provides a useful tool for probing the dynamics. Since the absorption and emission of light can be measured experimentally, corresponding theories and models can be tested for their applicability. If experiment validates thus the theoretical model, then it can be in turn used to explain the experimental results, providing microscopic information that is often not available by means of experiment. Nowadays, especially computer simulations serve as a bridge between the experimental observations and the theoretical models describing the underlying dynamics. Due to the rapid increase of the computational capabilities in the last decades, one is able to investigate more and more complex systems by means of simulations.

At the beginning of the twentieth century, physicists found the classical physics unable to describe several phenomena measured in the experiment. For example the radiation of a black body [1] or the interference of scattered electrons [2] could not be explained by the theories existing at that time. In order to predict the correct dynamics, physics had to be extended by quantum mechanics. Here, two fundamental contributions were Werner Heisenberg's matrix mechanics [3] and Erwin Schrödinger's wave mechanics [4]. As a third contribution, the so-called Wigner formulation of quantum mechanics was introduced independently by Eugene Wigner [5] and Hermann Weyl [6]. The focus of this thesis is on yet another, path integral (PI), formulation of quantum mechanics [7] introduced by Richard Feynman in 1948. It turns out that all four approaches to quantum physics are fully equivalent. With the theoretical basis at hand, the exact description of the system's dynamics would require a rigorous treatment of one of the theories. Achieving this goal for realistic systems consisting of numerous nuclei and electrons is in most cases impossible analytically and not feasible numerically due to the "curse of dimensionality", that is the exponential scaling with the number of particles. Thus, it becomes necessary to employ approximations. One of the most common is the Born-Oppenheimer approximation (BOA) [8]. Here, one assumes that the electron's dynamics can be separated

1. Introduction

from the nuclei's one. Since the latter are at least three orders of magnitude heavier than the former, both dynamics proceed on completely different time scales. In other words, an electron reacts nearly instantaneously on a new core configuration. The charge density around the cores induces then an effective potential for the nuclei's motion. In a further step the effective potential can be parametrized to known analytical functions. Finally, the complete influence of the electrons is implicitly contained in a force field depending on a few parameters. The remaining task is to describe the nuclei's quantum dynamics in that force field explicitly and precisely, which is still unfeasible for realistic systems without further reductions.

Starting from the BOA, there are several methods to consider the nuclear dynamics. One possibility is to treat the nuclei as classical point particles and simulate the dynamics via the classical equations of motion. This method, called classical molecular dynamics (MD) yields useful results for many systems [8] but it obviously does not contain truly quantum mechanical properties, which could be crucial for certain systems, e.g. if light atoms like hydrogen are involved or if the phase information is important, as it is for spectra. Another possibility lies in Wigner-based semi-classical approaches [9], where one systematically expands the quantum equations of motion in orders of the reduced Planck's constant $\hbar$. A compromise between a full quantum and a pure classical description of dynamics is provided by quasi-classical methods based on Feynman's PI approach. Here, one makes use of the isomorphism between the quantum mechanical partition function and a purely classical configuration integral [10]. In a nutshell, each particle is now described by a more complicated classical object referred to as the ring polymer. To exploit this isomorphism, one can use well-established methods of classical mechanics to simulate static quantum mechanical properties, whereas the time evolution is not rigorously included in the formalism and, thus, the phase information is not recovered. Still, for calculating the spectrum, dynamics need to be involved. There exist two quasi-classical approximations based on PI, namely centroid molecular dynamics (CMD) [11] and ring polymer molecular dynamics (RPMD) [12]. Within both methods dynamical information is *ad hoc* extracted from the ring polymer propagated according to the classical equations of motion. Although both methods yield a quasi-classical approximation to quantum dynamics, they suffer from intrinsic artifacts. The RPMD method exhibits artificial resonances in infrared spectra [13], whereas spectra for stretching vibrations obtained via CMD are unphysically redshifted due to the "curvature problem" [14, 13]. Although the authors of Ref. [15] claim that the curvature problem has no consequences for the OH/OD vibration of HOD in a surrounding of H_2O or D_2O molecules, the magnitude of the redshift for an arbitrary vibrational system is

1. Introduction

still unknown in the absence of exact benchmarks. As a reliable quantum reference the authors of Ref. [15] suggested the mixed quantum-classical scheme [16, 17], which is bound to several approximations and assumptions.

It is in general a demanding task to develop a methodology that can produce exact (or very precise) benchmarks, that can in turn be used for validating of classical or quasi- and semi-classical approximations. In the vast majority of cases, a complex molecular system can be partitioned into a small subsystem and a bath consisting of the remaining numerous particles. Usually, the dynamics of the subsystem are of interest, whereas the knowledge of the bath's time evolution is not desired explicitly. An exact solution of the time-dependent Schrödinger equation for the system would require the treatment of the high-dimensional wave function that contains all, necessary and unnecessary, dynamical information of the system-bath complex (SBC). A more attractive approach to a pure quantum description of the dynamics is provided by the real time PI formalism. Here, the motion of a quantum object from one point to another can be described by the integration over an infinite number of classical paths that connect the two points. It has to be emphasized that in contrast to the quasi-classical CMD and RPMD, no *ad hoc* assumptions are involved and, thus, the full quantum character of the system and all phase information are covered. Referring to [18], the PI can be formulated such that the bath can be treated implicitly via the so-called influence functional. In case the system-bath interaction is described by the multi-mode Brownian oscillator (MBO) model [19, 20, 21], the expression for the influence functional can be carried out analytically [18]. Moreover, the MBO model provides an unified framework for treating quantum and (quasi-)classical dynamics of the system in contact with a non-Markovian bath on equal footing. Thus, it is ideally tailored for the present purpose.

In spite of the great profit of treating the numerous bath particles implicitly via the influence functional, the evaluation of the PI is far from being a simple task. Since an analytical solution is not known for any realistic SBC, a numerical scheme is required that is able to treat the PI discretely in time and space with the nowadays computer capabilities. The attempt to discretize the PI directly leads to a high-dimensional integral with a complex integrand, thus, the use of the well-established Monte-Carlo methods is prohibited [22, 23]. Since two and a half decades the research group of Nancy Makri[1] progresses successfully in formulating a feasible numerical approach to real time PIs, mostly applied to electronic transfer problems.

---

[1]Department of Physics, University of Illinois, Urbana, USA; Department of Chemistry, University of Illinois, Urbana, USA

3

1. Introduction

With a specific factorization of the time evolution operators it is possible to discretize the time into rather long time slices [24]. Moreover, the discretization of space is optimized by the use of the so-called discrete variable representation (DVR) [25]. In order to calculate time-dependent expectation values for an arbitrary long time, the discrete PI can be reformulated as an iterative propagation scheme [26, 27]. It turns out that not all paths contribute significantly to the PI, thus, unimportant paths can be filtered out [28], which reduces the numerical effort dramatically. The ideas for calculating the real time PI have been then transferred to a complex time PI that can be used to extract time-dependent equilibrium properties [29, 30] like the time-correlation function, that is the key quantity for linear spectroscopy. Moreover, this methodology can also be extended to non-linear spectroscopy [30]. In the last three years, several improvements of the numerical algorithms have been published [31, 32]. Additionally a PI methodology has been presented, where the system is treated quantum mechanically, whereas the bath is approximated purely classically [33, 34]. With the given references at hand, the implementation of the PI formalism as an exact quantum reference and its application to vibrational systems in a realistic environments is the goal of this thesis. The focus is then put on the applicability to the special system consisting of the OH/OD bond solvated in liquid H_2O or D_2O, in order to shed light on the magnitude of artifacts induced by the curvature problem.

The thesis is organized as follows. The first chapter serves as a theoretical basis for the quantum dynamics of system-bath complexes, where the quantities of interest are introduced, namely time-dependent expectation values and equilibrium correlation functions. In the second chapter, the continuous PI expressions of these two quantities are derived. The focus of the third chapter is on quantum dynamical quantities expressed as discrete PIs, which are recast into an iterative propagation scheme. In the first section of the fourth chapter, a comparison to literature data is performed. Then, in the second section, the applicability of the discrete PI formalism to vibrational systems is debated. Finally in the fifth chapter, a conclusion and an outlook are given.

2. Quantum dynamics of a system coupled to a bath

2.1. Theoretical basics

The goal of this chapter is to present a formalism which is capable to describe the quantum dynamics of a system S with a coordinate and a momentum operators $\hat{s}$ and $\hat{p}$, respectively, in contact with a bath B. The bath is characterized by a vector of D coordinate operators $\hat{\mathbf{Q}} = (\hat{Q}_1, \ldots, \hat{Q}_D)^{\mathrm{T}}$ with conjugate momentum operators $\hat{\mathbf{P}} = (\hat{P}_1, \ldots, \hat{P}_D)^{\mathrm{T}}$. Such a situation is described by the Hamiltonian

$$
\begin{aligned}
\hat{H}(\hat{s}, \hat{p}; \hat{\mathbf{Q}}, \hat{\mathbf{P}}) &= \frac{\hat{p}^2}{2m} + \hat{V}_{\mathrm{S}}(\hat{s}) + \sum_{i=1}^{D} \frac{\hat{P}_i^2}{2M_i} + \hat{V}_{\mathrm{B}}(\hat{\mathbf{Q}}) + \hat{V}_{\mathrm{int}}(\hat{s}, \hat{\mathbf{Q}}) && (2.1) \\
&\equiv \hat{H}_{\mathrm{S}}(\hat{s}, \hat{p}) \qquad + \hat{H}_{\mathrm{B}}(\hat{\mathbf{Q}}, \hat{\mathbf{P}}) \qquad + \hat{V}_{\mathrm{int}}(\hat{s}, \hat{\mathbf{Q}}) && (2.2) \\
&\equiv \hat{H}_{\mathrm{S}}(\hat{s}, \hat{p}) \qquad\qquad + \hat{H}_{\mathrm{SB}}(\hat{s}, \hat{\mathbf{Q}}, \hat{\mathbf{P}}) \ , && (2.3)
\end{aligned}
$$

where $\hat{H}_{\mathrm{S}}(\hat{s}, \hat{p})$ depends only on the degrees of freedom (DOFs) of the system, $\hat{H}_{\mathrm{B}}(\hat{\mathbf{Q}}, \hat{\mathbf{P}})$ corresponds to an isolated bath B, $\hat{V}_{\mathrm{S}}(\hat{s})$ and $\hat{V}_{\mathrm{B}}(\hat{\mathbf{Q}})$ are respective potential operators and $\hat{V}_{\mathrm{int}}(\hat{s}, \hat{\mathbf{Q}})$ takes the coordinate-dependent interaction between the system and the bath into account. This definition of system, bath and their mutual interaction is employed throughout the thesis and the arguments of the aforementioned Hamiltonians and potentials will be omitted in the following. In general, the time evolution of a pure state $|\Psi(t)\rangle$ of the SBC is given by the formal solution of the time-dependent Schrödinger equation

$$
|\Psi(t)\rangle = \hat{U}(t) |\Psi(0)\rangle, \quad \hat{U}(t) = \exp\left\{-i\hat{H}t/\hbar\right\} \ , \tag{2.4}
$$

where $\hat{U}(t)$ is the Heisenberg time evolution operator. Since the bath is usually large, if not macroscopic, a calculation of $|\Psi(t)\rangle$ in any basis is not possible analytically apart from special cases, and is hardly feasible numerically. Moreover, the wavefunction contains dynamical information for the bath, which is in many cases not of explicit interest. In order to circumvent the redundancy of the information, the SBC is first described by the density operator instead of the wavefunction

$$|\Psi(t)\rangle \rightarrow \hat{\rho}(t) \ . \tag{2.5}$$

The great benefit of such a description is the ability to consider reduced dynamics of the system, which will be subject of Sec. 3.1. It is worth mentioning, that a density operator can be naturally used for treating mixed states. The time evolution of $\hat{\rho}(t)$, which can be found as the formal solution of the von Neumann equation, reads

$$\hat{\rho}(t) = \hat{U}(t)\hat{\rho}(0)\hat{U}^{\dagger}(t) \ , \tag{2.6}$$

where the symbol $\hat{U}^{\dagger}(t)$ stands for the adjoint of the time evolution operator. If one assumes that the interaction $\hat{V}_{\text{int}}$ is switched on at $t = 0$, then the system and the bath are initially uncorrelated, thereby setting the initial condition as

$$\hat{\rho}(0) \equiv \left(\hat{\rho}_{\text{S}}(0) \otimes \hat{1}_{\text{B}}\right) \cdot \left(\hat{1}_{\text{S}} \otimes \hat{\rho}_{\text{B}}(0)\right) \ , \tag{2.7}$$

where $\otimes$ is the tensorial product. If the bath has a macroscopic number of DOFs the density operator has the limit

$$\lim_{t \to \infty} \hat{\rho}(t) = \frac{1}{Z(\beta)} e^{-\beta \hat{H}} \ , \qquad Z(\beta) = \text{Tr}\left[e^{-\beta \hat{H}}\right] \ , \tag{2.8}$$

where $\beta = 1/(k_{\text{B}}T)$ is the inverse temperature, Z denotes the partition function and the trace is taken in any orthonormal basis of the SBC. This limit is referred to as the canonical equilibrium or Boltzmann operator and is independent of the initial preparation of the system.

The definitions given in this section serve as basis for what follows. In the next section the connection of the operators to measurable quantities is briefly discussed.

2.2. Expectation values and spectra

2.2.1. Time-dependent expectation values

In the previous section it was mentioned that the dynamics of the system are described by the time evolution of the density operator $\hat{\rho}(t)$. The advantage of that description is the possibility to formulate reduced dynamics. The key quantity here is the reduced density operator of the system S defined as

$$\hat{\rho}_\text{S}(t) \equiv \text{Tr}_\text{B}\left[\hat{\rho}(t)\right] \quad, \tag{2.9}$$

where the trace is taken in any orthonormal basis of the bath's Hilbert space and, thus, the bath's DOFs are integrated out and do not enter the dynamics of the system explicitly. If the state of the system is known at a certain time, then the reduced density operator can be propagated to arbitrarily long times. With the knowledge of this time evolution, one is able to extract dynamical information of any system operator $\hat{\Omega}$ in the form of a complex function of time. The particular function is referred to as the *expectation value* of $\hat{\Omega}$ and is calculated via

$$\left\langle \hat{\Omega} \right\rangle_t \equiv \text{Tr}_\text{S}\left[\hat{\rho}_\text{S}(t)\hat{\Omega}\right] \quad, \tag{2.10}$$

where the trace is now taken in any orthonormal basis of the system's Hilbert space. In case $\hat{\Omega}$ is a Hermitian operator, that is if $\hat{\Omega} = \hat{\Omega}^\dagger$, the expectation value represents a measurable quantity. Hence, results for $\left\langle \hat{\Omega} \right\rangle_t$ obtained by theoretical means can be compared to an experiment and, thus, the given theoretical framework can be validated.

2.2.2. The linear absorption spectrum

As it was stated in the introduction, the study of linear absorption spectra gives an insight into the microscopic dynamics of a system. A detailed theoretical fundament for linear spectroscopy can be found in Refs. [35, 20, 36]. The starting point is the Lambert-Beer absorption law

$$I(d,\omega) = I_0 \text{e}^{-\gamma(\omega)d} \quad. \tag{2.11}$$

that describes quantitatively the light absorption of a considered system or medium. It can be verbally formulated as: the loss of the intensity $I(d,\omega)$ of an incoming monochromatic electromagnetic wave with frequency ω and an initial intensity I_0 depends on the thickness of the

medium d and its frequency-dependent linear absorption coefficient $\gamma(\omega)$. The idea behind linear spectroscopy is thus to vary the radiated frequency and to measure the intensity as a function of ω. The logarithm of the resulting $I(d, \omega)$ yields the desired linear absorption coefficient. In order to assign the measured features to microscopic characteristics of the system one has to derive the theoretical counterpart of $\gamma(\omega)$. This can be achieved by treating the interactions between the system and the incoming electro-magnetic field in the dipole approximation [20, 35] by means of the first order perturbation theory[36]

$$\gamma(\omega) \sim \frac{\omega}{2\pi\hbar} \left(1 - \mathrm{e}^{-\beta\hbar\omega}\right) \Re \left\{ \int\limits_{-\infty}^{\infty} \mathrm{d}t\, \mathrm{e}^{-i\omega t} C_{\mu\mu}(t) \right\} \ , \tag{2.12}$$

where $\Re$ stands for the real part. The key quantity that connects the experimentally available $\gamma(\omega)$ and microscopic dynamics of the system is the equilibrium dipole auto-correlation function

$$C_{\mu\mu}(t) \equiv \frac{1}{Z(\beta)} \mathrm{Tr} \left[\mathrm{e}^{-\beta\hat{H}} \hat{\mu}\, \hat{U}^{\dagger}(t) \hat{\mu}\, \hat{U}(t) \right] \ , \tag{2.13}$$

where $\hat{\mu}$ is the system's dipole operator, which is usually assumed to be directly proportional to the position operator. Since we are interested in the absorption behavior of the system, this assumption implies $\hat{\mu} \sim \hat{s}$.

In the following chapter it will be shown that the operators $\hat{U}(t)$ and $\mathrm{e}^{-\beta\hat{H}}$ can be alternatively represented as functional integrals, namely the PIs. With that representation at hand, one is able to formulate also the time-evolution of the reduced density operator and the equilibrium correlation function within that framework.

3. Quantum dynamics in path integral formulation

3.1. Reduced dynamics in PI formulation

In this section it will be shown that the time evolution of the reduced density operator can be expressed as a path integral, whereas the influence of the macroscopic bath will be implicitly contained in the so-called influence functional.

The starting point to the PI formulation of Eq. (2.9) is the reduced density operator in the system's coordinate basis

$$\rho_{\mathrm{s}}(s_+, s_-; t) \equiv \langle s_+ | \hat{\rho}_{\mathrm{s}}(t) | s_- \rangle \quad , \tag{3.1}$$

which is then a time-dependent function of two arguments s_+, s_- with $\hat{s} | s_\pm \rangle = s_\pm | s_\pm \rangle$. Note in anticipation of the next steps that red-colored coordinates correspond to paths the system follows forward in time, whereas blue-colored coordinates form the paths that are followed backward in time. The trace over bath DOFs in Eq. (2.9) is taken in the coordinate basis of the bath

$$\rho_{\mathrm{s}}(s_+, s_-; t) = \int_{-\infty}^{\infty} \mathrm{d}\mathbf{Q} \left\langle s_+ \mathbf{Q} \left| \hat{U}(t) \hat{\rho}(0) \hat{U}^\dagger(t) \right| s_- \mathbf{Q} \right\rangle \quad , \tag{3.2}$$

where $\int_{-\infty}^{\infty} \mathrm{d}\mathbf{Q} \equiv \prod_{i=1}^{D} \int_{-\infty}^{\infty} \mathrm{d}Q_i$, $\quad |s\mathbf{Q}\rangle \equiv |s\rangle \otimes |Q_1\rangle \otimes |Q_2\rangle \cdots \otimes |Q_D\rangle$ with $\hat{Q}_i |Q_i\rangle = Q_i |Q_i\rangle$. Inserting the closures

$$\hat{1} = \int_{-\infty}^{\infty} \mathrm{d}s_0^+ \int_{-\infty}^{\infty} \mathrm{d}\mathbf{Q_0^+} \left| s_0^+ \mathbf{Q_0^+} \right\rangle \left\langle s_0^+ \mathbf{Q_0^+} \right| = \int_{-\infty}^{\infty} \mathrm{d}s_0^- \int_{-\infty}^{\infty} \mathrm{d}\mathbf{Q_0^-} \left| s_0^- \mathbf{Q_0^-} \right\rangle \left\langle s_0^- \mathbf{Q_0^-} \right| \tag{3.3}$$

3. Quantum dynamics in path integral formulation

on the right of $\hat{U}(t)$ and on the left of $\hat{U}^\dagger(t)$ in Eq. (3.2), respectively, yields after rearrangement

$$\rho_{\mathrm{s}}(s_+, s_-; t) = \int\limits_{-\infty}^{\infty} \mathrm{d}\mathbf{Q} \int\limits_{-\infty}^{\infty} \mathrm{d}s_0^+ \int\limits_{-\infty}^{\infty} \mathrm{d}s_0^- \int\limits_{-\infty}^{\infty} \mathrm{d}\mathbf{Q_0^+} \int\limits_{-\infty}^{\infty} \mathrm{d}\mathbf{Q_0^-}$$

$$\times \left\langle s_0^+ \mathbf{Q_0^+} \middle| \hat{\rho}(0) \middle| s_0^- \mathbf{Q_0^-} \right\rangle \left\langle s_0^- \mathbf{Q_0^-} \middle| \hat{U}^\dagger(t) \middle| s_- \mathbf{Q} \right\rangle \left\langle s_+ \mathbf{Q} \middle| \hat{U}(t) \middle| s_0^+ \mathbf{Q_0^+} \right\rangle . \quad (3.4)$$

Reading the integrand from the right to the left permits the following interpretation. The SBC is propagated from the initial coordinate state $\left| s_0^+ \mathbf{Q_0^+} \right\rangle$ at time 0 *forward* in time via $\hat{U}(t)$ to the final coordinate state $\left| s_+ \mathbf{Q} \right\rangle$ at time t. Then the SBC is propagated from another final state $\left| s_- \mathbf{Q} \right\rangle$ at time t *backward* in time via $\hat{U}^\dagger(t)$ to the initial coordinate state $\left| s_0^- \mathbf{Q_0^-} \right\rangle$ at time 0. Subsequently the integrand is weighted by the complex number $\left\langle s_0^+ \mathbf{Q_0^+} \middle| \hat{\rho}(0) \middle| s_0^- \mathbf{Q_0^-} \right\rangle$ related to the initial density operator $\hat{\rho}(0)$ and the initial states $\left| s_0^+ \mathbf{Q_0^+} \right\rangle$, $\left| s_0^- \mathbf{Q_0^-} \right\rangle$. The reduced density $\rho_{\mathrm{s}}(s_+, s_-; t)$ is then the result of an integration over all initial coordinate states of the entire SBC and all final coordinate states of the bath as a result of the trace. The propagation of the SBC *in time* can be described by the *time contour c_t* as it is depicted in Fig. 3.1. The quantity $\left\langle s_+ \mathbf{Q} \middle| \hat{U}(t) \middle| s_0^+ \mathbf{Q_0^+} \right\rangle$ in Eq. (3.4) is the *probability amplitude* that the SBC evolves from the state $\left| s_0^+ \mathbf{Q_0^+} \right\rangle$ at time 0 to $\left| s_+ \mathbf{Q} \right\rangle$ at time t. The expression $\left\langle s_0^- \mathbf{Q_0^-} \middle| \hat{U}^\dagger(t) \middle| s_- \mathbf{Q} \right\rangle$ would then correspond to the probability amplitude that the SBC evolves from the state $\left| s_- \mathbf{Q} \right\rangle$ at time t to

Figure 3.1.: **Time contour c_t**. See text for explanation.

$\left| s_0^- \mathbf{Q_0^-} \right\rangle$ at time 0. The possibility to express the probability amplitude as a *functional* integral is at the heart of the PI formulation of quantum mechanics, which is briefly sketched in the following. In particular, one can show (App. A) that

$$\left\langle s \middle| \exp\left\{ \mp i \left(\hat{p}^2/(2m) + \hat{V}(\hat{s}) \right) t/\hbar \right\} \middle| s_0 \right\rangle = \int\limits_{s_0}^{s} \mathrm{D}_{(0,t)} \mathfrak{s}(\tau) \, \exp\left\{ \pm \frac{i}{\hbar} A_{(0,t)} [\mathfrak{s}(\tau)] \right\} , \quad (3.5)$$

where $\int_{s_0}^{s} \mathrm{D}_{(0,t)} \mathfrak{s}(\tau)$ is defined as the functional integral over the complete space of continuous functions $\mathfrak{s}(\tau)$, defined on the interval $(0,t)$ with boundaries $\mathfrak{s}(0) = s_0$, $\mathfrak{s}(t) = s$. Note that the parentheses $(\cdot, \cdot)$ denote a *closed* interval, whereas the brackets $[\cdot]$ are reserved for functional

arguments. The quantity $A_{(0,t)}[\mathfrak{s}(\tau)]$ is the *classical action*

$$A_{(0,t)}[\mathfrak{s}(\tau)] \equiv \int\limits_0^t \mathrm{d}\tau \left\{ \frac{1}{2}m\dot{\mathfrak{s}}^2(\tau) - V\left(\mathfrak{s}(\tau)\right) \right\} \ , \tag{3.6}$$

where $V(s)$ is the classical counterpart of $\hat{V}(\hat{s})$. If one first focuses on the upper sign in Eq. (3.5), which corresponds to the normal time evolution forward in time, then the following interpretation for the aforementioned equivalence emerges [37]. The probability amplitude that the *quantum* system evolves from a state $|s_0\rangle$ at time 0 to a state $|s\rangle$ at time t is a complex-weighted superposition of *all* possible histories the *classical* counterpart of the system could have had if it would go from s_0 and s within time t, see Fig. 3.2.
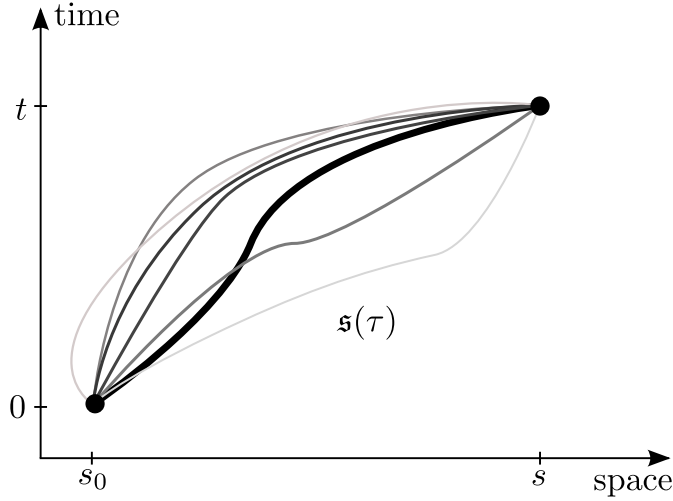
Figure 3.2.: **Superposition of classical histories.** The thickest line symbolizes the classical path. For further explanations see text.

Each history is characterized by a continuous function $\mathfrak{s}(\tau)$ which can be considered as a classical trajectory or *path*. The phases $\exp\left\{\frac{i}{\hbar}A_{(0,t)}[\mathfrak{s}(\tau)]\right\}$ are determined by the classical action along a particular system path $\mathfrak{s}(\tau)$. In contrast to this summation over all paths, the time-evolution in classical mechanics is fully determined by *one* path, namely the path for which the action is extremal. Paths in the vicinity of the classical path are stationary and, hence, they are weighted by similar phases with the same sign. These paths have consequently a large contribution to the integral. Conversely, for non-stationary paths, far away from the extremum, the integrand changes its sign rapidly and, hence, contributions of these paths cancel each other.

3. Quantum dynamics in path integral formulation

For the lower sign in Eq. (3.5) the same interpretation holds with the system following the path backward in time from $\mathfrak{s}(t) = s$ to $\mathfrak{s}(0) = s_0$. In the following these paths are called *backward paths* denoted by $\mathfrak{s}^-(\tau)$, whereas paths resulting from the normal time-evolution are called *forward paths* denoted by $\mathfrak{s}^+(\tau)$. It is worth mentioning that one could take the right hand side of Eq. (3.5) as a starting point for a quantum description of mechanics, then the Schrödinger equation and fundamental commutator relations would follow [7].

With Eq. (3.5) at hand, one can now recast the reduced density in Eq. (3.4) as a PI

$$\rho_{\mathrm{s}}(s_+, s_-; t) = \int\limits_{-\infty}^{\infty} \mathrm{d}\mathbf{Q} \int\limits_{-\infty}^{\infty} \mathrm{d}\mathbf{Q}_0^+ \int\limits_{-\infty}^{\infty} \mathrm{d}\mathbf{Q}_0^- \int\limits_{-\infty}^{\infty} \mathrm{d}s_0^+ \int\limits_{-\infty}^{\infty} \mathrm{d}s_0^-$$

$$\times \int\limits_{\mathbf{Q}_0^+}^{\mathbf{Q}} \mathrm{D}_{(0,t)}\mathfrak{Q}^+(\tau) \int\limits_{\mathbf{Q}_0^-}^{\mathbf{Q}} \mathrm{D}_{(0,t)}\mathfrak{Q}^-(\tau) \int\limits_{s_0^+}^{s_+} \mathrm{D}_{(0,t)}\mathfrak{s}^+(\tau) \int\limits_{s_0^-}^{s_-} \mathrm{D}_{(0,t)}\mathfrak{s}^-(\tau)$$

$$\times \rho(\mathfrak{s}^+(0), \mathfrak{s}^-(0), \mathfrak{Q}^+(0), \mathfrak{Q}^-(0); t) \cdot \exp\left\{ -\frac{i}{\hbar}\left(A_{(0,t)}^{\mathrm{S}}[\mathfrak{s}^-(\tau)] + A_{(0,t)}^{\mathrm{SB}}[\mathfrak{s}^-(\tau), \mathfrak{Q}^-(\tau)] \right) \right\}$$

$$\times \exp\left\{ \frac{i}{\hbar}\left(A_{(0,t)}^{\mathrm{S}}[\mathfrak{s}^+(\tau)] + A_{(0,t)}^{\mathrm{SB}}[\mathfrak{s}^+(\tau), \mathfrak{Q}^+(\tau)] \right) \right\} \ , \tag{3.7}$$

where $\mathbf{Q} = (Q_1, \ldots, Q_D)^{\mathrm{T}}$, $\mathfrak{Q}(\tau) = (\mathfrak{Q}_1(\tau), \ldots, \mathfrak{Q}_D(\tau))^{\mathrm{T}}$, $\int_{\mathbf{Q}_0}^{\mathbf{Q}} \mathrm{D}_{(0,t)}\mathfrak{Q}(\tau) \equiv \prod_{i=1}^{D} \int_{Q_{0,i}}^{Q_i} \mathrm{D}_{(0,t)}\mathfrak{Q}_i(\tau)$. In the exponents the classical actions of the bare system and the interacting bath appear according to Eq. (3.6) as

$$A_{(0,t)}^{\mathrm{S}}[\mathfrak{s}(\tau)] \equiv \int\limits_0^t \mathrm{d}\tau \left\{ \frac{1}{2}m\dot{\mathfrak{s}}^2(\tau) - V_{\mathrm{s}}\left(\mathfrak{s}(\tau)\right) \right\} \tag{3.8}$$

$$A_{(0,t)}^{\mathrm{SB}}[\mathfrak{s}(\tau), \mathfrak{Q}(\tau)] \equiv \int\limits_0^t \mathrm{d}\tau \left\{ \sum_{i=1}^{D} \frac{1}{2}M_i\dot{\mathfrak{Q}}_i^2(\tau) - V_{\mathrm{B}}\left(\mathfrak{Q}(\tau)\right) - V_{\mathrm{int}}(\mathfrak{s}(\tau); \mathfrak{Q}(\tau)) \right\} \ . \tag{3.9}$$

The initial density operator is now represented by the multi-dimensional complex function

$$\rho(\mathfrak{s}^+(0), \mathfrak{s}^-(0), \mathfrak{Q}^+(0), \mathfrak{Q}^-(0); t) \equiv \left\langle s_0^+ \mathbf{Q}_0^+ \right| \hat{\rho}(0) \left| s_0^- \mathbf{Q}_0^- \right\rangle \ , \tag{3.10}$$

depending on the coordinates of the forward and backward paths at time zero. Due to the absence of initial correlation, as it is assumed in Eq. (2.7), the initial condition can be separated

into

$$\rho(\mathfrak{s}^+(0),\, \mathfrak{s}^-(0),\, \mathfrak{Q}^+(0),\, \mathfrak{Q}^-(0);\, t) = \rho_{\mathrm{S}}(\mathfrak{s}^+(0),\, \mathfrak{s}^-(0);\, 0) \cdot \rho_{\mathrm{B}}(\mathfrak{Q}^+(0),\, \mathfrak{Q}^-(0);\, 0) \; . \qquad (3.11)$$

Since the integrand in Eq. (3.7) just consists of complex numbers, one can rearrange it such that bare system and system-bath parts are separated. Then the bath's DOFs can be formally integrated out

$$\rho_{\mathrm{S}}(s_+,\, s_-;\, t) = \int\limits_{-\infty}^{\infty} \mathrm{d}s_0^+ \int\limits_{-\infty}^{\infty} \mathrm{d}s_0^- \int\limits_{s_0^+}^{s_+} \mathrm{D}_{(0,t)}\mathfrak{s}^+(\tau) \int\limits_{s_0^-}^{s_-} \mathrm{D}_{(0,t)}\mathfrak{s}^-(\tau)$$

$$\times\, F_{(0,t)}[\mathfrak{s}^+(\tau),\, \mathfrak{s}^-(\tau)] \cdot \rho_{\mathrm{S}}(\mathfrak{s}^+(0),\, \mathfrak{s}^-(0);\, 0) \cdot \exp\left\{ \frac{i}{\hbar} \left(A_{(0,t)}^{\mathrm{S}}[\mathfrak{s}^+(\tau)] - A_{(0,t)}^{\mathrm{S}}[\mathfrak{s}^-(\tau)] \right) \right\} \quad (3.12)$$

with

$$F_{(0,t)}[\mathfrak{s}^+(\tau),\, \mathfrak{s}^-(\tau)] \equiv \int\limits_{-\infty}^{\infty} \mathrm{d}\mathbf{Q} \int\limits_{-\infty}^{\infty} \mathrm{d}\mathbf{Q}_0^+ \int\limits_{-\infty}^{\infty} \mathrm{d}\mathbf{Q}_0^- \int\limits_{\mathbf{Q}_0^+}^{\mathbf{Q}} \mathrm{D}_{(0,t)}\mathfrak{Q}^+(\tau) \int\limits_{\mathbf{Q}_0^-}^{\mathbf{Q}} \mathrm{D}_{(0,t)}\mathfrak{Q}^-(\tau)$$

$$\times\, \rho_{\mathrm{B}}(\mathfrak{Q}^+(0),\, \mathfrak{Q}^-(0);\, 0) \cdot \exp\left\{ \frac{i}{\hbar} \left(A_{(0,t)}^{\mathrm{SB}}[\mathfrak{s}^+(\tau),\, \mathfrak{Q}^+(\tau)] - A_{(0,t)}^{\mathrm{SB}}[\mathfrak{s}^-(\tau),\, \mathfrak{Q}^-(\tau)] \right) \right\} \; . \quad (3.13)$$

Equation (3.13) defines the *influence functional*, which contains the information about all interactions between system and bath if the system follows the forward path $\mathfrak{s}^+(\tau)$ and the backward path $\mathfrak{s}^-(\tau)$. This representation of the system's reduced density operator was first introduced by R. Feynman and F. Vernon in their seminal work [18]. Note that the subscript $(0,t)$ in $F_{(0,t)}[\mathfrak{s}^+(\tau),\, \mathfrak{s}^-(\tau)]$ takes account for the total duration of the system-bath interaction. For the sake of brevity the following notations are introduced

$$S_{(0,t)}\left[\mathfrak{s}^\pm(\tau)\right] \equiv \exp\left\{ \frac{i}{\hbar} \left(A_{(0,t)}^{\mathrm{S}}[\mathfrak{s}^+(\tau)] - A_{(0,t)}^{\mathrm{S}}[\mathfrak{s}^-(\tau)] \right) \right\} \qquad (3.14)$$

$$\int\limits^{s_\pm} \mathrm{D}_{(0,t)}\mathfrak{s}^\pm(\tau) \equiv \int\limits_{-\infty}^{\infty} \mathrm{d}s_0^+ \int\limits_{-\infty}^{\infty} \mathrm{d}s_0^- \int\limits_{s_0^+}^{s_+} \mathrm{D}_{(0,t)}\mathfrak{s}^+(\tau) \int\limits_{s_0^-}^{s_-} \mathrm{D}_{(0,t)}\mathfrak{s}^-(\tau) \qquad (3.15)$$

$$R\left[\mathfrak{s}^\pm(\tau)\right] \equiv \rho_{\mathrm{S}}(\mathfrak{s}^+(0),\, \mathfrak{s}^-(0);\, 0) \; . \qquad (3.16)$$

3. Quantum dynamics in path integral formulation

The functional which is defined by Eq. (3.14) is referred to as the *bare system part* of the PI. The functional integral in Eq. (3.15) means now an integral over *all combinations* of forward and backward paths $\mathfrak{s}^+(\tau)$, $\mathfrak{s}^-(\tau)$ spanning the time t with fixed points $\mathfrak{s}^\pm(t) = s_\pm$. Equation (3.16) defines the *multi-time reduced density functional* $R\left[\mathfrak{s}^\pm(\tau)\right] \equiv \rho_s(\mathfrak{s}^+(0), \mathfrak{s}^-(0); 0)$, which plays an important role in the numerical implementation (Sec. 4.1.1). Note that the term is inspired by Ref. [28], where the authors introduce the "extended multi-time reduced density matrix". With the given notations the time evolution of the system's reduced density operator in its PI formulation has the compact form

$$\rho_s(s_\pm; t) = \int^{s_\pm} D_{(0,t)} \mathfrak{s}^\pm(\tau) \, F_{(0,t)}\left[\mathfrak{s}^\pm(\tau)\right] \cdot R\left[\mathfrak{s}^\pm(\tau)\right] \cdot S_{(0,t)}\left[\mathfrak{s}^\pm(\tau)\right] \;, \tag{3.17}$$

with the abbreviations $\rho_s(s_\pm; t) \equiv \rho_s(s_+, s_-; t)$ and $F_{(0,t)}\left[\mathfrak{s}^\pm(\tau)\right] \equiv F_{(0,t)}[\mathfrak{s}^+(\tau), \mathfrak{s}^-(\tau)]$. The value of the integrand in Eq. (3.17) depends on three mutual independent quantities. First, the functional $S_{(0,t)}\left[\mathfrak{s}^\pm(\tau)\right]$ takes account of the bare system that is propagated along the forward path $\mathfrak{s}^+(\tau)$ and the backward path $\mathfrak{s}^-(\tau)$. Second, the integrand is weighted by the multi-time reduced density functional $R\left[\mathfrak{s}^\pm(\tau)\right]$ related to the initial reduced density operator $\hat{\rho}_s(0)$ and the coordinates $\mathfrak{s}^\pm(0)$. Third, the integrand is additionally weighted by influence functional $F_{(0,t)}\left[\mathfrak{s}^\pm(\tau)\right]$, which contains implicitly the interaction between system and bath.

To extract time-dependent expectation values for a system operator $\hat{\Omega}$ one has to perform the additional integration over the end points

$$\left\langle \hat{\Omega} \right\rangle_t = \int_{-\infty}^{\infty} ds_\pm \, \Omega(s_\mp) \int^{s_\pm} D_{(0,t)} \mathfrak{s}^\pm(\tau) \, F_{(0,t)}\left[\mathfrak{s}^\pm(\tau)\right] \cdot R\left[\mathfrak{s}^\pm(\tau)\right] \cdot S_{(0,t)}\left[\mathfrak{s}^\pm(\tau)\right] \;, \tag{3.18}$$

with $\int_{-\infty}^{\infty} ds_\pm \equiv \int_{-\infty}^{\infty} ds_+ \int_{-\infty}^{\infty} ds_-$ and $\Omega(s_\mp) \equiv \left\langle s_- \left| \hat{\Omega} \right| s_+ \right\rangle$. The expectation value can be considered as the integral over all bare system forward and backward paths that are *quasi-connected* at time zero via $\hat{\rho}_s(0)$ and at time t via $\hat{\Omega}$, see Fig. 3.3. A quasi-connection means that the forward-backward time evolution is not necessarily continuous.
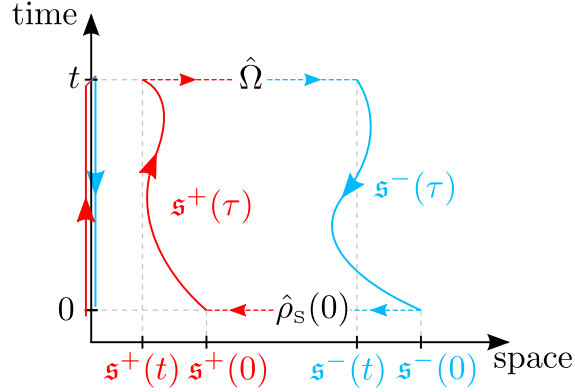
Figure 3.3.: **Bare system propagation in time and space.** Note that the time contour c_t in Fig. 3.1 is the projection of the entire path on the time axis.

3.2. Equilibrium time-correlation functions in PI formulation

Equilibrium TCFs contain important information about the dynamics of the system, e.g., for the calculation of absorption spectra. In this section it is shown that there exists a PI expression for the TCF, which is formally similar to Eq. (3.18). The derivation would show that this expression includes an integration over paths that span an imaginary time interval stemming from the Boltzmann operator.

The time-correlation function $C_{\Gamma\Omega}(t)$ of two arbitrary operators $\hat{\Gamma}$ and $\hat{\Omega}$ which act in the Hilbert space of the system is defined as the ensemble average over the entire SBC

$$C_{\Gamma\Omega}(t) \equiv \frac{1}{Z(\beta)}\mathrm{Tr}\left[\mathrm{e}^{-\beta\hat{H}}\hat{\Gamma}\,\hat{U}^{\dagger}(t)\hat{\Omega}\,\hat{U}(t)\right] \ . \tag{3.19}$$

To find the PI expression of Eq. (3.19) the trace is taken in the coordinate space of the SBC

$$C_{\Gamma\Omega}(t) = \frac{1}{Z(\beta)}\int\limits_{-\infty}^{\infty}\mathrm{d}s_0\int\limits_{-\infty}^{\infty}\mathrm{d}\mathbf{Q}_0\,\langle s_0\mathbf{Q}_0|\,\mathrm{e}^{-\beta\hat{H}/2}\,\hat{\Gamma}\,\hat{U}^{\dagger}(t)\,\hat{\Omega}\,\hat{U}(t)\,\mathrm{e}^{-\beta\hat{H}/2}\,|s_0\mathbf{Q}_0\rangle \ , \tag{3.20}$$

where the invariance of the trace under cyclic exchange of operators was exploited. The specific splitting of the Boltzmann operator in Eq. (3.20) is advantageous for the purposes of the numerical implementation presented in Sec. 4.2. Note in anticipation of the next steps that

variables colored in green correspond to imaginary time paths. Analogously to Eq. (3.4) spatial closures are inserted in between the operators yielding

$$
C_{\Gamma\Omega}(t) = \frac{1}{Z(\beta)} \int\limits_{-\infty}^{\infty} \mathrm{d}s_0 \int\limits_{-\infty}^{\infty} \mathrm{d}s_0^+ \int\limits_{-\infty}^{\infty} \mathrm{d}s_0^- \int\limits_{-\infty}^{\infty} \mathrm{d}s_\Omega \int\limits_{-\infty}^{\infty} \mathrm{d}s_t \int\limits_{-\infty}^{\infty} \mathrm{d}s_\Gamma \int\limits_{-\infty}^{\infty} \mathrm{d}\mathbf{Q}_0 \int\limits_{-\infty}^{\infty} \mathrm{d}\mathbf{Q}_t \int\limits_{-\infty}^{\infty} \mathrm{d}\mathbf{Q}_0^+ \int\limits_{-\infty}^{\infty} \mathrm{d}\mathbf{Q}_0^-
$$

$$
\times \left\langle s_0 \mathbf{Q}_0 \right| \mathrm{e}^{-\beta\hat{H}/2} \left| s_\Gamma \mathbf{Q}_0^- \right\rangle \left\langle s_\Gamma \right| \hat{\Gamma} \left| s_0^- \right\rangle \left\langle s_0^- \mathbf{Q}_0^- \right| \hat{U}^\dagger(t) \left| s_t \mathbf{Q}_t \right\rangle
$$

$$
\times \left\langle s_t \right| \hat{\Omega} \left| s_\Omega \right\rangle \left\langle s_\Omega \mathbf{Q}_t \right| \hat{U}(t) \left| s_0^+ \mathbf{Q}_0^+ \right\rangle \left\langle s_0^+ \mathbf{Q}_0^+ \right| \mathrm{e}^{-\beta\hat{H}/2} \left| s_0 \mathbf{Q}_0 \right\rangle \ . \quad (3.21)
$$

Note that the operator $\hat{\Gamma}$ does not act on bath states, thus, $\langle s\mathbf{Q}| \hat{\Gamma} |s'\mathbf{Q}'\rangle = \langle s| \hat{\Gamma} |s'\rangle \delta\left(\mathbf{Q} - \mathbf{Q}'\right)$. The integration over $\mathbf{Q}'$ or $\mathbf{Q}$ can then be performed immediately, yielding $\left\langle s_\Gamma \right| \hat{\Gamma} \left| s_0^- \right\rangle$ in the equation above. The very same is valid for $\hat{\Omega}$ yielding $\left\langle s_t \right| \hat{\Omega} \left| s_\Omega \right\rangle$ therein. In order to interpret Eq. (3.21), the following isomorphism is exploited. The time evolution operator $\hat{U}(t)$ acts in the same way as $\exp(-\beta\hat{H}/2)$ if one would virtually set $t = -i\beta\hbar/2$. For that reason one can claim that the operator $\exp(-\beta\hat{H}/2)$ propagates the SBC in the *imaginary* time from zero to $-i\beta\hbar/2$. Note that the imaginary time $-i\beta\hbar/2$ is exclusively determined by the temperature and does not depend on the *real* time t. Analogously to Eq. (3.4) one can now read the integrand in Eq. (3.21) from the right to the left. The SBC starts in the state $|s_0\mathbf{Q}_0\rangle$ and is propagated within the imaginary time $-i\beta\hbar/2$ to $\left|s_0^+ \mathbf{Q}_0^+\right\rangle$. Further the SBC evolves *forward* in the real time to $|s_\Omega\mathbf{Q}_t\rangle$ at time t. At this point the SBC has reached the *complex time*

$$
\chi \equiv t - i\beta\hbar/2 \qquad (3.22)
$$

After the operator $\hat{\Omega}$ has been evaluated, the SBC goes *backward* in the real time from $\left|s_t\mathbf{Q}_t\right\rangle$ to $\left|s_0^- \mathbf{Q}_0^-\right\rangle$ at time $-i\beta\hbar/2$. Here, the evaluation of $\hat{\Gamma}$ takes place. In the final step the SBC is propagated from the state $\left|s_\Gamma\mathbf{Q}_0^-\right\rangle$ to the initial state $|s_0\mathbf{Q}_0\rangle$ at time $-i\beta\hbar$. The propagation in time can be characterized by the *complex time contour* $\mathfrak{c}_\chi$ visualized in Fig. 3.4. As a result of the trace in Eq. (3.19), the TCF has the form of an integral over all coordinate states the SBC occupies during the propagation. In order to express the TCF as a PI, one follows the same line of reasoning as for the reduced density operator in Eq. (3.4). It can be shown that
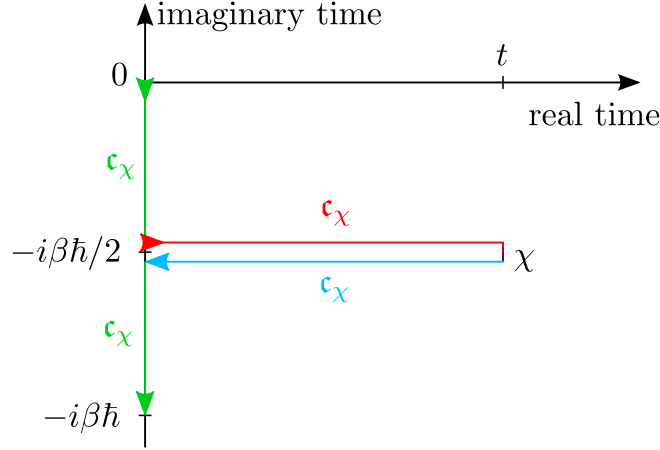
Figure 3.4.: **Complex time contour** $\mathfrak{c}_\chi$.

the following equivalence (App. A) holds

$$\left\langle s \left| \exp\left\{ -\beta/2 \left(\hat{p}^2/(2m) + \hat{V}(\hat{s}) \right) \right\} \right| s_0 \right\rangle = \int\limits_{s_0}^{s} \mathrm{D}_{(0,\beta\hbar/2)} \mathfrak{s}(\tau) \, \exp\left\{ -\frac{1}{\hbar} E_{(0,\beta\hbar/2)}[\mathfrak{s}(\tau)] \right\} \quad, \quad (3.23)$$

with the so-called *Euclidean action*

$$E_{(0,\beta\hbar/2)}[\mathfrak{s}(\tau)] = \int\limits_0^{\beta\hbar/2} \mathrm{d}\tau \left[\frac{1}{2} m \dot{\mathfrak{s}}^2(\tau) + V\left(\mathfrak{s}(\tau)\right) \right] \quad. \qquad (3.24)$$

Note that the Euclidean action differs from the classical action in the sign of the potential energy. The paths appearing in Eqs. (3.23,3.24) do not depend on the real time, thus they can not be considered as classical trajectories, but they can be interpreted as paths spanning the imaginary time $-i\beta\hbar/2$. Following Tuckerman [37], the variation of the Euclidean action yields the same Euler-Lagrange equation as the variation of the classical action. Thus, if the classical path provides the minimum of the classical action, then the Euclidian action also becomes minimal for this particular path. If a path differs crucially from the classical one, the Euclidean action has a high magnitude, thus, its contribution to the PI in Eq. (3.23) is damped strongly due to the exponential integrand. In contrast, paths similar to the classical one have a large contribution, since their Euclidean action is close to the minimal one. With the Eqs. (3.5,3.23) at hand, one can express the TCF in Eq. (3.21) as an integral over forward/backward paths

$\mathfrak{s}_{\text{re}}^+(\tau)$, $\mathfrak{s}_{\text{re}}^-(\tau)$ spanning the real part of the complex time χ and paths $\mathfrak{s}_{\text{im}}^+(\tau)$, $\mathfrak{s}_{\text{im}}^-(\tau)$ that span the imaginary part. Note that for the latter paths the superscript $\pm$ does not imply a forward or backward direction in imaginary time. Inspired by Ref. [30], the paths $\mathfrak{s}_{\text{im}}^+(\tau)$ span the imaginary time interval $(0, -i\beta\hbar/2)$, whereas $\mathfrak{s}_{\text{im}}^-(\tau)$ span the interval $(-i\beta\hbar/2, -i\beta\hbar)$. The TCF rewritten as a PI then reads

$$
C_{\Gamma\Omega}(t) = \frac{1}{Z(\beta)} \int\limits_{-\infty}^{\infty} \mathrm{d}s_0 \int\limits_{-\infty}^{\infty} \mathrm{d}s_0^- \int\limits_{-\infty}^{\infty} \mathrm{d}s_0^+ \int\limits_{-\infty}^{\infty} \mathrm{d}s_t \int\limits_{-\infty}^{\infty} \mathrm{d}s_\Gamma \int\limits_{-\infty}^{\infty} \mathrm{d}s_\Omega
$$

$$
\times \int\limits_{s_0}^{s_0^+} \mathrm{D}_{(0,\beta\hbar/2)}\mathfrak{s}_{\text{im}}^+(\tau) \int\limits_{s_0^+}^{s_\Gamma} \mathrm{D}_{(0,t)}\mathfrak{s}_{\text{re}}^+(\tau) \int\limits_{s_0^-}^{s_t} \mathrm{D}_{(0,t)}\mathfrak{s}_{\text{re}}^-(\tau) \int\limits_{s_\Gamma}^{s_0} \mathrm{D}_{(0,\beta\hbar/2)}\mathfrak{s}_{\text{im}}^-(\tau)
$$

$$
\times \exp\left\{ \frac{i}{\hbar} \left(A_{(0,t)}^{\text{S}}[\mathfrak{s}_{\text{re}}^+(\tau)] - A_{(0,t)}^{\text{S}}[\mathfrak{s}_{\text{re}}^-(\tau)] \right) - \frac{1}{\hbar} \left(E_{(0,\beta\hbar/2)}^{\text{S}}[\mathfrak{s}_{\text{im}}^+(\tau)] + E_{(0,\beta\hbar/2)}^{\text{S}}[\mathfrak{s}_{\text{im}}^-(\tau)] \right) \right\}
$$

$$
\times \mathscr{F}_{(0,\chi)}[\mathfrak{s}_{\text{re}}^+(\tau), \, \mathfrak{s}_{\text{re}}^-(\tau), \, \mathfrak{s}_{\text{im}}^+(\tau), \, \mathfrak{s}_{\text{im}}^-(\tau)] \cdot \left\langle \mathfrak{s}_{\text{im}}^-(0) \right| \hat{\Gamma} \left| \mathfrak{s}_{\text{re}}^-(0) \right\rangle \left\langle \mathfrak{s}_{\text{re}}^-(t) \right| \hat{\Omega} \left| \mathfrak{s}_{\text{re}}^+(t) \right\rangle \quad , \quad (3.25)
$$

where

$$
\left\langle \mathfrak{s}_{\text{im}}^-(0) \right| \hat{\Gamma} \left| \mathfrak{s}_{\text{re}}^-(0) \right\rangle \left\langle \mathfrak{s}_{\text{re}}^-(t) \right| \hat{\Omega} \left| \mathfrak{s}_{\text{re}}^+(t) \right\rangle \equiv \left\langle s_\Gamma \right| \hat{\Gamma} \left| s_0^- \right\rangle \left\langle s_t \right| \hat{\Omega} \left| s_\Omega \right\rangle \tag{3.26}
$$

and the *complex time influence functional* is defined as

$$
\mathscr{F}_{(0,\chi)}[\mathfrak{s}_{\text{re}}^+(\tau), \, \mathfrak{s}_{\text{re}}^-(\tau), \, \mathfrak{s}_{\text{im}}^+(\tau), \, \mathfrak{s}_{\text{im}}^-(\tau)] \equiv \int\limits_{-\infty}^{\infty} \mathrm{d}\mathbf{Q}_0 \int\limits_{-\infty}^{\infty} \mathrm{d}\mathbf{Q}_t \int\limits_{-\infty}^{\infty} \mathrm{d}\mathbf{Q}_0^+ \int\limits_{-\infty}^{\infty} \mathrm{d}\mathbf{Q}_0^-
$$

$$
\times \int\limits_{\mathbf{Q}_0}^{\mathbf{Q}_0^+} \mathrm{D}_{(0,\beta\hbar/2)}\mathfrak{Q}_{\text{im}}^+(\tau) \int\limits_{\mathbf{Q}_0^+}^{\mathbf{Q}_t} \mathrm{D}_{(0,t)}\mathfrak{Q}_{\text{re}}^+(\tau) \int\limits_{\mathbf{Q}_0^-}^{\mathbf{Q}_t} \mathrm{D}_{(0,t)}\mathfrak{Q}_{\text{re}}^-(\tau) \int\limits_{\mathbf{Q}_0^-}^{\mathbf{Q}_0} \mathrm{D}_{(0,\beta\hbar/2)}\mathfrak{Q}_{\text{im}}^-(\tau)
$$

$$
\times \exp\left\{ \frac{i}{\hbar} \left(A_{(0,t)}^{\text{SB}}[\mathfrak{s}_{\text{re}}^+(\tau), \, \mathfrak{Q}_{\text{re}}^+(\tau)] - A_{(0,t)}^{\text{SB}}[\mathfrak{s}_{\text{re}}^-(\tau), \, \mathfrak{Q}_{\text{re}}^-(\tau)] \right) \right\}
$$

$$
\times \exp\left\{ -\frac{1}{\hbar} \left(E_{(0,\beta\hbar/2)}^{\text{SB}}[\mathfrak{s}_{\text{im}}^+(\tau), \, \mathfrak{Q}_{\text{im}}^+(\tau)] + E_{(0,\beta\hbar/2)}^{\text{SB}}[\mathfrak{s}_{\text{im}}^-(\tau), \, \mathfrak{Q}_{\text{im}}^-(\tau)] \right) \right\} \quad (3.27)
$$

with the Euclidean actions

$$E^{\mathrm{SB}}_{(0,\beta\hbar/2)}[\mathfrak{s}(\tau),\mathfrak{Q}(\tau)] = \int\limits_0^{\beta\hbar/2} \mathrm{d}\tau \left\{ \sum_{i=1}^{D} \frac{1}{2}M_i\dot{\mathfrak{Q}}_i^{\,2}(\tau) + V_{\mathrm{B}}\left(\mathfrak{Q}(\tau)\right) + V_{\mathrm{int}}\left(\mathfrak{s}(\tau);\mathfrak{Q}(\tau)\right) \right\} \qquad (3.28)$$

$$E^{\mathrm{S}}_{(0,\beta\hbar/2)}[\mathfrak{s}(\tau)] = \int\limits_0^{\beta\hbar/2} \mathrm{d}\tau \left[\frac{1}{2}m\dot{\mathfrak{s}}^2(\tau) + V_{\mathrm{s}}\left(\mathfrak{s}(\tau)\right) \right] \;. \qquad (3.29)$$

As it was done in Sec. 3.1, the PI expression can be compressed with the introduction of the *complex time bare system part* of the path integral

$$\mathscr{S}^{\Gamma\Omega}_{(0,\chi)}\left[\mathfrak{s}^{\pm}_{\mathrm{re}}(\tau),\mathfrak{s}^{\pm}_{\mathrm{im}}(\tau)\right] \equiv \left\langle \mathfrak{s}^{-}_{\mathrm{im}}(0)\right|\hat{\Gamma}\left|\mathfrak{s}^{-}_{\mathrm{re}}(0)\right\rangle \left\langle \mathfrak{s}^{-}_{\mathrm{re}}(t)\right|\hat{\Omega}\left|\mathfrak{s}^{+}_{\mathrm{re}}(t)\right\rangle$$

$$\times \exp\left\{ \frac{i}{\hbar}\left(A^{\mathrm{S}}_{(0,t)}[\mathfrak{s}^{+}_{\mathrm{re}}(\tau)] - A^{\mathrm{S}}_{(0,t)}[\mathfrak{s}^{-}_{\mathrm{re}}(\tau)] \right) - \frac{1}{\hbar}\left(E^{\mathrm{S}}_{(0,\beta\hbar/2)}[\mathfrak{s}^{+}_{\mathrm{im}}(\tau)] + E^{\mathrm{S}}_{(0,\beta\hbar/2)}[\mathfrak{s}^{-}_{\mathrm{im}}(\tau)] \right) \right\} \qquad (3.30)$$

and the notation

$$\int\limits_{s_0}^{\cdot} \mathrm{D}_{(0,\beta\hbar/2)}\mathfrak{s}^{+}_{\mathrm{im}}(\tau) \int \mathrm{D}_{(0,t)}\mathfrak{s}^{+}_{\mathrm{re}}(\tau) \int \mathrm{D}_{(0,t)}\mathfrak{s}^{-}_{\mathrm{re}}(\tau) \int\limits^{s_0} \mathrm{D}_{(0,\beta\hbar/2)}\mathfrak{s}^{-}_{\mathrm{im}}(\tau) \equiv$$

$$\int\limits_{-\infty}^{\infty} \mathrm{d}s_0^+ \int\limits_{-\infty}^{\infty} \mathrm{d}s_0^- \int\limits_{-\infty}^{\infty} \mathrm{d}s_t \int\limits_{-\infty}^{\infty} \mathrm{d}s_\Omega \int\limits_{-\infty}^{\infty} \mathrm{d}s_\Gamma$$

$$\times \int\limits_{s_0}^{s_0^+} \mathrm{D}_{(0,\beta\hbar/2)}\mathfrak{s}^{+}_{\mathrm{im}}(\tau) \int\limits_{s_0^+}^{s_\Omega} \mathrm{D}_{(0,t)}\mathfrak{s}^{+}_{\mathrm{re}}(\tau) \int\limits_{s_0^-}^{s_t} \mathrm{D}_{(0,t)}\mathfrak{s}^{-}_{\mathrm{re}}(\tau) \int\limits_{s_\Gamma}^{s_0} \mathrm{D}_{(0,\beta\hbar/2)}\mathfrak{s}^{-}_{\mathrm{im}}(\tau) \;. \qquad (3.31)$$

The functional integral in Eq. (3.31) is taken over all imaginary paths $\mathfrak{s}^{+}_{\mathrm{im}}(\tau)$ that start at the coordinate s_0 and end where the forward path $\mathfrak{s}^{+}_{\mathrm{re}}(\tau)$ starts, i.e. $\mathfrak{s}^{+}_{\mathrm{im}}(\beta\hbar/2) = \mathfrak{s}^{+}_{\mathrm{re}}(0)$ as indicated by the dots. The paths $\mathfrak{s}^{+}_{\mathrm{re}}(\tau)$ and $\mathfrak{s}^{-}_{\mathrm{re}}(\tau)$ as well as $\mathfrak{s}^{-}_{\mathrm{re}}(\tau)$ and $\mathfrak{s}^{-}_{\mathrm{im}}(\tau)$ are not connected continuously. Note that the imaginary path $\mathfrak{s}^{-}_{\mathrm{im}}(\tau)$ ends where $\mathfrak{s}^{+}_{\mathrm{im}}(\tau)$ starts, namely at the coordinate s_0, as the result of the trace in Eq. (3.19). Employing these definitions, the TCF in the path integral formulation finally reads
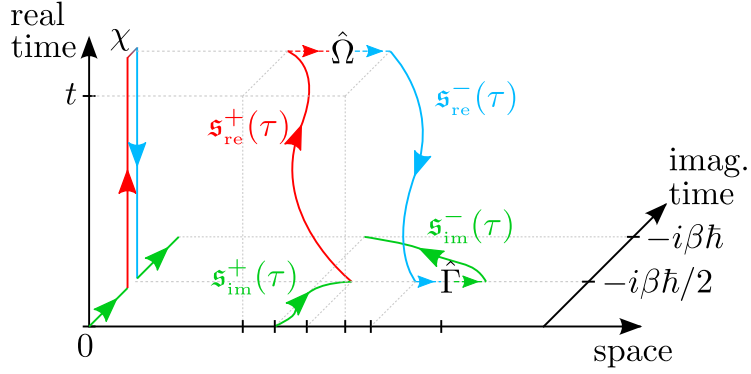
Figure 3.5.: **Bare system propagation in complex time and space.** The marked coordinates on the space axis are from the left to the right $\mathfrak{s}_{\mathrm{re}}^{+}(t)$, $\mathfrak{s}_{\mathrm{im}}^{+}(0) = \mathfrak{s}_{\mathrm{im}}^{-}(\beta\hbar/2)$, $\mathfrak{s}_{\mathrm{im}}^{+}(\beta\hbar/2) = \mathfrak{s}_{\mathrm{re}}^{+}(0)$, $\mathfrak{s}_{\mathrm{re}}^{-}(t)$, $\mathfrak{s}_{\mathrm{re}}^{-}(0)$, $\mathfrak{s}_{\mathrm{im}}^{-}(0)$. Note that the time contour $\mathfrak{c}_{\chi}$ in Fig. 3.4 is the projection of the entire path on the complex time plane.

$$C_{\Gamma\Omega}(t) = \frac{1}{Z(\beta)} \int\limits_{-\infty}^{\infty} \mathrm{d}s_0 \int\limits_{s_0}^{\cdot} \mathrm{D}_{(0,\beta\hbar/2)}\mathfrak{s}_{\mathrm{im}}^{+}(\tau) \int \mathrm{D}_{(0,t)}\mathfrak{s}_{\mathrm{re}}^{+}(\tau) \int \mathrm{D}_{(0,t)}\mathfrak{s}_{\mathrm{re}}^{-}(\tau) \int\limits_{\cdot}^{s_0} \mathrm{D}_{(0,\beta\hbar/2)}\mathfrak{s}_{\mathrm{im}}^{-}(\tau)$$

$$\times \mathscr{F}_{(0,\chi)}[\mathfrak{s}_{\mathrm{re}}^{\pm}(\tau), \mathfrak{s}_{\mathrm{im}}^{\pm}(\tau)] \cdot \mathscr{S}_{(0,\chi)}^{\Gamma\Omega}[\mathfrak{s}_{\mathrm{re}}^{\pm}(\tau), \mathfrak{s}_{\mathrm{im}}^{\pm}(\tau)] \quad . \quad (3.32)$$

The integrand is determined by two mutually independent factors. First, the value of the functional $\mathscr{S}_{(0,\chi)}^{\Gamma\Omega}[\mathfrak{s}_{\mathrm{re}}^{\pm}(\tau), \mathfrak{s}_{\mathrm{im}}^{\pm}(\tau)]$, that depends on the system operators $\hat{\Gamma}$ and $\hat{\Omega}$ and takes account of the bare system that follows the paths $\mathfrak{s}_{\mathrm{re}}^{\pm}(\tau)$, $\mathfrak{s}_{\mathrm{im}}^{\pm}(\tau)$ in the complex time. Second, the complex time influence functional weights the integrand according to the interaction between the system and bath. The value of the TCF can then be considered as an integral over *all* bare system paths, that are *quasi-closed* in space, see Fig. 3.5. Here, quasi-closed means that the paths $\mathfrak{s}_{\mathrm{re}}^{+}(\tau)$ and $\mathfrak{s}_{\mathrm{re}}^{-}(\tau)$ are discontinuously connected by the operator $\hat{\Omega}$ and $\mathfrak{s}_{\mathrm{re}}^{-}(\tau)$ and $\mathfrak{s}_{\mathrm{im}}^{-}(\tau)$ are discontinuously connected by $\hat{\Gamma}$, whereas the starting point of $\mathfrak{s}_{\mathrm{im}}^{+}(\tau)$ and the end point of $\mathfrak{s}_{\mathrm{im}}^{-}(\tau)$ coincide.

4. Numerical treatment of path integrals

The first part of this chapter contains a derivation of the time evolution of the reduced density operator formulated as a *discrete* PI. In order to obtain closed expressions for the discrete influence functional the bath is described by an ensemble of uncoupled harmonic oscillators with an arbitrary spectral density, whereas system-bath coupling is linear. This particular description of system and bath is referred to as the multi-mode Brownian oscillator model (MBO) [19, 20, 21]. The discrete PI formalism derived in this chapter serves as a basis for an iterative propagation scheme and related algorithms [26, 27, 28, 31]. The second part is focused on the application of the very same ideas to the propagation of equilibrium time-correlation functions [30, 29].

4.1. Propagation of the reduced density operator

4.1.1. Derivation of the discrete PI

The goal of this subsection is to construct the discrete counterpart of Eq. (3.17), which then can be used as a basis for a numerical implementation. Note that a direct discretization of Eq. (3.17) causes problems as stated in Introduction. Therefore, the starting point is the general time evolution of the reduced density operator

$$\hat{\rho}_{\mathrm{s}}(t) = \mathrm{Tr}_{\mathrm{B}}\left[\hat{U}(t)\hat{\rho}(0)\hat{U}^{\dagger}(t)\right] \quad . \tag{4.1}$$

The time t is formally discretized into N time slices by using the identity

$$\exp\left\{\mp i\hat{H}t/\hbar\right\} = \left(\exp\left\{\mp i\hat{H}\Delta t/\hbar\right\}\right)^{N} \quad , \tag{4.2}$$

where $\Delta t \equiv t/N$. Equation (4.1) can then be rewritten as

$$\hat{\rho}_{\mathrm{S}}(t) = \mathrm{Tr}_{\mathrm{B}} \left[\underbrace{\mathrm{e}^{-i\hat{H}\Delta t/\hbar} \cdots \mathrm{e}^{-i\hat{H}\Delta t/\hbar}}_{N \text{ times}} \hat{\rho}(0) \underbrace{\mathrm{e}^{i\hat{H}\Delta t/\hbar} \cdots \mathrm{e}^{i\hat{H}\Delta t/\hbar}}_{N \text{ times}} \right] . \tag{4.3}$$

The next step consists of an insertion of a set of $2N$ spatial closures for a system coordinate

$$\hat{1}_{\mathrm{S}} = \int\limits_{-\infty}^{\infty} \mathrm{d}s \, |s\rangle\langle s| \tag{4.4}$$

in between each pair of operators in Eq. (4.3). The integrals inserted on the left of $\hat{\rho}(0)$ are performed over the variables s_k^+, whereas the integrals on the right go over s_k^- with $k = 0, \ldots, N-1$. In anticipation of what follows, the coordinates colored in red will form discrete forward paths and blue-colored coordinates will correspond to discrete backward paths. The reduced density operator in the coordinate representation can then be written as

$$\langle s_+ |\hat{\rho}_{\mathrm{S}}(t)| s_-\rangle = \mathrm{Tr}_{\mathrm{B}} \left[\int\limits_{-\infty}^{\infty} \mathrm{d}s_0^+ \cdots \int\limits_{-\infty}^{\infty} \mathrm{d}s_{N-1}^+ \int\limits_{-\infty}^{\infty} \mathrm{d}s_0^- \cdots \int\limits_{-\infty}^{\infty} \mathrm{d}s_{N-1}^- \right.$$

$$\left\langle s_+ \left| \mathrm{e}^{-i\hat{H}\Delta t/\hbar} \right| s_{N-1}^+ \right\rangle \left\langle s_{N-1}^+ \left| \mathrm{e}^{-i\hat{H}\Delta t/\hbar} \right| s_{N-2}^+ \right\rangle \cdots \left\langle s_1^+ \left| \mathrm{e}^{-i\hat{H}\Delta t/\hbar} \right| s_0^+ \right\rangle$$

$$\times \left. \left\langle s_0^+ \left| \hat{\rho}(0) \right| s_0^- \right\rangle \left\langle s_0^- \left| \mathrm{e}^{i\hat{H}\Delta t/\hbar} \right| s_1^- \right\rangle \cdots \left\langle s_{N-2}^- \left| \mathrm{e}^{i\hat{H}\Delta t/\hbar} \right| s_{N-1}^- \right\rangle \left\langle s_{N-1}^- \left| \mathrm{e}^{i\hat{H}\Delta t/\hbar} \right| s_- \right\rangle \right] , \tag{4.5}$$

where $\hat{s}\,|s_\pm\rangle = s_\pm\,|s_\pm\rangle$. For a numerical treatment the continuous space coordinate s is approximated by a set of M discrete *grid points* $\tilde{s}_i$ leading to the quadrature rule

$$\hat{1}_{\mathrm{S}} = \int\limits_{-\infty}^{\infty} \mathrm{d}s \, |s\rangle\langle s| \approx \sum_{i=0}^{M-1} \Delta\tilde{s}_i \cdot |\tilde{s}_i\rangle\langle\tilde{s}_i| , \tag{4.6}$$

where $\hat{s}\,|\tilde{s}_i\rangle = \tilde{s}_i\,|\tilde{s}_i\rangle$ and $\Delta\tilde{s}_i$ is the weight of the i-th grid point. Since the states $|\tilde{s}_i\rangle$ are not orthonormal, the normalized *spatial grid states* are defined as

$$|\underline{\tilde{s}_i}\rangle \equiv \sqrt{\Delta\tilde{s}_i}\,|\tilde{s}_i\rangle , \tag{4.7}$$

which obey

$$\hat{1}_{\mathrm{s}} \approx \sum_{i=0}^{M-1} |\tilde{s}_i\rangle\langle\tilde{s}_i| \tag{4.8}$$

and

$$\hat{s}|\tilde{s}_i\rangle = \tilde{s}_i|\tilde{s}_i\rangle, \quad \langle\tilde{s}_i|\tilde{s}_j\rangle = \delta_{ij} \ , \tag{4.9}$$

where δ_{ij} is the Kronecker delta. Combining Eqs. (4.8,4.9) implies that the M states $|\tilde{s}_i\rangle$ related to the spatial grid

$$\mathbb{S}_M \equiv \{\tilde{s}_i\} \tag{4.10}$$

form an *orthonormal* basis for an M-dimensional subspace of the system's Hilbert space. Note that the approximation in Eq. (4.6) is exact for $M \to \infty$. In order to recast Eq. (4.5) into a numerically approachable expression, two steps are performed. First, the reduced density operator is represented as a time-dependent matrix $\tilde{\boldsymbol{\rho}}^{\mathrm{s}}(N\Delta t) \in \mathbb{C}^{M\times M}$ in the basis of the spatial grid states. The matrix $\tilde{\boldsymbol{\rho}}^{\mathrm{s}}(N\Delta t)$ is referred to as the *reduced density matrix* (RDM) of the system and has the elements

$$\tilde{\rho}^{\mathrm{s}}_{+,-}(N\Delta t) \equiv \langle\tilde{s}_+|\hat{\rho}_{\mathrm{s}}(t)|\tilde{s}_-\rangle \ , \tag{4.11}$$

where "+" and "−" symbolically represent the integer numbers $0,\ldots, M-1$. Second, the integrals in Eq. (4.5) are replaced by sums

$$\int_{-\infty}^{\infty} \mathrm{d}s_k^+ \, |s_k^+\rangle\langle s_k^+| \to \sum_{i_k^+=0}^{M-1} |\tilde{s}_{i_k^+}\rangle\langle\tilde{s}_{i_k^+}| \ , \quad \int_{-\infty}^{\infty} \mathrm{d}s_k^- \, |s_k^-\rangle\langle s_k^-| \to \sum_{i_k^-=0}^{M-1} |\tilde{s}_{i_k^-}\rangle\langle\tilde{s}_{i_k^-}| \ , \tag{4.12}$$

according to Eq. (4.6). The final result is the time propagation of the RDM elements on a discrete spatial grid

$$\tilde{\rho}^{\text{S}}_{+,-}(N\Delta t) = \text{Tr}_{\text{B}}\left[\sum_{i_0^+=0}^{M-1}\cdots\sum_{i_{N-1}^+=0}^{M-1}\sum_{i_0^-=0}^{M-1}\cdots\sum_{i_{N-1}^-=0}^{M-1}\right.$$

$$\left\langle \tilde{s}_+ \left| e^{-i\hat{H}\Delta t/\hbar} \right| \tilde{s}_{i_{N-1}^+} \right\rangle\left\langle \tilde{s}_{i_{N-1}^+} \left| e^{-i\hat{H}\Delta t/\hbar} \right| \tilde{s}_{i_{N-2}^+} \right\rangle\cdots\left\langle \tilde{s}_{i_1^+} \left| e^{-i\hat{H}\Delta t/\hbar} \right| \tilde{s}_{i_0^+} \right\rangle$$

$$\times\left\langle \tilde{s}_{i_0^+} \left| \hat{\rho}(0) \right| \tilde{s}_{i_0^-} \right\rangle\left\langle \tilde{s}_{i_0^-} \left| e^{i\hat{H}\Delta t/\hbar} \right| \tilde{s}_{i_1^-} \right\rangle\cdots\left\langle \tilde{s}_{i_{N-2}^-} \left| e^{i\hat{H}\Delta t/\hbar} \right| \tilde{s}_{i_{N-1}^-} \right\rangle\left\langle \tilde{s}_{i_{N-1}^-} \left| e^{i\hat{H}\Delta t/\hbar} \right| \tilde{s}_- \right\rangle\left.\right] \quad . \quad (4.13)$$

In the following, the time evolution by a time-step Δt of the entire system is approximated by the Trotter factorization

$$\exp\left\{-\frac{i}{\hbar}\hat{H}\Delta t\right\} \approx \exp\left\{-\frac{i}{2\hbar}\hat{H}_{\text{SB}}\Delta t\right\}\exp\left\{-\frac{i}{\hbar}\hat{H}_{\text{S}}\Delta t\right\}\exp\left\{-\frac{i}{2\hbar}\hat{H}_{\text{SB}}\Delta t\right\} \quad . \quad (4.14)$$

Note that this factorization is only an approximation, since the system's momentum operator $\hat{p}$ in $\hat{H}_{\text{S}}$ does not commute with the system's position operator $\hat{s}$ in $\hat{H}_{\text{SB}}$. The error induced by this approximation is proportional to Δt^3 [24], thus, in the limit of $N \to \infty$ it becomes exact for an arbitrarily long but finite time t. With this approximation the quantities in Eq. (4.13) can be further evaluated, e.g.

$$\left\langle \tilde{s}_{i_{k+2}^+} \left| e^{-i\hat{H}\Delta t/\hbar} \right| \tilde{s}_{i_{k+1}^+} \right\rangle\left\langle \tilde{s}_{i_{k+1}^+} \left| e^{-i\hat{H}\Delta t/\hbar} \right| \tilde{s}_{i_k^+} \right\rangle \approx$$

$$\exp\left\{-\frac{i}{2\hbar}\hat{H}_{\text{SB}}\left(\tilde{s}_{i_{k+2}^+}\right)\Delta t\right\}\exp\left\{-\frac{i}{\hbar}\hat{H}_{\text{SB}}\left(\tilde{s}_{i_{k+1}^+}\right)\Delta t\right\}\exp\left\{-\frac{i}{2\hbar}\hat{H}_{\text{SB}}\left(\tilde{s}_{i_k^+}\right)\Delta t\right\}$$

$$\times\left\langle \tilde{s}_{i_{k+2}^+} \left| e^{-i\hat{H}_{\text{S}}\Delta t/\hbar} \right| \tilde{s}_{i_{k+1}^+} \right\rangle\left\langle \tilde{s}_{i_{k+1}^+} \left| e^{-i\hat{H}_{\text{S}}\Delta t/\hbar} \right| \tilde{s}_{i_k^+} \right\rangle \quad , \quad (4.15)$$

where

$$\hat{H}_{\text{SB}}\left(\tilde{s}_{i_k^+}\right) \equiv \hat{H}_{\text{SB}}\left(\tilde{s}_{i_k^+}, \hat{\mathbf{Q}}, \hat{\mathbf{P}}\right) \quad (4.16)$$

is the system-bath interaction Hamiltonian depending parametrically on the system coordinate $\tilde{s}_{i_k^+}$. Note that operators of the bath's Hilbert space do not act on the states $\left| \tilde{s}_{i_k^+} \right\rangle$ and $\hat{H}_{\text{SB}}\left(\hat{s}, \hat{\mathbf{Q}}, \hat{\mathbf{P}}\right)\left| \tilde{s}_{i_k^+} \right\rangle = \hat{H}_{\text{SB}}\left(\tilde{s}_{i_k^+}, \hat{\mathbf{Q}}, \hat{\mathbf{P}}\right)\left| \tilde{s}_{i_k^+} \right\rangle$. Equation (4.15) can be easily transferred to the

quantities on the right hand side of $\hat{\rho}(0)$, that is depending on the variables $\tilde{s}_{i_k^-}$. Note that, according to Eq. (2.7), the following equality holds

$$\left\langle \tilde{s}_{i_0^+} \middle| \hat{\rho}(0) \middle| \tilde{s}_{i_0^-} \right\rangle = \left\langle \tilde{s}_{i_0^+} \middle| \hat{\rho}_{\mathrm{S}}(0) \middle| \tilde{s}_{i_0^-} \right\rangle \hat{\rho}_{\mathrm{B}}(0) \ . \tag{4.17}$$

By the insertion of the spatial closures, all operators in the system's Hilbert space are represented by complex numbers, see Eqs. (4.15-4.17). It is now possible to rearrange the quantities such that all bare system quantities in Eq. (4.13) are separated from that depending on the system *and* the bath or exclusively on the bath. The equation for the RDM rewritten this way reads

$$\tilde{\rho}_{+,-}^{\mathrm{S}}(N\Delta t) = \sum_{i_0^+=0}^{M-1} \cdots \sum_{i_{N-1}^+=0}^{M-1} \sum_{i_0^-=0}^{M-1} \cdots \sum_{i_{N-1}^-=0}^{M-1}$$

$$f\left(\tilde{s}_{i_0^+}, \ldots, \tilde{s}_{i_{N-1}^+}, \tilde{s}_+, \tilde{s}_{i_0^-}, \ldots, \tilde{s}_{i_{N-1}^-}, \tilde{s}_- \right) \left\langle \tilde{s}_{i_0^+} \middle| \hat{\rho}_{\mathrm{S}}(0) \middle| \tilde{s}_{i_0^-} \right\rangle$$

$$\times \left\langle \tilde{s}_{i_0^-} \middle| \mathrm{e}^{i\hat{H}_{\mathrm{S}}\Delta t/\hbar} \middle| \tilde{s}_{i_1^-} \right\rangle \cdots \left\langle \tilde{s}_{i_{N-2}^-} \middle| \mathrm{e}^{i\hat{H}_{\mathrm{S}}\Delta t/\hbar} \middle| \tilde{s}_{i_{N-1}^-} \right\rangle \left\langle \tilde{s}_{i_{N-1}^-} \middle| \mathrm{e}^{i\hat{H}_{\mathrm{S}}\Delta t/\hbar} \middle| \tilde{s}_- \right\rangle$$

$$\times \left\langle \tilde{s}_+ \middle| \mathrm{e}^{-i\hat{H}_{\mathrm{S}}\Delta t/\hbar} \middle| \tilde{s}_{i_{N-1}^+} \right\rangle \left\langle \tilde{s}_{i_{N-1}^+} \middle| \mathrm{e}^{-i\hat{H}_{\mathrm{S}}\Delta t/\hbar} \middle| \tilde{s}_{i_{N-2}^+} \right\rangle \cdots \left\langle \tilde{s}_{i_1^+} \middle| \mathrm{e}^{-i\hat{H}_{\mathrm{S}}\Delta t/\hbar} \middle| \tilde{s}_{i_0^+} \right\rangle \ , \tag{4.18}$$

where the multi-dimensional function

$$f\left(\tilde{s}_0^+, \ldots, \tilde{s}_{N-1}^+, \tilde{s}^+, \tilde{s}_0^-, \ldots, \tilde{s}_{N-1}^-, \tilde{s}^- \right) \equiv$$

$$\mathrm{Tr}_{\mathrm{B}}\left[\mathrm{e}^{-i\hat{H}_{\mathrm{SB}}(\tilde{s}^+,)\Delta t/(2\hbar)} \mathrm{e}^{-i\hat{H}_{\mathrm{SB}}(\tilde{s}_{N-1}^+)\Delta t/\hbar} \cdots \mathrm{e}^{-i\hat{H}_{\mathrm{SB}}(\tilde{s}_1^+)\Delta t/\hbar} \mathrm{e}^{-i\hat{H}_{\mathrm{SB}}(\tilde{s}_0^+)\Delta t/(2\hbar)} \hat{\rho}_{\mathrm{B}}(0) \right.$$

$$\left. \times \mathrm{e}^{i\hat{H}_{\mathrm{SB}}(\tilde{s}_0^-)\Delta t/(2\hbar)} \mathrm{e}^{i\hat{H}_{\mathrm{SB}}(\tilde{s}_1^-)\Delta t/\hbar} \cdots \mathrm{e}^{i\hat{H}_{\mathrm{SB}}(\tilde{s}_{N-1}^+)\Delta t/\hbar} \mathrm{e}^{i\hat{H}_{\mathrm{SB}}(\tilde{s}^-)\Delta t/(2\hbar)} \right] \ . \tag{4.19}$$

carries all the information about the system-bath interaction. The function f defines the *discrete* influence functional, as it would be pointed out below. Note at this point that the approximation due to discretization in time and space becomes exact in the limit

$$\lim_{\Delta t \to 0,\, M \to \infty} \tilde{\rho}_{+,-}^{\mathrm{S}}(N\Delta t) = \rho_{\mathrm{S}}(\tilde{s}_+, \tilde{s}_-; t) \ , \tag{4.20}$$

where $\Delta t \to 0$ induces $N \to \infty$. This implies that a numerical scheme based on Eq. (4.18) produces numerically exact results, i.e. up to a given accuracy. Equation (4.18) would be

rewritten in a more compact form in the following. The basis of this recast is the substitution of a grid point sequence $\tilde{s}_{i_0^+}, \ldots, \tilde{s}_{i_{N-1}^+}, \tilde{s}_+, \tilde{s}_{i_0^-}, \ldots, \tilde{s}_{i_{N-1}^-}, \tilde{s}_-$ by a new variable referred to as the *discrete forward backward path combination* (FBC)

$$\tilde{\mathfrak{s}}^{\pm} \equiv \begin{pmatrix} \tilde{\mathfrak{s}}_0^+ & \tilde{\mathfrak{s}}_1^+ & \cdots & \tilde{\mathfrak{s}}_{N-1}^+ \\ \tilde{\mathfrak{s}}_0^- & \tilde{\mathfrak{s}}_1^- & \cdots & \tilde{\mathfrak{s}}_{N-1}^- \end{pmatrix} = \begin{pmatrix} \tilde{s}_{i_0^+} & \tilde{s}_{i_1^+} & \cdots & \tilde{s}_{i_{N-1}^+} \\ \tilde{s}_{i_0^-} & \tilde{s}_{i_1^-} & \cdots & \tilde{s}_{i_{N-1}^-} \end{pmatrix} \tag{4.21}$$

with the *end points* $\tilde{s}_{\pm}$. Note that the end points are not included in the definition of $\tilde{\mathfrak{s}}^{\pm}$. This specific definition is more convenient for formulating the iterative propagation scheme later in Sec. 4.1.4. In order to motivate the introduction of FBCs in Eq. (4.21), let us restrict ourselves to the special case $N = M = 3$, where the time-space grid contains 4×3 points as it is depicted in Fig. 4.1. The focus is now put on the RDM element $\tilde{\rho}_{0,1}^{\mathrm{S}}(3\Delta t)$, i.e. "+"= 0, "−"= 1, which is determined by

$$\tilde{\rho}_{0,1}^{\mathrm{S}}(3\Delta t) = \sum_{i_0^+=0}^{2} \sum_{i_1^+=0}^{2} \sum_{i_2^+=0}^{2} \sum_{i_0^-=0}^{2} \sum_{i_1^-=0}^{2} \sum_{i_2^-=0}^{2}$$

$$f\left(\tilde{s}_{i_0^+}, \tilde{s}_{i_1^+}, \tilde{s}_{i_2^+}, \tilde{s}_0, \tilde{s}_{i_0^-}, \tilde{s}_{i_1^-}, \tilde{s}_{i_2^-}, \tilde{s}_1\right) \left\langle \tilde{s}_{i_0^+}\middle|\hat{\rho}_{\mathrm{S}}(0)\middle|\tilde{s}_{i_0^-}\right\rangle$$

$$\times \left\langle \tilde{s}_{i_0^-}\middle|e^{i\hat{H}_{\mathrm{S}}\Delta t/\hbar}\middle|\tilde{s}_{i_1^-}\right\rangle\left\langle \tilde{s}_{i_1^-}\middle|e^{i\hat{H}_{\mathrm{S}}\Delta t/\hbar}\middle|\tilde{s}_{i_2^-}\right\rangle\left\langle \tilde{s}_{i_2^-}\middle|e^{i\hat{H}_{\mathrm{S}}\Delta t/\hbar}\middle|\tilde{s}_1\right\rangle$$

$$\times \left\langle \tilde{s}_0\middle|e^{-i\hat{H}_{\mathrm{S}}\Delta t/\hbar}\middle|\tilde{s}_{i_2^+}\right\rangle\left\langle \tilde{s}_{i_2^+}\middle|e^{-i\hat{H}_{\mathrm{S}}\Delta t/\hbar}\middle|\tilde{s}_{i_1^+}\right\rangle\left\langle \tilde{s}_{i_1^+}\middle|e^{-i\hat{H}_{\mathrm{S}}\Delta t/\hbar}\middle|\tilde{s}_{i_0^+}\right\rangle , \tag{4.22}$$

In order to calculate a specific summand, called σ with $i_0^+ = 0$, $i_1^+ = 0$, $i_2^+ = 1$ and $i_0^- = 1$, $i_1^- = 2$, $i_2^- = 1$, the following operation has to be performed

$$\sigma = f\left(\tilde{s}_0, \tilde{s}_0, \tilde{s}_1, \tilde{s}_0, \tilde{s}_1, \tilde{s}_2, \tilde{s}_1, \tilde{s}_1\right) \left\langle \tilde{s}_0|\hat{\rho}_{\mathrm{S}}(0)|\tilde{s}_1\right\rangle$$

$$\times \left\langle \tilde{s}_1|e^{i\hat{H}_{\mathrm{S}}\Delta t/\hbar}|\tilde{s}_2\right\rangle\left\langle \tilde{s}_2|e^{i\hat{H}_{\mathrm{S}}\Delta t/\hbar}|\tilde{s}_1\right\rangle\left\langle \tilde{s}_1|e^{i\hat{H}_{\mathrm{S}}\Delta t/\hbar}|\tilde{s}_1\right\rangle$$

$$\times \left\langle \tilde{s}_0|e^{-i\hat{H}_{\mathrm{S}}\Delta t/\hbar}|\tilde{s}_1\right\rangle\left\langle \tilde{s}_1|e^{-i\hat{H}_{\mathrm{S}}\Delta t/\hbar}|\tilde{s}_0\right\rangle\left\langle \tilde{s}_0|e^{-i\hat{H}_{\mathrm{S}}\Delta t/\hbar}|\tilde{s}_0\right\rangle . \tag{4.23}$$

The calculation of σ can be divided into three mutually independent tasks; note that the expression has to be read from the right to the left.

First, the *bare* system is stepwise propagated *forward* in time on the spatial grid due to $\hat{H}_{\mathrm{S}}$, see Fig. 4.1. During this propagation the system is localized along the *discrete forward*
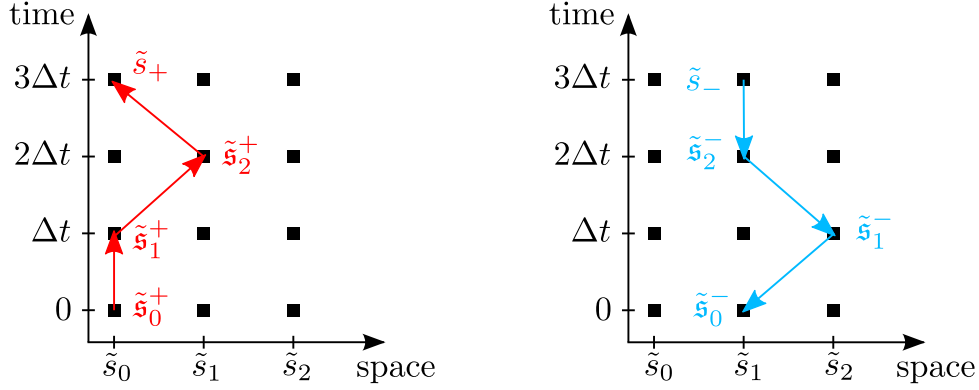
Figure 4.1.: **Propagation of the bare system on the space-time grid.** The forward/backward path is shown in the left/right panel, correspondingly.

path $\tilde{\mathfrak{s}}^+ \equiv \left(\tilde{\mathfrak{s}}_0^+, \tilde{\mathfrak{s}}_1^+, \tilde{\mathfrak{s}}_2^+ \right) = (\tilde{s}_0, \tilde{s}_0, \tilde{s}_1)$. Note that the *end point* $\tilde{s}_+ = \tilde{s}_0$, where the system is localized at time $3\Delta t$ is not included in the definition of $\tilde{\mathfrak{s}}^+$. Subsequently the system is propagated backward in time starting at the coordinate $\tilde{s}_- = \tilde{s}_1$ at time $3\Delta t$. Then the system follows *reversely* the *discrete backward path* $\tilde{\mathfrak{s}}^- \equiv \left(\tilde{\mathfrak{s}}_0^-, \tilde{\mathfrak{s}}_1^-, \tilde{\mathfrak{s}}_2^- \right) = (\tilde{s}_1, \tilde{s}_2, \tilde{s}_1)$. Note that the coordinates building the backward path are still ordered in the forward direction of time. In analogy to the discrete forward path, the coordinate $\tilde{s}_-$ is also referred to as the *end point* of the discrete backward path, despite that it is, in fact, the starting point of the backward propagation. According to the last two lines in Eq. 4.23, the first task in order to calculate σ requires the propagation of the bare system along the FBC

$$\tilde{\mathfrak{s}}^\pm = \begin{pmatrix} \tilde{\mathfrak{s}}_0^+ & \tilde{\mathfrak{s}}_1^+ & \tilde{\mathfrak{s}}_2^+ \\ \tilde{\mathfrak{s}}_0^- & \tilde{\mathfrak{s}}_1^- & \tilde{\mathfrak{s}}_2^- \end{pmatrix} \tag{4.24}$$

with the end points $\tilde{s}_\pm$. Note that the end points are exclusively determined by the RDM element on the right hand side of Eq. (4.23), thus, they are the same in all summands contributing to this particular RDM element.

The second task in order to calculate σ involves the weighting of the summand by the complex number $\left\langle \tilde{s}_{i_0^+} \middle| \hat{\rho}_{\rm s}(0) \middle| \tilde{s}_{i_0^-} \right\rangle = \left\langle \tilde{s}_0 \middle| \hat{\rho}_{\rm s}(0) \middle| \tilde{s}_1 \right\rangle = \left\langle \tilde{\mathfrak{s}}_0^+ \middle| \hat{\rho}_{\rm s}(0) \middle| \tilde{\mathfrak{s}}_0^- \right\rangle$, which is given by the initial RDM related to the first coordinate $\tilde{\mathfrak{s}}_0^+$ of the forward path and the first coordinate $\tilde{\mathfrak{s}}_0^-$ of the backward path.

The third task is to compute the multi-dimensional function f, which appears as an additional weighting factor in the first line of Eq. (4.23). According to Eq. (4.19), the function f in the
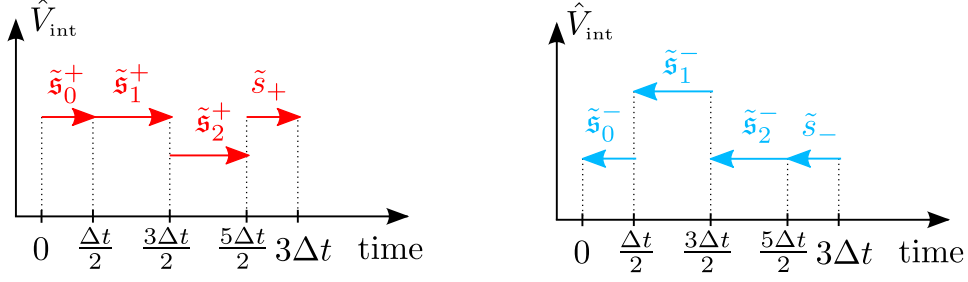
Figure 4.2.: **Interaction potential experienced by the bath.** The vertical axis is referred to the "strength" of the system-bath interaction. The forward/backward evolution in time is shown in the left/right panel, respectively.

case $N = M = 3$ reads as

$$
\begin{aligned}
f\left(\tilde{s}_0,\,\tilde{s}_0,\,\tilde{s}_1,\,\tilde{s}_0,\,\,\tilde{s}_1,\,\tilde{s}_2,\,\tilde{s}_1,\,\tilde{s}_1\right) = f\left(\tilde{\mathfrak{s}}_0^+,\,\tilde{\mathfrak{s}}_1^+,\,\tilde{\mathfrak{s}}_2^+,\,\tilde{s}_+,\,\tilde{\mathfrak{s}}_0^-,\,\tilde{\mathfrak{s}}_1^-,\,\tilde{\mathfrak{s}}_2^-,\,\tilde{s}_-\right) = \\
\int_{-\infty}^{\infty} \mathrm{d}\mathbf{Q} \int_{-\infty}^{\infty} \mathrm{d}\mathbf{Q}_0^+ \int_{-\infty}^{\infty} \mathrm{d}\mathbf{Q}_0^- \left\langle \mathbf{Q}_0^+ \middle| \hat{\rho}_{\mathrm{B}}(0) \middle| \mathbf{Q}_0^- \right\rangle \\
\times \left\langle \mathbf{Q}_0^- \middle| \mathrm{e}^{i\hat{H}_{\mathrm{SB}}(\tilde{\mathfrak{s}}_0^-)\Delta t/(2\hbar)} \mathrm{e}^{i\hat{H}_{\mathrm{SB}}(\tilde{\mathfrak{s}}_1^-)\Delta t/\hbar} \mathrm{e}^{i\hat{H}_{\mathrm{SB}}(\tilde{\mathfrak{s}}_2^-)\Delta t/\hbar} \mathrm{e}^{i\hat{H}_{\mathrm{SB}}(\tilde{s}_-)\Delta t/(2\hbar)} \middle| \mathbf{Q} \right\rangle \\
\times \left\langle \mathbf{Q} \middle| \mathrm{e}^{-i\hat{H}_{\mathrm{SB}}(\tilde{s}_+)\Delta t/(2\hbar)} \mathrm{e}^{-i\hat{H}_{\mathrm{SB}}(\tilde{\mathfrak{s}}_2^+)\Delta t/\hbar} \mathrm{e}^{-i\hat{H}_{\mathrm{SB}}(\tilde{\mathfrak{s}}_1^+)\Delta t/\hbar} \mathrm{e}^{-i\hat{H}_{\mathrm{SB}}(\tilde{\mathfrak{s}}_0^+)\Delta t/(2\hbar)} \middle| \mathbf{Q}_0^+ \right\rangle \;,
\end{aligned}
$$
$$(4.25)$$

where the trace is taken in the bath's coordinate basis and two spatial closures $\int_{-\infty}^{\infty} \mathrm{d}\mathbf{Q}_0^+ \left| \mathbf{Q}_0^+ \right\rangle\left\langle \mathbf{Q}_0^+ \right|$, $\int_{-\infty}^{\infty} \mathrm{d}\mathbf{Q}_0^- \left| \mathbf{Q}_0^- \right\rangle\left\langle \mathbf{Q}_0^- \right|$ are inserted on the left and on the right of $\hat{\rho}_{\mathrm{B}}(0)$, respectively. Note additionally that the sequence of the system coordinates $\tilde{s}_0,\,\tilde{s}_0,\,\tilde{s}_1,\,\tilde{s}_0,\,\tilde{s}_1,\,\tilde{s}_2,\,\tilde{s}_1,$ $\tilde{s}_1$ is now expressed in terms of the FBC $\tilde{\mathfrak{s}}^\pm$ with end points $\tilde{s}_\pm$. If the integrand is read from the right to the left, then the following interpretation emerges. The bath starts at time 0 from the initial state $\left| \mathbf{Q}_0^+ \right\rangle$, then it is propagated due to $\hat{H}_{\mathrm{SB}}(\tilde{\mathfrak{s}}_0^+)$ by a half time step forward in time. The downscaling of the time step by two is the result of the Trotter factorization in Eq. (4.14). Within the time $\Delta t/2$ the system coordinate is fixed to $\tilde{\mathfrak{s}}_0^+$ and, thus, the interaction potential is fixed to $\hat{V}_{\mathrm{int}}(\tilde{\mathfrak{s}}_0^+, \hat{\mathbf{Q}})$ accordingly, see Fig. 4.2. Afterwards the bath is propagated by two full time steps experiencing the fixed interaction $\hat{V}_{\mathrm{int}}(\tilde{\mathfrak{s}}_1^+, \hat{\mathbf{Q}})$ and $\hat{V}_{\mathrm{int}}(\tilde{\mathfrak{s}}_2^+, \hat{\mathbf{Q}})$, respectively, followed by a half step with $\hat{V}_{\mathrm{int}}(\tilde{s}_+, \hat{\mathbf{Q}})$. At this point the bath is in the final state $|\mathbf{Q}\rangle$ at time $3\Delta t$. The next propagation step evolves the bath $\Delta t/2$ backward in time, with the interaction potential being fixed to $\hat{V}_{\mathrm{int}}(\tilde{s}_-, \hat{\mathbf{Q}})$. Analogously to the propagation forward in time, two full steps and a

half step backward in time follow. At the end the bath is in the state $\left|\mathbf{Q}_0^-\right\rangle$ and the integrand is weighted by the complex number $\left\langle\mathbf{Q}_0^+\right|\hat{\rho}_{\mathrm{B}}(0)\left|\mathbf{Q}_0^-\right\rangle$ related to the initial density operator of the bath. The actual value of f is then the integral over all initial and final states the bath could have had within the described propagation.

To summarize, the specific summand σ is determined by the propagation of the bare system following the particular FBC $\tilde{\mathfrak{s}}^\pm$ with end points $\tilde{s}_\pm$. Then σ is weighted by the complex number $\left\langle\tilde{\mathfrak{s}}_0^+\right|\hat{\rho}_{\mathrm{s}}(0)\left|\tilde{\mathfrak{s}}_0^-\right\rangle$ related to the initial RDM and the initial coordinates of the forward and backward paths. The multi-dimensional function f additionally weights the summand σ. The value of f is calculated according to the averaged system-bath interaction, where the corresponding interaction potential can be described by an operator-like step function, see Fig. 4.2. The magnitude of the interaction potential depends on the coordinates of the particular FBC and its end points, see also Fig. 4.2. If one now calculates all other summands that contribute to the RDM element $\tilde{\rho}_{0,1}^{\mathrm{S}}(3\Delta t)$, then the values $\tilde{s}_+ = \tilde{s}_0$ and $\tilde{s}_- = \tilde{s}_1$ are fixed but the indices i_k^+, i_k^-, $k = 0, 1, 2$ are varying. Each summand represents a particular combination of forward and backward paths, which is combinatorially constructed out of $2N = 6$ spatial grid points contained in the set $\mathbb{S}_3$. That means the six-fold sum in Eq. (4.22) can be replaced by *one* sum over all possible FBCs that can be build out of six grid points. Since all considerations of this paragraph are easily transferable to arbitrary RDM elements and arbitrary N, M, one can transform Eq. (4.18) into a *discrete path integral* (DPI)

$$\tilde{\rho}_\pm^{\mathrm{S}}(N\Delta t) = \sum_{\tilde{\mathfrak{s}}^\pm \in \mathbb{P}_{N,M}} \tilde{F}_{(0,N)}\left[\tilde{\mathfrak{s}}^\pm, \tilde{s}_\pm\right] \tilde{S}_{(0,N)}\left[\tilde{\mathfrak{s}}^\pm, \tilde{s}_\pm\right] \tilde{R}\left[\tilde{\mathfrak{s}}^\pm\right] \quad, \tag{4.26}$$

where $\tilde{\rho}_\pm^{\mathrm{S}}(N\Delta t) \equiv \tilde{\rho}_{+,-}^{\mathrm{S}}(N\Delta t)$. The set $\mathbb{P}_{N,M}$ is the $2N$-fold Cartesian product of the spatial grid

$$\mathbb{P}_{N,M} \equiv \left(\mathbb{S}_M\right)^{2N} \tag{4.27}$$

and has the number of elements $L_{N,M}$ given by

$$L_{N,M} \equiv \left|\mathbb{P}_{N,M}\right| = M^{2N} \quad. \tag{4.28}$$

Each element of $\mathbb{P}_{N,M}$ is a FBC $\tilde{\mathfrak{s}}^\pm$ that spans $N-1$ time steps and is defined according to Eq. (4.21). Naturally the set $\mathbb{P}_{N,M}$ contains *all* FBCs that are possible on an $N \times M$ time-space grid. Each summand in Eq. (4.26) requires the calculation of three independent quantities.

4. Numerical treatment of path integrals

First, the *discrete bare system part* of the DPI is calculated via

$$\tilde{S}_{(0,N)}\left[\tilde{\mathfrak{s}}^{\pm}, s_{\pm}\right] \equiv \prod_{k=0}^{N-1} \tilde{S}_{(k,k+1)}\left(\tilde{\mathfrak{s}}_k^{\pm}, \tilde{\mathfrak{s}}_{k+1}^{\pm}\right) \quad, \tag{4.29}$$

where

$$\tilde{S}_{(k,k+1)}\left(\tilde{\mathfrak{s}}_k^{\pm}, \tilde{\mathfrak{s}}_{k+1}^{\pm}\right) \equiv \underline{\langle \tilde{\mathfrak{s}}_{k+1}^+|} e^{-i\hat{H}_{\mathrm{S}}\Delta t/\hbar} \underline{|\tilde{\mathfrak{s}}_k^+\rangle} \underline{\langle \tilde{\mathfrak{s}}_k^-|} e^{i\hat{H}_{\mathrm{S}}\Delta t/\hbar} \underline{|\tilde{\mathfrak{s}}_{k+1}^-\rangle} \quad, \tag{4.30}$$

is the *bare system point-to-point propagator,* which propagates the bare system from the time $k\Delta t$ to $(k+1)\Delta t$. Note that in Eqs. (4.29,4.30) for $k = N-1$ the following definition is valid

$$\tilde{\mathfrak{s}}_N^{\pm} = \tilde{s}_{\pm} \quad. \tag{4.31}$$

Second, the summand is weighted by the *discrete multi-time reduced density functional*

$$\tilde{R}\left[\tilde{\mathfrak{s}}^{\pm}\right] \equiv \underline{\langle \tilde{\mathfrak{s}}_0^+|} \hat{\rho}_{\mathrm{S}}(0) \underline{|\tilde{\mathfrak{s}}_0^-\rangle} \quad. \tag{4.32}$$

The value $\tilde{R}\left[\tilde{\mathfrak{s}}^{\pm}\right]$ for a particular FBC $\tilde{\mathfrak{s}}^{\pm}$ can be considered as one element of the *multi-time reduced density vector* $\tilde{\mathbf{R}} \in \mathbb{C}^{L_{N,M}}$. As it was already stated in Sec. 3.1, the importance of the definition in Eq. 4.32 would become clear in Sec. 4.1.4.

Third, the summand is additionally weighted by the *discrete influence functional* defined as

$$\tilde{F}_{(0,N)}\left[\tilde{\mathfrak{s}}^{\pm}, \tilde{s}_{\pm}\right] \equiv f\left(\tilde{\mathfrak{s}}_0^+, \ldots, \tilde{\mathfrak{s}}_{N-1}^+, \tilde{s}_+, \tilde{\mathfrak{s}}_0^-, \ldots, \tilde{\mathfrak{s}}_{N-1}^-, \tilde{s}_-\right) \quad. \tag{4.33}$$

The value of $\tilde{F}_{(0,N)}\left[\tilde{\mathfrak{s}}^{\pm}, \tilde{s}_{\pm}\right]$ depends on the particular FBC $\tilde{\mathfrak{s}}^{\pm}$ and the end points $\tilde{s}_{\pm}$, which span together the time interval $(0, N\Delta t)$. In order to calculate the time-dependent expectation value of an arbitrary system operator $\hat{\Omega}$, one has to perform an additional summation over the end points

$$
\begin{aligned}
\left\langle \hat{\Omega} \right\rangle_t &= \sum_{\pm=0}^{M-1} \tilde{\Omega}_{\mp} \cdot \tilde{\rho}_{\pm}^{\mathrm{S}}(N\Delta t) \\
&= \sum_{\pm=0}^{M-1} \tilde{\Omega}_{\mp} \cdot \sum_{\tilde{\mathfrak{s}}^{\pm} \in \mathbb{P}_{N,M}} \tilde{F}_{(0,N)}\left[\tilde{\mathfrak{s}}^{\pm}, \tilde{s}_{\pm}\right] \tilde{S}_{(0,N)}\left[\tilde{\mathfrak{s}}^{\pm}, \tilde{s}_{\pm}\right] \tilde{R}\left[\tilde{\mathfrak{s}}^{\pm}\right]
\end{aligned} \tag{4.34}
$$

where $\tilde{\Omega}_{\mp} \equiv \underline{\langle \tilde{s}_-|} \hat{\Omega} \underline{|\tilde{s}_+\rangle}$ and $\sum_{\pm=0}^{M-1}$ symbolically represents a two-fold sum over the indices "+"

and "−".

Equation (4.26) offers in principal a recipe to perform the time evolution of the RDM numerically. However, the feasibility of this approach is debatable due to the numbers of FBCs $L_{N,M}$ which contribute to the DPI. Here, two problems with respect to the numerical costs arise. The number of FBCs and, hence, the number of operations during the propagation strongly depend on M, see Eq. (4.28). Moreover, the numbers grow exponentially with the propagation step N. The first problem can be reduced by employing a system-dependent grid, which reasonably approximates the continuous system space by just few grid points. The construction of this specific grid is the subject of the following subsection. The second problem is due to the structure of Eq. (4.26). In order to propagate the RDM to a certain time step N, one always has to start from the initial condition at time 0. If N is incremented by one, the space-time grid grows by M spatial grid points, thus, the set $\mathbb{P}_{N,M}$ grows by M^2 elements. Such a propagation scheme is referred to as *global*. The aim is now to reformulate Eq. (4.26) such, that already calculated time steps can be used as starting points for following time steps. Within such a successive propagation, the number of FBCs is independent on the total propagation time. A scheme of this kind is called *iterative* and its application to the discrete PI is the subject of Sec. 4.1.4.

4.1.2. The discrete variable representation

As it was mentioned in the end of the previous subsection, the number of FBCs increases rapidly with the number M of spatial grid points. Hence, the aim of this subsection is to find a set of coordinates $\mathbb{S}_M = \{\tilde{s}_i\}$, with M being as small as possible, such that the approximation in Eq. (4.6) still remains reasonable.

As a starting point one assumes that the perturbation induced by the bath is small enough, such that the reduced density operator has approximately the limit

$$\lim_{t \to \infty} \hat{\rho}_{\mathrm{s}}(t) \approx \frac{1}{Z_{\mathrm{s}}(\beta)} \mathrm{e}^{-\beta \hat{H}_{\mathrm{s}}} \ , \tag{4.35}$$

which corresponds to the canonical equilibrium of the bare system with the system's partition function $Z_{\mathrm{s}}(\beta)$. The operator on the right hand side of Eq. (4.35) can be written down as a

sum over the system's eigenstate projectors

$$e^{-\beta \hat{H}_\text{S}} = \sum_{n=0}^{\infty} e^{-\beta \epsilon_n} |n\rangle \langle n| \quad, \tag{4.36}$$

where the states obey the stationary Schrödinger equation

$$\hat{H}_\text{S} |n\rangle = \epsilon_n |n\rangle \quad. \tag{4.37}$$

If one assumes additionally that the thermal energy $1/\beta = k_\text{B}T$ is much smaller than the energy differences $\epsilon_n - \epsilon_0$ for $n > 0$, the sum in Eq. (4.36) can be truncated after few summands. In other words, high energy states have negligible weight in the equilibrium statistics of the system in a weakly-coupled environment at typical temperatures. If the lowest M energy eigenstates of the system are sufficient to describe the equilibrium statistics without a loss of accuracy, one can claim that

$$\hat{1}_\text{S} \approx \sum_{n=0}^{M-1} |n\rangle \langle n| \tag{4.38}$$

is a *reasonable* approximation. Since the PI formulation of quantum dynamics requires the coordinate representation, the task is now to find a set of *position* eigenstates $\left\{ \left| \underline{\tilde{s}_i} \right\rangle \right\}$ that span the same subspace as the energy eigenstates in Eq. (4.38) do. This criterion is fulfilled if there exist coefficients T_{in} that obey

$$\left| \underline{\tilde{s}_i} \right\rangle = \sum_{n=0}^{M-1} T_{in} |n\rangle \quad, \tag{4.39}$$

under the condition

$$\left\langle \underline{\tilde{s}_i} \middle| \hat{s} \middle| \underline{\tilde{s}_j} \right\rangle = \tilde{s}_i \delta_{ij} \quad. \tag{4.40}$$

A combination of Eqs. (4.39,4.40) yields

$$\sum_{k=0}^{M-1} \sum_{l=0}^{M-1} T_{ik}^* \langle k| \hat{s} |l\rangle T_{jl} = \tilde{s}_i \delta_{ij} \quad, \tag{4.41}$$

which can be expressed as the diagonalization of a matrix $\mathbf{s}$ via the unitary transformation

$$\mathbf{T}^{\dagger}\mathbf{s}\mathbf{T} = \begin{pmatrix} \tilde{s}_0 & & \\ & \ddots & \\ & & \tilde{s}_{M-1} \end{pmatrix} , \qquad (4.42)$$

where $\mathbf{s}, \mathbf{T} \in \mathbb{C}^{M \times M}$ have the elements $s_{kl} = \langle k| \hat{s} |l\rangle$ and $T_{in} = \langle n|\tilde{s}_i\rangle$, respectively, and $\mathbf{T}^{\dagger} = \mathbf{T}^{-1}$. Note that $\mathbf{s}$ is the matrix representation of the system's position operator in the truncated basis formed by the M lowest energy eigenstates of the system itself. Consequently, the eigenvalues $\tilde{s}_0, \ldots, \tilde{s}_{M-1}$ form a *system-dependent* spatial grid and the corresponding basis given by the states $\left\{ |\tilde{s}_i\rangle \right\}$ is called the *discrete variable representation* (DVR). In comparison to another spatial discretization, the DVR indeed requires a very small number of grid points as it will be shown in Sec. 5.2.

To conclude, the recipe to determine a reasonable spatial grid is as follows. First, the stationary Schrödinger equation of the bare system has to be solved for the M lowest eigenstates, see Eq. (4.37). Subsequently the matrix $\mathbf{s}$ has to be calculated and diagonalized, see Eq. (4.42). The resulting eigenvalues are then the grid points. Additionally, the elements of the transformation matrix $\mathbf{T}$ can be employed to calculate the discrete bare system part in Eqs. (4.33,4.29) via

$$\langle \tilde{s}_i |\mathrm{e}^{\mp i\hat{H}_\mathrm{S}\Delta t/\hbar}| \tilde{s}_j \rangle = \sum_{n=0}^{M-1} \mathrm{e}^{\mp i\epsilon_n \Delta t/\hbar} \langle \tilde{s}_i|n\rangle \langle n|\tilde{s}_j\rangle = \sum_{n=0}^{M-1} \mathrm{e}^{\mp i\epsilon_n \Delta t/\hbar} T_{jn} T_{ni}^{\dagger} . \qquad (4.43)$$

4.1.3. The multi-mode Brownian oscillator model

The remaining task is to recast the global propagation of the RDM in Eq. (4.26) as an iterative scheme. First let us figure out the main obstacles hindering it. In Eq. (4.19) one notices that the influence functional depends on the coordinates of *all* time steps in the past simultaneously. In other words, the influence functional is *non-local in time* as a result of the bath's "memory". Thus, the RDM at the N-th time step depends *explicitly* on all previous time steps up to the zeroth. The goal of this subsection is to express the discrete influence functional as a product of point-to-point propagators similar to the discrete bare system part in Eqs. (4.29, 4.30). Since in the vast majority of cases the memory time of the bath is finite, this product can be truncated and, thus, the explicit dependence on very early time steps vanishes.

In order to derive a specific form of the influence functional, one assumes the *multi-mode*

4. Numerical treatment of path integrals

Brownian oscillator (MBO) model, whose system-bath Hamiltonian reads

$$\hat{H}(\hat{s}, \hat{p}; \hat{\mathbf{Q}}, \hat{\mathbf{P}}) = \frac{\hat{p}^2}{2m} + \hat{V}_{\mathrm{S}}(\hat{s}) + \sum_{i=1}^{D} \left\{ \frac{\hat{P}_i^2}{2M_i} + \frac{1}{2} M_i \omega_i^2 \left(\hat{Q}_i - \frac{g_i \hat{s}}{M_i \omega_i^2} \right)^2 \right\} \quad . \tag{4.44}$$

Here, the system with an arbitrary potential $\hat{V}_{\mathrm{S}}(\hat{s})$ is bilinearly coupled to the bath comprised by D harmonic oscillators with frequencies ω_i and masses M_i. The coupling to each oscillator is determined by the parameters g_i, which are given by the *spectral density*

$$J(\omega) = \frac{\pi}{2} \sum_{i=1}^{D} \frac{g_i^2}{M_i \omega_i} \delta(\omega - \omega_i) \quad . \tag{4.45}$$

The spectral density fully determines the characteristics of the bath and if the number of harmonic oscillators approaches infinity this function becomes continuous. Note that the harmonic oscillators are uncoupled from each other. This particular definition of the system-bath Hamiltonian is assumed for all following considerations. For the MBO Hamiltonian, the error resulting from the Trotter factorization in Eq. (4.14) can be explicitly given [24] to be proportional to

$$\Delta t^3 \sum_{i=1}^{D} \left[\hat{p}^2, \left[\hat{p}^2, \left(\hat{Q}_i - \frac{g_i \hat{s}}{M_i \omega_i^2} \right)^2 \right] \right] \quad , \tag{4.46}$$

where $[\cdot, \cdot]$ denotes the commutator. The major advantage of the MBO model is, that the influence functional in Eq. (4.33) can be expressed analytically. Thus, the calculation of $\tilde{F}_{(0,N)}\left[\tilde{\mathfrak{s}}^{\pm}, s_{\pm} \right]$ in Eq. (4.33) can be performed without treating the numerous bath's DOFs numerically. The possibility to find an analytical expression for the influence functional is a consequence of the particular assumption of the MBO Hamiltonian, as it is briefly sketched in the following. Each oscillator in the bath experiences individually the *external force*

$$\hat{K}_i^{\mathrm{ext}}(\hat{s}) \equiv \frac{i}{\hbar} \left[\hat{V}_{\mathrm{int}}(\hat{s}, \hat{\mathbf{Q}}), \, \hat{P}_i \right] = g_i \hat{1}_{\mathrm{B}} \hat{s} \quad , \tag{4.47}$$

according to the Heisenberg equation of motion, where $\hat{V}_{\mathrm{int}}(\hat{s}, \hat{\mathbf{Q}}) = -\hat{Q}_i \hat{s} + g_i^2/(M_i \omega_i^2)\hat{s}^2$. Due to the bilinear coupling between system and bath, the force scales just linearly with the system coordinate $\hat{s}$. In the framework of the PI formalism, as presented in Sec. 3.1, the system coordinate is described by a combination of a forward path $\mathfrak{s}^+(\tau)$ and a backward path $\mathfrak{s}^-(\tau)$.

Consequently, the force in Eq. (4.47) in the PI formulation depends on the system path and, thus, it is parametrically time-dependent

$$\hat{K}_i^{\text{ext},\pm}(\tau) \equiv g_i \hat{1}_{\text{B}} \mathfrak{s}^{\pm}(\tau) \ .$$

(4.48)

Following Feynman [18], the *continuous* influence functional can then be written down analytically as

$$F_{(0,t)}\left[\mathfrak{s}^{\pm}(\tau)\right] = \exp\left\{-\frac{1}{\hbar}\int_0^t \mathrm{d}\tau \int_0^\tau \mathrm{d}\tau' \ \left(B(\tau-\tau')\mathfrak{s}^+(\tau') - B^*(\tau-\tau')\mathfrak{s}^-(\tau')\right) \cdot \left(\mathfrak{s}^+(\tau) - \mathfrak{s}^-(\tau)\right)\right\}$$

$$\times \exp\left\{-i\frac{\pi}{\hbar}\int_0^\infty \mathrm{d}\omega \frac{J(\omega)}{\omega}\int_0^t \mathrm{d}\tau \ \left(\mathfrak{s}^+(\tau)^2 - \mathfrak{s}^-(\tau)^2\right)\right\} \ . \quad (4.49)$$

Note that it is additionally assumed that the bath is in the canonical equilibrium at time zero

$$\hat{\rho}_{\text{B}}(0) = \frac{1}{Z_{\text{B}}}\mathrm{e}^{-\beta\hat{H}_{\text{B}}} \ .$$

(4.50)

All characteristics of the bath are contained in the *bath response function*

$$B(\tau-\tau') \equiv \frac{1}{\pi}\int_0^\infty \mathrm{d}\omega J(\omega)\frac{\cos\left(\omega\left(\tau-\tau'+i\beta\hbar/2\right)\right)}{\sinh\left(\beta\hbar\omega/2\right)} \ .$$

(4.51)

Referring back to the *discrete* PI in Eq. (4.26), the interaction potential appearing in the discrete influence functional is a step function as depicted in Fig. 4.2. The magnitude depends on the FBC $\tilde{\mathfrak{s}}^{\pm}$ and the end points $s_{\pm}$, thus, in the discrete case the external force can be expressed accordingly

$$\hat{K}_i^{\text{ext},\pm}(\tau) = g_i \hat{1}_{\text{B}} \cdot \begin{cases} \tilde{\mathfrak{s}}_0^{\pm}, & 0 \leq \tau < \Delta t/2 \\ \tilde{\mathfrak{s}}_k^{\pm}, & \left(k-\frac{1}{2}\right)\Delta t \leq \tau < \left(k+\frac{1}{2}\right)\Delta t, \ k = 1,\ldots N-1 \\ s_{\pm}, & \left(N-\frac{1}{2}\right)\Delta t \leq \tau \leq N\Delta t \ , \end{cases}$$

(4.52)

where the first and the last time interval are half-sized as the result of the Trotter factorization in Eq. (4.14). By inserting this special form of the external force into Eq. (4.49), the time

integration can be carried out, yielding the discrete influence functional [26]

$$\tilde{F}_{(0,N)}\left[\tilde{\mathfrak{s}}^{\pm}, \tilde{s}_{\pm}\right] = \exp\left\{-\frac{1}{\hbar}\sum_{k=0}^{N}\sum_{k'=0}^{k}\left(\eta_{k'k}\tilde{\mathfrak{s}}_{k'}^{+} - \eta_{k'k}^{*}\tilde{\mathfrak{s}}_{k'}^{-}\right)\cdot\left(\tilde{\mathfrak{s}}_{k}^{+} - \tilde{\mathfrak{s}}_{k}^{-}\right)\right\}\,, \tag{4.53}$$

with the *memory coefficients*

$$\eta_{k'k} = \int_{\tau_k}^{\tau_{k+1}}\mathrm{d}\tau\int_{\tau_{k'}}^{\tau_{k'+1}}\mathrm{d}\tau' B(\tau - \tau')\,, \quad k \neq k' \tag{4.54}$$

$$\eta_{kk} = \int_{\tau_k}^{\tau_{k+1}}\mathrm{d}\tau\left(\int_{\tau_k}^{\tau_{k+1}}\mathrm{d}\tau' B(\tau - \tau') + i\pi\int_{0}^{\infty}\mathrm{d}\omega\frac{J(\omega)}{\omega}\right)\,, \tag{4.55}$$

where the times τ_k match the time intervals given in Eq. (4.52)

$$\tau_k = \begin{cases} 0\,, & k = 0 \\ \left(k - \frac{1}{2}\right)\Delta t\,, & k = 1,\ldots,N \\ N\Delta t\,, & k = N+1 \end{cases}. \tag{4.56}$$

The memory coefficients $\eta_{k,k}$ can be formulated as closed expressions depending on the spectral density and are given in App. B.1. One can show that $\eta_{k'k}$ depend only on the difference $\Delta k = k - k'$ if $k, k' \neq 0$ and $k, k' \neq N$. The Eq. (4.53) permits the following interpretation. The exclusively bath-dependent coefficients $\eta_{k'k}$ are connecting points $\tilde{\mathfrak{s}}_{k'}^{\pm}$ in the past with present points $\tilde{\mathfrak{s}}_{k}^{\pm}$ of a system path. That means the coefficients are mediating the memory of the bath to the dynamics of the system and the non-locality in time, therefore, manifests itself in $\eta_{k'k}$. Since the primitive of the integrand in Eq. (4.51) is proportional to $1/(\tau - \tau')$, one can expect the limit

$$\lim_{\tau - \tau' \to \infty} B(\tau - \tau') = 0\,, \tag{4.57}$$

see Fig. 4.3 for an example. The limit in Eq. (4.57) implies that also the memory coefficients $\eta_{k'k}$ tend to zero if $k' \ll k$. This behavior accounts for the *finite memory* of the bath, which is mandatory for the iterative procedure as presented in the following subsection.

The initially formulated goal of this subsection is to recast the discrete influence functional
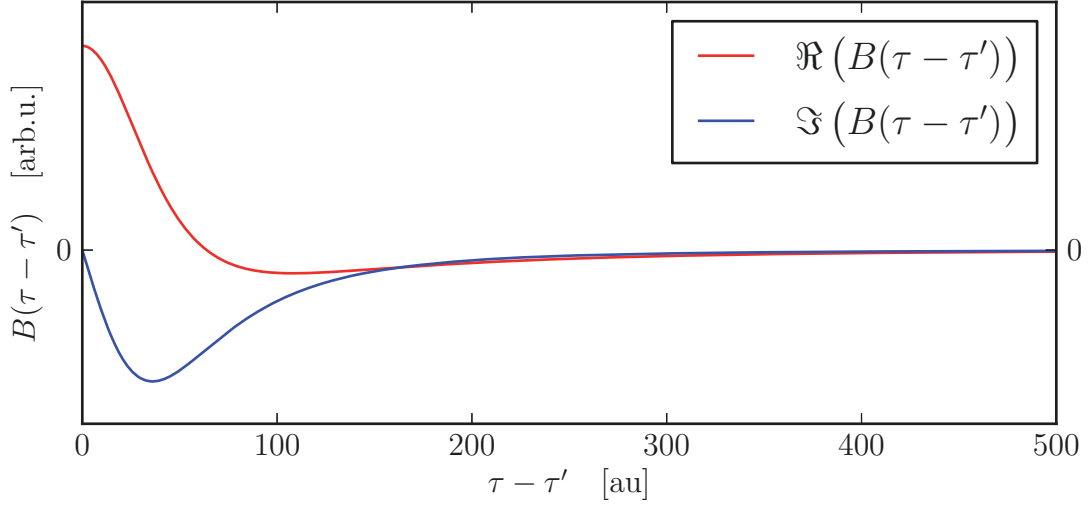
Figure 4.3.: **Bath response function for an Ohmic spectral density.** The graph corresponds to the Ohmic spectral density $J(\omega) = \frac{\pi}{2} \hbar \xi \omega \exp\left(-\omega/\omega_c\right)$.

as a product of point-to-point propagators. By applying the MBO model this aim is fulfilled, since Eq. (4.53) can be written as

$$
\tilde{F}_{(0,N)} \left[\tilde{\mathfrak{s}}^{\pm}, \tilde{s}_{\pm} \right] = \prod_{k=0}^{N} \prod_{k'=0}^{k} \tilde{F}_{(k',k)} \left(\tilde{\mathfrak{s}}_{k'}^{\pm}, \tilde{\mathfrak{s}}_{k}^{\pm} \right) \quad , \tag{4.58}
$$

with the *point-to-point influence*

$$
\tilde{F}_{(k',k)} \left(\tilde{\mathfrak{s}}_{k'}^{\pm}, \tilde{\mathfrak{s}}_{k}^{\pm} \right) \equiv \exp \left\{ -\frac{1}{\hbar} \left(\eta_{k'k} \tilde{\mathfrak{s}}_{k'}^{+} - \eta_{k'k}^{*} \tilde{\mathfrak{s}}_{k'}^{-} \right) \cdot \left(\tilde{\mathfrak{s}}_{k}^{+} - \tilde{\mathfrak{s}}_{k}^{-} \right) \right\} \quad . \tag{4.59}
$$

In order to simplify the derivation of the iterative scheme, the identity

$$
\prod_{k=0}^{N} \prod_{k'=0}^{k} \tilde{F}_{(k',k)} \left(\tilde{\mathfrak{s}}_{k'}^{\pm}, \tilde{\mathfrak{s}}_{k}^{\pm} \right) = \prod_{k'=0}^{N} \prod_{k=k'}^{N} \tilde{F}_{(k',k)} \left(\tilde{\mathfrak{s}}_{k'}^{\pm}, \tilde{\mathfrak{s}}_{k}^{\pm} \right) \tag{4.60}
$$

is employed in the following. The effect of the point-to-point influences can be visualized if one writes the double product on the right hand side of Eq. (4.58) in a more pictorial way and omitting the arguments, see Figs. 4.4. After substitution of Eq. (4.58) in Eq. (4.26) the RDM is

$$\tilde{F}_{(0,N)}\left[\tilde{\mathfrak{s}}^{\pm}, s_{\pm}\right] =$$

$$\tilde{F}_{(0,0)}\tilde{F}_{(0,1)}\tilde{F}_{(0,2)}\tilde{F}_{(0,3)}\tilde{F}_{(0,4)}$$

$$\times \tilde{F}_{(1,1)}\tilde{F}_{(1,2)}\tilde{F}_{(1,3)}\tilde{F}_{(1,4)}$$

$$\times \tilde{F}_{(2,2)}\tilde{F}_{(2,3)}\tilde{F}_{(2,4)}$$

$$\times \tilde{F}_{(3,3)}\tilde{F}_{(3,4)}$$
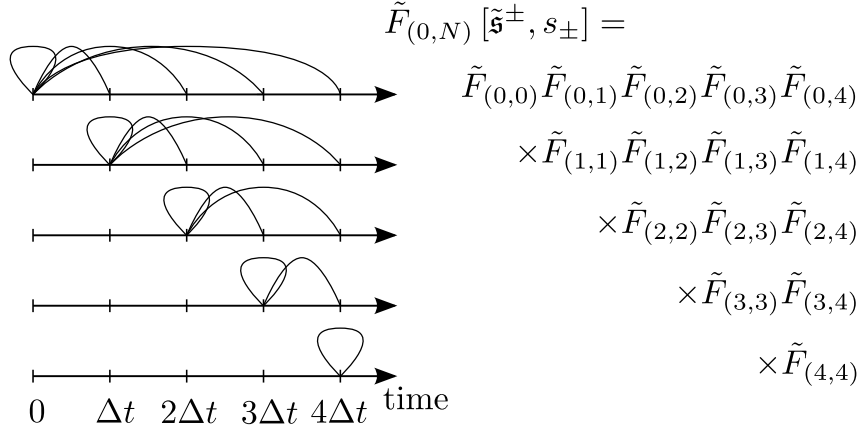
$$\times \tilde{F}_{(4,4)}$$

Figure 4.4.: **Effect of the point-to-point influences.** Shown for the special case $N = 4$. Each point in the past influences each point in the future.

propagated globally via

$$\tilde{\rho}_{\pm}^{\mathrm{S}}(N\Delta t) = \sum_{\tilde{\mathfrak{s}}^{\pm}\in\mathbb{P}_{N,M}} \left(\prod_{k'=0}^{N}\prod_{k=k'}^{N}\tilde{F}_{(k',k)}\left(\tilde{\mathfrak{s}}_{k'}^{\pm}, \tilde{\mathfrak{s}}_{k}^{\pm}\right)\right) \left(\prod_{k=0}^{N-1}\tilde{S}_{(k,k+1)}\left(\tilde{\mathfrak{s}}_{k}^{\pm}, \tilde{\mathfrak{s}}_{k+1}^{\pm}\right)\right) \tilde{R}\left[\tilde{\mathfrak{s}}^{\pm}\right] \quad. \tag{4.61}$$

In the following subsection the global propagation scheme in Eq. (4.61) is transfered into an iterative one.

4.1.4. The iterative calculation of the PI

As it was mentioned in the previous subsection, the memory coefficients $\eta_{k'k}$ appearing in the discrete influence functional tend to zero if $k' \ll k$. Here and further we thus assume that $\eta_{k'k}$ can be neglected without loss of accuracy if $k - k' > \kappa$, which corresponds to a finite memory or *correlation time* $t_{\kappa} \equiv \kappa\Delta t$ of the bath. For any $\kappa > 0$ the bath is referred to as a *non-Markovian* bath. A point-to-point influence in Eq. (4.61) that connects two points separated by a time larger than t_{κ} acts like unity, thus, the double product in Eq. (4.58) can be truncated

$$\tilde{F}_{(0,N)}\left[\tilde{\mathfrak{s}}^{\pm}, s_{\pm}\right] = \prod_{k'=0}^{N}\prod_{k=k'}^{\min\{N, k'+\kappa\}}\tilde{F}_{(k',k)}\left(\tilde{\mathfrak{s}}_{k'}^{\pm}, \tilde{\mathfrak{s}}_{k}^{\pm}\right) \quad. \tag{4.62}$$

$$\tilde{F}_{(0,N)}\left[\tilde{\mathfrak{s}}^{\pm}, s_{\pm}\right] =$$

$$\tilde{F}_{(0,0)}\tilde{F}_{(0,1)}\tilde{F}_{(0,2)}\tilde{F}_{(0,3)}$$

$$\times \tilde{F}_{(1,1)}\tilde{F}_{(1,2)}\tilde{F}_{(1,3)}$$

$$\times \tilde{F}_{(2,2)}\tilde{F}_{(2,3)}$$
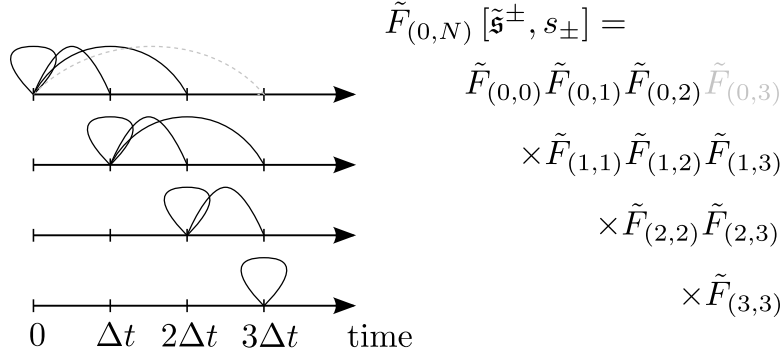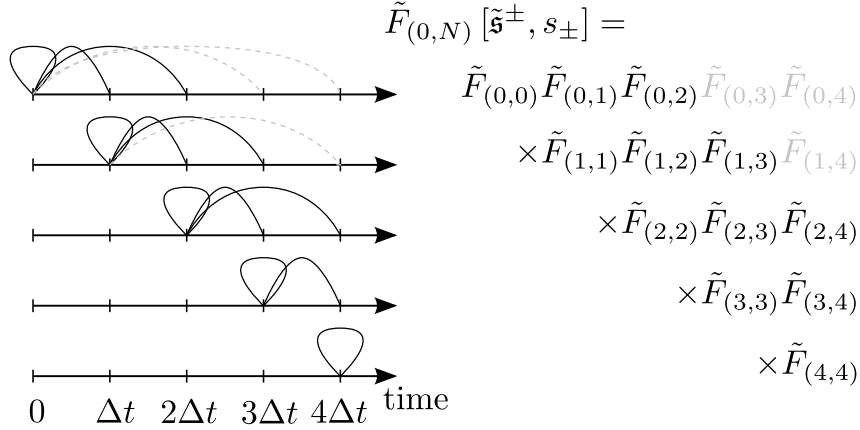
$$\times \tilde{F}_{(3,3)}$$

Figure 4.5.: **Truncation of the point-to-point influences.** Shown for the special case $N = 3$. The grey-colored factor is equal to one, thus, the influence visualized by the grey dashed line is neglected.

In a practical application the value κ is determined by the correlation time of the bath. The truncation in Eq. (4.62) can now be employed to recast the global propagation in Eq. (4.26) into an iterative scheme. For the sake of illustration we consider the special case $\kappa = 2$. The effect of the truncation on the mutual influence of the time steps is shown in Figs. 4.5, 4.6. Here, it becomes visible that the set of interactions in Fig. 4.6 can be built upon the set at the previous time step visualized in Fig. 4.5. The same would hold for the next time step $(N = 5)$ and also for following time steps. The number of additional interactions is constantly $\kappa + 1$ and, thus, independent of N. One can expect that the discrete PI can be formulated such that the number of arithmetic operations is constant for arbitrary N in contrast to an exponential increase, typical for global propagation schemes. To illustrate that it is indeed possible, let us first focus on the special case $N = 3$, $\kappa = 2$. The sum over the set $\mathbb{P}_{N,M}$ in Eq. (4.61) is now unfolded back into the $2N$-fold sum in Eq. (4.18). According to Eq. (4.61) an arbitrary RDM element is calculated via

$$\tilde{\rho}_{\pm}^{\mathrm{S}}(3\Delta t) = \sum_{i_0^+=0}^{M-1}\sum_{i_1^+=0}^{M-1}\sum_{i_2^+=0}^{M-1}\sum_{i_0^-=0}^{M-1}\sum_{i_1^-=0}^{M-1}\sum_{i_2^-=0}^{M-1}$$

$$\left(\prod_{k'=0}^{3}\prod_{k=k'}^{\min\{3,k'+2\}}\tilde{F}_{(k',k)}\left(\tilde{s}_{i_{k'}^{\pm}}, \tilde{s}_{i_k^{\pm}}\right)\right) \cdot \left(\prod_{k=0}^{2}\tilde{S}_{(k,k+1)}\left(\tilde{s}_{i_k^{\pm}}, \tilde{s}_{i_{k+1}^{\pm}}\right)\right) \left\langle \tilde{s}_{i_0^+}\middle|\hat{\rho}_{\mathrm{S}}(0)\middle|\tilde{s}_{i_0^-}\right\rangle . \quad (4.63)$$

All quantities that depend on the indices i_0^+, i_0^- and, thus, $k = k' = 0$ can be grouped together, such that the summation over these indices can be done separately. Note especially that the

$$\tilde{F}_{(0,N)}\left[\tilde{\mathfrak{s}}^{\pm}, s_{\pm}\right] =$$

$$\tilde{F}_{(0,0)}\tilde{F}_{(0,1)}\tilde{F}_{(0,2)}\tilde{F}_{(0,3)}\tilde{F}_{(0,4)}$$

$$\times\tilde{F}_{(1,1)}\tilde{F}_{(1,2)}\tilde{F}_{(1,3)}\tilde{F}_{(1,4)}$$

$$\times\tilde{F}_{(2,2)}\tilde{F}_{(2,3)}\tilde{F}_{(2,4)}$$

$$\times\tilde{F}_{(3,3)}\tilde{F}_{(3,4)}$$

$$\times\tilde{F}_{(4,4)}$$

Figure 4.6.: **Truncation of the point-to-point influences.** Shown for the special case $N = 4$. The grey-colored factors are equal to one, thus, the influences visualized by the grey dashed lines are neglected.

point-to-point influences with $k' = 0$ are pulled out of the double product in Eq. (4.62). After the rearrangement the propagation of the RDM can be expressed as

$$\tilde{\rho}_{\pm}^{\mathrm{S}}(3\Delta t) = \sum_{i_1^+=0}^{M-1}\sum_{i_2^+=0}^{M-1}\sum_{i_1^-=0}^{M-1}\sum_{i_2^-=0}^{M-1}\left(\prod_{k'=1}^{3}\prod_{k=k'}^{\min\{3,\,k'+2\}}\tilde{F}_{(k',k)}\left(\tilde{s}_{i_{k'}^{\pm}},\,\tilde{s}_{i_k^{\pm}}\right)\right)\cdot\left(\prod_{k=1}^{2}\tilde{S}_{(k,k+1)}\left(\tilde{s}_{i_k^{\pm}},\,\tilde{s}_{i_{k+1}^{\pm}}\right)\right)$$

$$\times\sum_{i_0^+=0}^{M-1}\sum_{i_0^-=0}^{M-1}\left(\prod_{k=0}^{\min\{3,2\}}\tilde{F}_{(0,k)}\left(\tilde{s}_{i_0^{\pm}},\,\tilde{s}_{i_k^{\pm}}\right)\right)\cdot\tilde{S}_{(0,1)}\left(\tilde{s}_{i_0^{\pm}},\,\tilde{s}_{i_1^{\pm}}\right)\left\langle\tilde{s}_{i_0^+}\Big|\hat{\rho}_{\mathrm{S}}(0)\Big|\tilde{s}_{i_0^-}\right\rangle . \quad (4.64)$$

Note that $\prod_{k'=1}^{3}\prod_{k=k'}^{\min\{3,\,k'+2\}}$ can be replaced by $\prod_{k'=1}^{3}\prod_{k=k'}^{3}$ and $\prod_{k=0}^{\min\{3,2\}}\tilde{F}_{(0,k)}\left(\tilde{s}_{i_0^{\pm}},\,\tilde{s}_{i_{\Delta k}^{\pm}}\right) = \prod_{k=0}^{2}\tilde{F}_{(0,k)}\left(\tilde{s}_{i_0^{\pm}},\,\tilde{s}_{i_{\Delta k}^{\pm}}\right)$ corresponds to the uppermost row of factors in Figs. 4.5, 4.6. A new quantity that corresponds to the last line in Eq. (4.64) can be defined as

$$r\left(\tilde{s}_{i_1^{\pm}},\tilde{s}_{i_2^{\pm}};\Delta t\right) \equiv \sum_{i_0^+=0}^{M-1}\sum_{i_0^-=0}^{M-1}\left(\prod_{k=0}^{2}\tilde{F}_{(0,k)}\left(\tilde{s}_{i_0^{\pm}},\,\tilde{s}_{i_k^{\pm}}\right)\right)\cdot\tilde{S}_{(0,1)}\left(\tilde{s}_{i_0^{\pm}},\,\tilde{s}_{i_1^{\pm}}\right)\left\langle\tilde{s}_{i_0^+}\Big|\hat{\rho}_{\mathrm{S}}(0)\Big|\tilde{s}_{i_0^-}\right\rangle . \quad (4.65)$$

Note that $r\left(\tilde{s}_{i_1^{\pm}},\tilde{s}_{i_2^{\pm}};\Delta t\right)$ does not depend on the indices $i_0^{\pm}$ since they are summed over. The complete information of the zeroth time step is now implicitly contained in $r\left(s_{i_1^{\pm}},s_{i_2^{\pm}};\Delta t\right)$. If one calculates the elements of the RDM for the next time step, that is for $N = 4$, the following

equation emerges

$$\tilde{\rho}_{\pm}^{\mathrm{S}}(4\Delta t) = \sum_{i_0^+=0}^{M-1}\sum_{i_1^+=0}^{M-1}\sum_{i_2^+=0}^{M-1}\sum_{i_3^+=0}^{M-1}\sum_{i_0^-=0}^{M-1}\sum_{i_1^-=0}^{M-1}\sum_{i_2^-=0}^{M-1}\sum_{i_3^-=0}^{M-1}$$

$$\left(\prod_{k'=0}^{4}\prod_{k=k'}^{\min\{4,\,k'+2\}}\tilde{F}_{(k',k)}\left(\tilde{s}_{i_{k'}^{\pm}},\,\tilde{s}_{i_k^{\pm}}\right)\right)\cdot\left(\prod_{k=0}^{3}\tilde{S}_{(k,k+1)}\left(\tilde{s}_{i_k^{\pm}},\tilde{s}_{i_{k+1}^{\pm}}\right)\right)\left\langle\tilde{s}_{i_0^+}\left|\hat{\rho}_{\mathrm{S}}(0)\right|\tilde{s}_{i_0^-}\right\rangle\;. \quad (4.66)$$

At this point, the definition of $r\left(\tilde{s}_{i_1^{\pm}},\tilde{s}_{i_2^{\pm}};\Delta t\right)$ can be inserted and all quantities depending on indices $i_1^{\pm}$ and, thus, $k = k' = 1$ can be grouped together leading to

$$\tilde{\rho}_{\pm}^{\mathrm{S}}(4\Delta t) = \sum_{i_2^+=0}^{M-1}\sum_{i_3^+=0}^{M-1}\sum_{i_2^-=0}^{M-1}\sum_{i_3^-=0}^{M-1}\left(\prod_{k'=2}^{4}\prod_{k=k'}^{\min\{4,\,k'+2\}}\tilde{F}_{(k',k)}\left(\tilde{s}_{i_{k'}^{\pm}},\,\tilde{s}_{i_k^{\pm}}\right)\right)\cdot\left(\prod_{k=2}^{3}\tilde{S}_{(k,k+1)}\left(\tilde{s}_{i_k^{\pm}},\tilde{s}_{i_{k+1}^{\pm}}\right)\right)$$

$$\times\sum_{i_1^+=0}^{M-1}\sum_{i_1^-=0}^{M-1}\left(\prod_{k=1}^{\min\{4,3\}}\tilde{F}_{(1,k)}\left(\tilde{s}_{i_1^{\pm}},\tilde{s}_{i_k^{\pm}}\right)\right)\cdot\tilde{S}_{(1,2)}\left(\tilde{s}_{i_1^{\pm}},\tilde{s}_{i_2^{\pm}}\right)r\left(\tilde{s}_{i_1^{\pm}},\tilde{s}_{i_2^{\pm}};\Delta t\right)\;. \quad (4.67)$$

Note again that $\prod_{k'=2}^{4}\prod_{k=k'}^{\min\{4,\,k'+2\}} = \prod_{k'=2}^{4}\prod_{k=k'}^{4}$ and $\prod_{k=1}^{\min\{4,3\}}\tilde{F}_{(1,k)}\left(\tilde{s}_{i_1^{\pm}},\,\tilde{s}_{i_k^{\pm}}\right) = \prod_{k=1}^{3}\tilde{F}_{(1,k)}\left(\tilde{s}_{i_1^{\pm}},\,\tilde{s}_{i_k^{\pm}}\right)$ corresponds to the second rows in Figs. 4.5, 4.6. Equation (4.67) is formally identical to Eq. (4.64) if all indices therein are shifted by one and $\left\langle\tilde{s}_{i_0^+}\left|\hat{\rho}_{\mathrm{S}}(0)\right|\tilde{s}_{i_0^-}\right\rangle$ is substituted by $r\left(\tilde{s}_{i_1^{\pm}},\tilde{s}_{i_2^{\pm}};\Delta t\right)$. This similarity between the previous and the current time step is at the heart of an iterative propagation scheme. As the next step, the complete information of the first two time steps reduces to the quantity

$$r(\tilde{s}_{i_2^{\pm}},\tilde{s}_{i_3^{\pm}};2\Delta t) \equiv \sum_{i_1^+=0}^{M-1}\sum_{i_1^-=0}^{M-1}\left(\prod_{k=1}^{3}\tilde{F}_{(1,k)}\left(\tilde{s}_{i_1^{\pm}},\tilde{s}_{i_k^{\pm}}\right)\right)\cdot\tilde{S}_{(1,2)}\left(\tilde{s}_{i_1^{\pm}},\tilde{s}_{i_2^{\pm}}\right)r\left(\tilde{s}_{i_1^{\pm}},\tilde{s}_{i_2^{\pm}};\Delta t\right) \quad (4.68)$$

and so on. It is straightforward to generalize the presented iterative procedure to arbitrary κ and $N > \kappa$. To calculate the RDM for the N-th step, one has to perform the following steps.

41

4. Numerical treatment of path integrals

First, the quantity r has to be propagated step by step via

$$
r\left(\tilde{s}_{i_{N-\kappa}^\pm}, \ldots, \tilde{s}_{i_{N-1}^\pm}; (N-\kappa)\Delta t\right) = \sum_{i_{N-\kappa-1}^+=0}^{M-1} \sum_{i_{N-\kappa-1}^-=0}^{M-1} \left(\prod_{k=N-\kappa-1}^{N-1} \tilde{F}_{(N-\kappa-1,k)}\left(\tilde{s}_{i_{N-\kappa-1}^\pm}, \tilde{s}_{i_k^\pm}\right) \right)
$$
$$
\times \tilde{S}_{(N-\kappa-1,N-\kappa)}\left(\tilde{s}_{i_{N-\kappa-1}^\pm}, \tilde{s}_{i_{N-\kappa}^\pm}\right) r\left(\tilde{s}_{i_{N-\kappa-1}^\pm}, \ldots \tilde{s}_{i_{N-2}^\pm}; (N-\kappa-1)\Delta t\right) \ . \quad (4.69)
$$

The initial condition is given by

$$
r\left(\tilde{s}_{i_0^\pm}, \ldots \tilde{s}_{i_{\kappa-1}^\pm}; 0\right) \equiv \left\langle \tilde{s}_{i_0^+} \left| \hat{\rho}_\mathrm{S}(0) \right| \tilde{s}_{i_0^-} \right\rangle \ . \quad (4.70)
$$

Second, the additional summation has to be performed

$$
\tilde{\rho}_\pm^\mathrm{S}(N\Delta t) = \sum_{i_{N-\kappa}^+=0}^{M-1} \cdots \sum_{i_{N-1}^+=0}^{M-1} \sum_{i_{N-\kappa}^-=0}^{M-1} \cdots \sum_{i_{N-1}^-=0}^{M-1} \left(\prod_{k'=N-\kappa}^{N} \prod_{k=k'}^{N} \tilde{F}_{(k',k)}\left(\tilde{s}_{i_{k'}^\pm}, \tilde{s}_{i_k^\pm}\right) \right)
$$
$$
\times \left(\prod_{k=N-\kappa}^{N-1} \tilde{S}_{(k,k+1)}\left(\tilde{s}_{i_k^\pm}, \tilde{s}_{i_{k+1}^\pm}\right) \right) r\left(\tilde{s}_{i_{N-\kappa}^\pm}, \ldots, \tilde{s}_{i_{N-1}^\pm}; (N-\kappa)\Delta t\right) \ . \quad (4.71)
$$

Equations (4.70-4.71) represent an iterative scheme for the propagation of the RDM, since the quantity $r\left(\tilde{s}_{i_{N-\kappa}^\pm}, \ldots, \tilde{s}_{i_{N-1}^\pm}; (N-\kappa)\Delta t\right)$ is exclusively constructed out of its counterpart at the previous time step. Note that for $0 < N \le \kappa$, the RDM is propagated globally with details given in App. C. Importantly, there is no possibility to propagate the RDM iteratively within the correlation time of the bath, since the influence functional can not be truncated in this case.

In analogy to Eq. (4.26), the iterative scheme for any $N > \kappa$ is reformulated in terms of FBC *segments* $\tilde{\mathfrak{s}}^\pm = \begin{pmatrix} \tilde{\mathfrak{s}}_0^+ & \cdots & \tilde{\mathfrak{s}}_{\kappa-1}^+ \\ \tilde{\mathfrak{s}}_0^- & \cdots & \tilde{\mathfrak{s}}_{\kappa-1}^- \end{pmatrix}$ with the end points $\tilde{s}_\pm$ employing the following substitutions.

First, the discrete influence functional can be found by index shifting and grouping the

coordinates $\tilde{s}_{i_k^\pm}$ to path segments $\tilde{\mathfrak{s}}^\pm$

$$\prod_{k'=N-\kappa}^{N} \prod_{k=k'}^{\min\{N,\,k'+\kappa\}} \tilde{F}_{(k',k)}\left(\tilde{s}_{i_{k'}^\pm},\,\tilde{s}_{i_k^\pm}\right) \xrightarrow{k'\to k'+N-\kappa} \prod_{k'=0}^{\kappa} \prod_{k=k'}^{\kappa} \tilde{F}_{(k'+N-\kappa,\,k+N-\kappa)}\left(\tilde{\mathfrak{s}}_{k'}^\pm,\,\tilde{\mathfrak{s}}_k^\pm\right) = \tilde{F}_{(N-\kappa,N)}\left[\tilde{\mathfrak{s}}^\pm,\,\tilde{s}_\pm\right] \quad,$$

(4.72)

where, according to Eq. (4.59)

$$\tilde{F}_{(k'+N-\kappa,\,k+N-\kappa)}\left(\tilde{\mathfrak{s}}_{k'}^\pm,\,\tilde{\mathfrak{s}}_k^\pm\right) = \exp\left\{-\frac{1}{\hbar}\left(\eta_{k'+N-\kappa,k+N-\kappa}\,\tilde{\mathfrak{s}}_{k'}^+ - \eta_{k'+N-\kappa,k+N-\kappa}^*\,\tilde{\mathfrak{s}}_{k'}^-\right)\cdot\left(\tilde{\mathfrak{s}}_k^+ - \tilde{\mathfrak{s}}_k^-\right)\right\} \quad.$$

(4.73)

Note that the indices k, k' are now in the range $0, \ldots, \kappa$.

Second, the discrete bare system part is obtained likewise

$$\prod_{k=N-\kappa}^{N-1} \tilde{S}_{(k,k+1)}\left(\tilde{s}_{i_k^\pm},\,\tilde{s}_{i_{k+1}^\pm}\right) \xrightarrow{k'\to k'+N-\kappa} \prod_{k=0}^{\kappa-1} \tilde{S}_{(k,k+1)}\left(\tilde{\mathfrak{s}}_k^\pm,\,\tilde{\mathfrak{s}}_{k+1}^\pm\right) = \tilde{S}_{(N-\kappa,N)}\left[\tilde{\mathfrak{s}}^\pm,\,\tilde{s}_\pm\right] \quad,$$

(4.74)

where, according to Eq. (4.30)

$$\tilde{S}_{(k,k+1)}\left(\tilde{\mathfrak{s}}_k^\pm,\,\tilde{\mathfrak{s}}_{k+1}^\pm\right) = \underline{\langle\tilde{\mathfrak{s}}_{k+1}^+|}\,\mathrm{e}^{-i\hat{H}_\mathrm{S}\Delta t/\hbar}\,\underline{|\tilde{\mathfrak{s}}_k^+\rangle}\underline{\langle\tilde{\mathfrak{s}}_k^-|}\,\mathrm{e}^{i\hat{H}_\mathrm{S}\Delta t/\hbar}\,\underline{|\tilde{\mathfrak{s}}_{k+1}^-\rangle} \quad.$$

(4.75)

Note that the bare system part is independent of the total propagation time and, thus, $\tilde{S}_{(N-\kappa,N)}\left[\tilde{\mathfrak{s}}^\pm,\,\tilde{s}_\pm\right] = \tilde{S}_{(0,\kappa)}\left[\tilde{\mathfrak{s}}^\pm,\,\tilde{s}_\pm\right]$, whereas the point-to-point influences in Eq. (4.73) depend explicitly on N due to the memory coefficients. The virtual character of the memory coefficient's time-dependence is shown in Sec. 4.1.5. In Eqs. (4.72-4.75) the end points enter as $\tilde{\mathfrak{s}}_\kappa^\pm \equiv \tilde{s}_\pm$.

Third, the quantity $r\left(\tilde{s}_{i_{N-\kappa}^\pm},\ldots,\tilde{s}_{i_{N-1}^\pm};(N-\kappa)\Delta t\right)$ is replaced by the *time-dependent* discrete multi-time reduced density functional $\tilde{R}\left[\tilde{\mathfrak{s}}^\pm;(N-\kappa)\Delta t\right]$ with $\tilde{s}_{i_{N-\kappa}^\pm} \to \tilde{\mathfrak{s}}_0^\pm,\ldots,\tilde{s}_{i_{N-1}^\pm} \to \tilde{\mathfrak{s}}_{\kappa-1}^\pm$. Here each value $\tilde{R}\left[\tilde{\mathfrak{s}}^\pm;(N-\kappa)\Delta t\right]$ for a particular $\tilde{\mathfrak{s}}^\pm$ can be considered as an element of the *time-dependent* multi-time reduced density vector $\tilde{\mathbf{R}}\left((N-\kappa)\Delta t\right) \in \mathbb{C}^{L_{\kappa,M}}$.

- Fourth, the quantity $r\left(\tilde{s}_{i_{N-\kappa-1}^\pm},\ldots\tilde{s}_{i_{N-2}^\pm};(N-\kappa-1)\Delta t\right)$ at the previous time step is substituted by $\tilde{R}\left[\tilde{\mathfrak{r}}^\pm;(N-\kappa-1)\Delta t\right]$, where $\tilde{s}_{i_{N-\kappa-1}^\pm} \to \tilde{\mathfrak{r}}_0^\pm,\ldots,\tilde{s}_{i_{N-2}^\pm} \to \tilde{\mathfrak{r}}_{\kappa-1}^\pm$, that is $\tilde{\mathfrak{s}}^\pm$ shifted by one time step. Note that the third and the fourth substitution imply

$$\tilde{\mathfrak{r}}_1^\pm = \tilde{\mathfrak{s}}_0^\pm,\ldots,\tilde{\mathfrak{r}}_{\kappa-1}^\pm = \tilde{\mathfrak{s}}_{\kappa-2}^\pm \quad.$$

(4.76)

Fifth, the weighting factor in Eq. (4.69) defines the *lambda propagator*

$$
\left(\prod_{k=N-\kappa-1}^{N-1} \tilde{F}_{(N-\kappa-1,k)}\left(\tilde{s}_{i_{N-\kappa-1}^{\pm}}, \tilde{s}_{i_k^{\pm}} \right) \right) \tilde{S}_{(N-\kappa-1,N-\kappa)}\left(\tilde{s}_{i_{N-\kappa-1}^{\pm}}, \tilde{s}_{i_{N-\kappa}^{\pm}} \right) \xrightarrow{k \to k+(N-\kappa-1)}
$$

$$
\tilde{S}_{(0,1)}\left(\tilde{\mathfrak{r}}_0^{\pm}, \tilde{\mathfrak{r}}_1^{\pm} \right) \left(\prod_{k=0}^{\kappa-1} \tilde{F}_{(N-\kappa-1,k+N-\kappa-1)}\left(\tilde{\mathfrak{r}}_0^{\pm}, \tilde{\mathfrak{r}}_k^{\pm} \right) \right) \tilde{F}_{(N-\kappa-1,N-1)}\left(\tilde{\mathfrak{r}}_0^{\pm}, \tilde{\mathfrak{s}}_{\kappa-1}^{\pm} \right)
$$

$$
\equiv \Lambda_{(N-\kappa-1,N-1)}\left[\tilde{\mathfrak{r}}^{\pm}, \tilde{\mathfrak{s}}^{\pm} \right] \quad . \tag{4.77}
$$

With the given substitutions at hand, the iterative scheme can be formulated as follows. If one wants to calculate the RDM element $\tilde{\rho}_{\mathrm{s},\pm}(N\Delta t)$, where $N > \kappa$, one has to propagate each element of $\tilde{\mathbf{R}}(k\Delta t)$ time step by time step up to $k = N - \kappa$ via

$$
\tilde{R}\left[\tilde{\mathfrak{s}}^{\pm}; (N-\kappa)\Delta t \right] = \sum_{\tilde{\mathfrak{r}}^{\pm} \in \mathbb{P}_{\kappa,M}\left[\tilde{\mathfrak{s}}^{\pm} \right]} \Lambda_{(N-\kappa-1,N-1)}\left[\tilde{\mathfrak{r}}^{\pm}, \tilde{\mathfrak{s}}^{\pm} \right] \cdot \tilde{R}\left[\tilde{\mathfrak{r}}^{\pm}; (N-\kappa-1)\Delta t \right] \quad . \tag{4.78}
$$

with the initial condition

$$
\tilde{R}\left[\tilde{\mathfrak{s}}^{\pm}; 0 \right] \equiv \left\langle \tilde{\mathfrak{s}}_0^{+} \middle| \hat{\rho}_{\mathrm{s}}(0) \middle| \tilde{\mathfrak{s}}_0^{-} \right\rangle \quad . \tag{4.79}
$$

The set $\mathbb{P}_{\kappa,M}\left[\tilde{\mathfrak{s}}^{\pm} \right]$ is a subset of $\mathbb{P}_{\kappa,M} = (\mathbb{S}_M)^{2\kappa}$ and it contains the FBCs $\tilde{\mathfrak{r}}^{\pm}$ that share all points except the first with $\tilde{\mathfrak{s}}^{\pm}$ according to Eq. (4.76)

$$
\mathbb{P}_{\kappa,M}\left[\tilde{\mathfrak{s}}^{\pm} \right] \equiv \left\{ \tilde{\mathfrak{r}}^{\pm} \in \mathbb{P}_{\kappa,M} \;\middle|\; \tilde{\mathfrak{r}}_k^{\pm} = \tilde{\mathfrak{s}}_{k-1}^{\pm}, \; k = 1, \ldots, \kappa-1 \right\}, \quad \tilde{\mathfrak{s}}^{\pm} \in \mathbb{P}_{\kappa,M} \quad . \tag{4.80}
$$

Within the propagation in Eq. (4.7) each element of $\tilde{\mathbf{R}}(k\Delta t)$ is the complex-weighted superposition of certain elements of the previous $\tilde{\mathbf{R}}\left((k-1)\Delta t \right)$, where the weight is given by the lambda propagator. The elements $\tilde{R}\left[\tilde{\mathfrak{r}}^{\pm}; (k-1)\Delta t \right]$, which contribute to a certain $\tilde{R}\left[\tilde{\mathfrak{s}}^{\pm}; k\Delta t \right]$ correspond to the FBC segments $\tilde{\mathfrak{r}}^{\pm} \in \mathbb{P}_{\kappa,M}\left[\tilde{\mathfrak{s}}^{\pm} \right]$. This can be interpreted as the set $\mathbb{P}_{\kappa,M}\left[\tilde{\mathfrak{s}}^{\pm} \right]$ contains all possible histories $\tilde{\mathfrak{r}}^{\pm}$ of the FBC segment $\tilde{\mathfrak{s}}^{\pm}$ within the correlation time, see Fig. 4.7. Since $\tilde{\mathbf{R}}(k\Delta t)$ can be determined exclusively with the knowledge of $\tilde{\mathbf{R}}\left((k-1)\Delta t \right)$ at the previous time step, the propagation of the multi-time reduced density vector is *local in time* or in other words, its time evolution is *effectively Markovian*. Note that the specific form of Eq. (4.78) could not have been written down, if the end points $\tilde{s}_{\pm}$ would be included in the definition of $\tilde{\mathfrak{s}}^{\pm}$. The final step to calculate $\tilde{\rho}_{\mathrm{s},\pm}(N\Delta t)$ is the summation over all FBCs that span the correlation
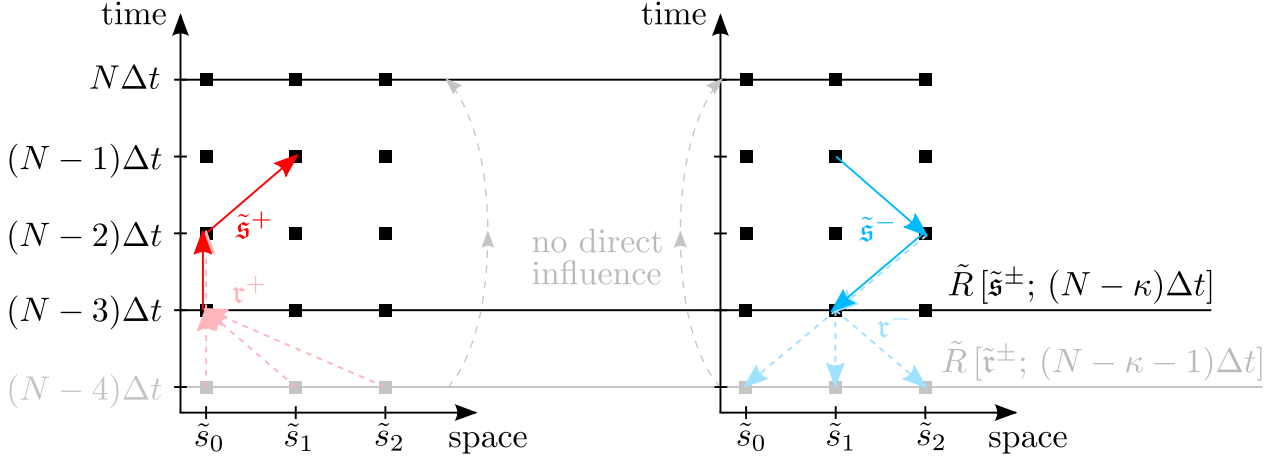
Figure 4.7.: **Propagation of the discrete multi-time reduced density vector.** Shown for the special $M = 3$, $\kappa = 3$. Forward/Backward paths are shown in left/right panel, respectively.

time together with the end points $\tilde{s}_{\pm}$

$$\tilde{\rho}_{\pm}^{\mathrm{s}}(N\Delta t) = \sum_{\tilde{\mathfrak{s}}^{\pm} \in \mathbb{P}_{\kappa,M}} \tilde{F}_{(N-\kappa,N)}\left[\tilde{\mathfrak{s}}^{\pm}, \tilde{s}_{\pm}\right] \tilde{R}\left[\tilde{\mathfrak{s}}^{\pm}; (N-\kappa)\Delta t\right] \tilde{S}_{(N-\kappa,N)}\left[\tilde{\mathfrak{s}}^{\pm}, \tilde{s}_{\pm}\right] \quad . \tag{4.81}$$

The vector $\tilde{\mathbf{R}}\big((N-\kappa)\Delta t\big)$ serves as a starting point for this summation, see Fig. 4.8. It is worth mentioning that in contrast to Eq. (4.26), the set $\mathbb{P}_{\kappa,M}$ in Eq. (4.81) contains $L_{\kappa,M} = M^{2\kappa}$ elements *independently* of N. Each element of $\mathbb{P}_{\kappa,M}$ is an FBC segment containing a constant number of coordinates. However, the fixed initial condition $\tilde{R}\left[\tilde{\mathfrak{s}}^{\pm}\right]$ in Eq. (4.26) is now replaced by $\tilde{R}\left[\tilde{\mathfrak{s}}^{\pm}; (N-\kappa)\Delta t\right]$, which depends explicitly on the global time step N, thus, the key quantity of the iterative scheme is the discrete multi-time reduced density functional $\tilde{R}\left[\tilde{\mathfrak{s}}^{\pm}; (N-\kappa)\Delta t\right]$.

The task of this subsection is fulfilled and the RDM propagation has been recast into an iterative scheme. Note at this point that the RDM calculated via Eq. (4.81) has the limit

$$\lim_{\Delta t \to 0,\, M, \kappa \to \infty} \tilde{\rho}_{\pm}^{\mathrm{s}}(N\Delta t) = \rho_{\mathrm{s}}(\tilde{s}_{\pm}; t) \quad , \tag{4.82}$$

which permits numerical convergence. The number of FBCs entering the propagation is constant (though usually very large) within the whole propagation. That is the gross improvement against the exponentially growing number of FBCs within the global scheme. The following
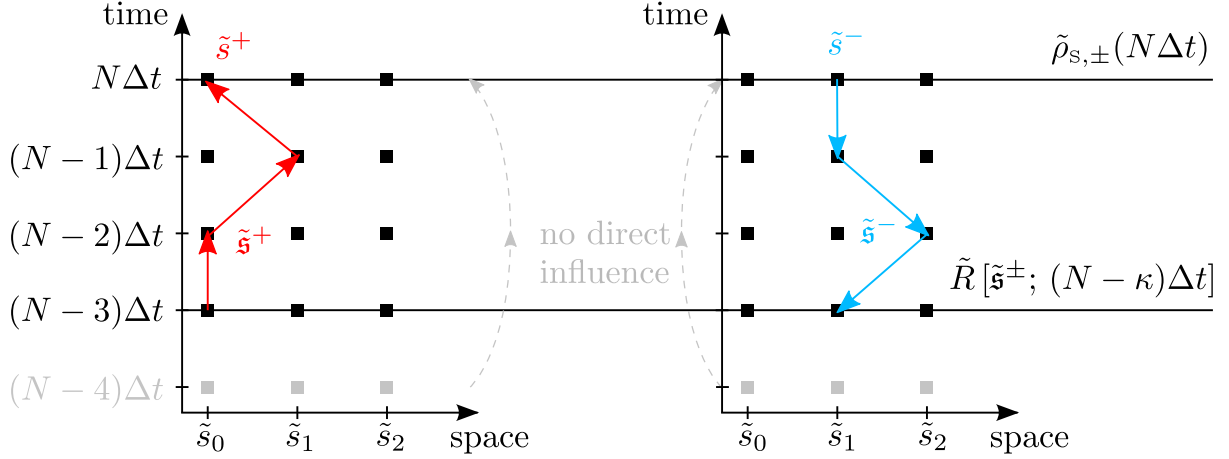
Figure 4.8.: **Iterative propagation of the RDM.** Shown for the special $M = 3$, $\kappa = 3$. Forward/Backward paths are shown in left/right panel, correspondingly.

section will show that this number can be further reduced if unimportant paths are filtered out.

4.1.5. Virtual time-dependence of the memory coefficients

To recapitulate, the memory coefficients $\eta_{k'k}$ depend on the absolute value of k if one of k and k' is equal to zero or N. It is shown in App. B.1 that coefficients like $\eta_{k'+N-\kappa,k+N-\kappa}$ in Eq. (4.72) with $k', k = 0, \ldots \kappa$ do not depend on N if $N > \kappa$, hence, they do not change during the iteration. These coefficients are called $\eta_{k'k}^{\text{mid-fin}}$ in the following. Accordingly, the influence functional for any $N > \kappa$ reads

$$\tilde{F}_{(N-\kappa,N)}\left[\tilde{\mathfrak{s}}^{\pm}, \tilde{s}_{\pm}\right] = \tilde{F}_{(0,\kappa)}^{\text{mid-fin}}\left[\tilde{\mathfrak{s}}^{\pm}, \tilde{s}_{\pm}\right] \equiv \prod_{k=0}^{\kappa} \prod_{k=k'}^{\kappa} \tilde{F}_{(k',k)}^{\text{mid-fin}}\left(\tilde{\mathfrak{s}}_{k'}^{\pm}, \tilde{\mathfrak{s}}_{k}^{\pm}\right) \quad, \tag{4.83}$$

with

$$\tilde{F}_{(k',k)}^{\text{mid-fin}}\left(\tilde{\mathfrak{s}}_{k'}^{\pm}, \tilde{\mathfrak{s}}_{k}^{\pm}\right) \equiv \exp\left\{-\frac{1}{\hbar}\left(\eta_{k'k}^{\text{mid-fin}}\tilde{\mathfrak{s}}_{k'}^{+} - \left(\eta_{k'k}^{\text{mid-fin}}\right)^{*}\tilde{\mathfrak{s}}_{k'}^{-}\right) \cdot \left(\tilde{\mathfrak{s}}_{k}^{+} - \tilde{\mathfrak{s}}_{k}^{-}\right)\right\} \quad. \tag{4.84}$$

For the case $N \leq \kappa$ the coefficients, referred to as $\eta_{k'k}^{\text{init-fin}}$, depend explicitly on N, see App. B.1 for the expressions. The corresponding $\tilde{F}_{(0,N)}^{\text{init-fin}}\left[\tilde{\mathfrak{s}}^{\pm}, \tilde{s}_{\pm}\right]$ and $\tilde{F}_{(k',k)}^{\text{init-fin}}\left(\tilde{\mathfrak{s}}_{k'}^{\pm}, \tilde{\mathfrak{s}}_{k}^{\pm}\right)$ are given by Eqs. (4.83,4.84) if $\eta_{k'k}^{\text{mid-fin}}$ is replaced by $\eta_{k'k}^{\text{init-fin}}$. For the lambda propagator in Eq. (4.77) the coefficients $\eta_{k'k}$ in the point-to-point influence depend only on $\Delta k = k - k'$ if $N > \kappa + 1$, hence, they are also fixed within the propagation, see App. B.1. Consequently, the lambda propagator itself does

not depend on the absolute propagation time. The memory coefficients for $N > \kappa + 1$ are labeled by $\eta_{k'k}^{\mathrm{mid}}$ and

$$\Lambda_{(N-\kappa-1,N-1)}\left[\tilde{\mathfrak{r}}^{\pm},\,\tilde{\mathfrak{s}}^{\pm}\right] = \Lambda_{(0,\kappa)}^{\mathrm{mid}}\left[\tilde{\mathfrak{r}}^{\pm},\,\tilde{\mathfrak{s}}^{\pm}\right] \equiv \tilde{S}_{(0,1)}\left(\tilde{\mathfrak{r}}_0^{\pm},\tilde{\mathfrak{r}}_1^{\pm}\right) \prod_{k=0}^{\kappa-1} \tilde{F}_{(0,k)}^{\mathrm{mid}}\left(\tilde{\mathfrak{r}}_0^{\pm},\tilde{\mathfrak{r}}_k^{\pm}\right) \cdot \tilde{F}_{(0,\kappa)}^{\mathrm{mid}}\left(\tilde{\mathfrak{r}}_0^{\pm},\tilde{\mathfrak{s}}_{\kappa-1}^{\pm}\right) \quad, \tag{4.85}$$

with

$$\tilde{F}_{(0,k)}^{\mathrm{mid}}\left(\tilde{\mathfrak{s}}_0^{\pm},\,\tilde{\mathfrak{s}}_k^{\pm}\right) \equiv \exp\left\{-\frac{1}{\hbar}\left(\eta_{0k}^{\mathrm{mid}}\tilde{\mathfrak{s}}_0^+ - \left(\eta_{0k}^{\mathrm{mid}}\right)^*\tilde{\mathfrak{s}}_0^-\right)\cdot\left(\tilde{\mathfrak{s}}_k^+ - \tilde{\mathfrak{s}}_k^-\right)\right\} \quad. \tag{4.86}$$

For $N = \kappa + 1$ the coefficients, labeled $\eta_{k'k}^{\mathrm{init\text{-}mid}}$, are given in App. B.1. The corresponding $\Lambda_{(0,\kappa)}^{\mathrm{init\text{-}mid}}\left[\tilde{\mathfrak{r}}^{\pm},\,\tilde{\mathfrak{s}}^{\pm}\right]$ and point-to-point influence $\tilde{F}_{(0,k)}^{\mathrm{init\text{-}mid}}\left(\tilde{\mathfrak{s}}_0^{\pm},\,\tilde{\mathfrak{s}}_k^{\pm}\right)$ are given by Eqs. (4.85,4.86) if η_{0k}^{mid} is replaced by $\eta_{0k}^{\mathrm{init\text{-}mid}}$. Due to the behavior of the coefficients it is sufficient to recalculate the point-to-point influences only for the first $\kappa + 1$ time steps. For all following time steps the propagators are fixed.

4.1.6. Path filtering

As it was derived in the previous section, the RDM can be propagated for arbitrary long times by summing over a constant set of $M^{2\kappa}$ path segments. This is already much more feasible than the number M^{2N} growing exponentially with the propagation time in the global scheme. Still, the number $M^{2\kappa}$ depends exponentially on the correlation time of the bath, which can be large for particular SBCs as discussed in Sec. 5.2. In this section it will be shown that it is not necessary to sum over all possible FBCs, thus, the number of arithmetic operations can be significantly reduced further.

According to Eq. (4.81) the absolute value of an RDM element with $N > \kappa$ can be estimated via the triangular inequality as

$$\left|\tilde{\rho}_{\pm}^{\mathrm{S}}(N\Delta t)\right| \leq \sum_{\tilde{\mathfrak{s}}^{\pm}\in\mathbb{P}_{\kappa,M}} \left|\tilde{F}_{(0,\kappa)}^{\mathrm{mid\text{-}fin}}\left[\tilde{\mathfrak{s}}^{\pm},\tilde{s}_{\pm}\right]\tilde{S}_{(0,\kappa)}\left[\tilde{\mathfrak{s}}^{\pm},\tilde{s}_{\pm}\right]\tilde{R}\left[\tilde{\mathfrak{s}}^{\pm};(N-\kappa)\Delta t\right]\right| \tag{4.87}$$

$$\leq |\mathcal{C}| \sum_{\tilde{\mathfrak{s}}^{\pm}\in\mathbb{P}_{\kappa,M}} \left|\left(\prod_{k'=0}^{\kappa-1}\prod_{k=k'}^{\kappa-1}\tilde{F}_{(k',k)}^{\mathrm{mid\text{-}fin}}\left(\tilde{\mathfrak{s}}_{k'}^{\pm},\,\tilde{\mathfrak{s}}_k^{\pm}\right)\right)\prod_{k=0}^{\kappa-2}\tilde{S}_{(k,k+1)}\left(\tilde{\mathfrak{s}}_k^{\pm},\,\tilde{\mathfrak{s}}_{k+1}^{\pm}\right)\right| \quad, \tag{4.88}$$

where

$$\mathcal{C} \equiv \max_{\tilde{\mathfrak{s}}^{\pm} \in \mathbb{P}_{\kappa,M}} \left\{ \tilde{R} \left[\tilde{\mathfrak{s}}^{\pm}; (N-\kappa)\Delta t \right] \left(\prod_{k'=0}^{\kappa} \tilde{F}_{(k',\kappa)}^{\text{mid-fin}} \left(\tilde{\mathfrak{s}}_{k'}^{\pm}, \tilde{s}_{\pm} \right) \right) \tilde{S}_{(\kappa-1,\kappa)} \left(\tilde{\mathfrak{s}}_{\kappa-1}^{\pm}, \tilde{s}_{\pm} \right) \right\} \tag{4.89}$$

Note that $\mathcal{C}$ is defined such that the sum in Eq. (4.88) is neither time-dependent nor depends on the end points $\tilde{s}_{\pm}$, thus all terms in the sum are equal for any N and any RDM element. The summand for particular $\tilde{\mathfrak{s}}^{\pm}$ is now defined as its *path weight*

$$w_{\kappa-1} \left[\tilde{\mathfrak{s}}^{\pm} \right] \equiv \left| \left(\prod_{k'=0}^{\kappa-1} \prod_{k=k'}^{\kappa-1} \tilde{F}_{(k',k)}^{mid\text{-}fin} \left(\tilde{\mathfrak{s}}_{k'}^{\pm}, \tilde{\mathfrak{s}}_{k}^{\pm} \right) \right) \prod_{k=0}^{\kappa-2} \tilde{S}_{(k,k+1)} \left(\tilde{\mathfrak{s}}_{k}^{\pm}, \tilde{\mathfrak{s}}_{k+1}^{\pm} \right) \right| . \tag{4.90}$$

Due to the complex exponential character of the point-to-point influences and the bare system point-to-point propagators, the value $w_{\kappa-1} \left[\tilde{\mathfrak{s}}^{\pm} \right]$ for some FBCs might approach unity. Therefore, one can assume that paths, for which $w_{\kappa-1} \left[\tilde{\mathfrak{s}}^{\pm} \right] \ll 1$, do not contribute significantly to discrete PI. It in turn means that one can replace the set $\mathbb{P}_{\kappa,M}$ in Eq. (4.81) by the *filtered* subset

$$\mathbb{P}_{\kappa,M}^{\theta} \equiv \left\{ \tilde{\mathfrak{s}}^{\pm} \in \mathbb{P}_{\kappa,M} \mid w_{\kappa-1} \left[\tilde{\mathfrak{s}}^{\pm} \right] > \theta \right\} \tag{4.91}$$

without changing the propagation of the RDM crucially for a given *threshold* θ, where the actual value of θ serves as a convergence parameter. The subset $\mathbb{P}_{\kappa,M} \left[\tilde{\mathfrak{s}}^{\pm} \right]$ appearing in the propagation of the multi-time reduced density vector is filtered accordingly

$$\mathbb{P}_{\kappa,M}^{\theta} \left[\tilde{\mathfrak{s}}^{\pm} \right] \equiv \left\{ \tilde{\mathfrak{r}}^{\pm} \in \mathbb{P}_{\kappa,M}^{\theta} \mid \tilde{\mathfrak{r}}_{k}^{\pm} = \tilde{\mathfrak{s}}_{k-1}^{\pm}, \, k = 1, \ldots, \kappa-1 \right\} \, , \quad \tilde{\mathfrak{s}}^{\pm} \in \mathbb{P}_{\kappa,M}^{\theta}. \tag{4.92}$$

Depending on the system and its interaction with the bath, a noticeable part of $\mathbb{P}_{\kappa,M}$ could be filtered out, thus, the number of paths can be reduced significantly with respect to $M^{2\kappa}$. The actual impact of the system characteristics on the quality of the filtering is discussed in Sec. 5.2.

Note that the RDM calculated iteratively as a sum over the filtered set of FBCs has still the exact limit with $\theta \to 0$

$$\lim_{\Delta t, \theta \to 0, M, \kappa \to \infty} \tilde{\rho}_{\pm}^{\text{s}}(N\Delta t) = \rho_{\text{s}}(\tilde{s}_{\pm}; t) \, . \tag{4.93}$$

Recapitulating the similar limits presented in the previous subsections, Eqs. (4.20,4.82,4.93), the number of convergence parameters has subsequently increased to four at this point.

4.2. Propagation of the equilibrium TCF

4.2.1. Derivation of the discrete PI

In this subsection the discrete counterpart for the equilibrium TCF in Eq. (3.32) is derived. As it was explained in the Introduction, the direct discretization is hindered by numerical obstacles. Analogously to the propagation of the RDM, the starting point of this derivation is the general expression

$$C_{\Gamma\Omega}(t) \equiv \frac{1}{Z(\beta)} \mathrm{Tr} \left[\mathrm{e}^{-\beta\hat{H}/2} \hat{\Gamma} \, \hat{U}^\dagger(t) \hat{\Omega} \, \hat{U}(t) \mathrm{e}^{-\beta\hat{H}/2} \right] \quad . \tag{4.94}$$

First, the imaginary time $-i\beta\hbar/2$ is split into P slices with the length $\Delta\beta \equiv \beta\hbar/(2P)$ leading to the equality

$$\exp\left\{-\beta\hat{H}/2\right\} = \left(\exp\left\{-\hat{H}\Delta\beta/\hbar\right\}\right)^P \quad . \tag{4.95}$$

Remember that β is the inverse temperature. The real time t is again divided into N time slices with the length Δt as in Eq. (4.2). With the given definitions Eq. (4.94) takes the form

$$C_{\Gamma\Omega}(N\Delta t) = \frac{1}{Z(\beta)}$$
$$\times \mathrm{Tr} \left[\underbrace{\mathrm{e}^{-\hat{H}\Delta\beta/\hbar} \cdots \mathrm{e}^{-\hat{H}\Delta\beta/\hbar}}_{P \text{ times}} \hat{\Gamma} \underbrace{\mathrm{e}^{i\hat{H}\Delta t/\hbar} \cdots \mathrm{e}^{i\hat{H}\Delta t/\hbar}}_{N \text{ times}} \hat{\Omega} \underbrace{\mathrm{e}^{-i\hat{H}\Delta t/\hbar} \cdots \mathrm{e}^{-i\hat{H}\Delta t/\hbar}}_{N \text{ times}} \underbrace{\mathrm{e}^{-\hat{H}\Delta\beta/\hbar} \cdots \mathrm{e}^{-\hat{H}\Delta\beta/\hbar}}_{P \text{ times}} \right] \quad . \tag{4.96}$$

In the following the trace in the system's Hilbert space is taken in the coordinate basis, whereas the trace in the bath's Hilbert space is left arbitrary, i.e.

$$\mathrm{Tr}\left[\,\cdot\,\right] = \mathrm{Tr}_{\mathrm{B}} \left[\int_{-\infty}^{\infty} \mathrm{d}s_0 \, \langle s_0| \, \cdot \, |s_0\rangle \right] \quad . \tag{4.97}$$

As the next step one inserts a set of $2(N + P)$ spatial closures in Eq. (4.96), where $N > 0$. The special case $N = 0$ corresponds to a pure imaginary time propagation and is considered in App. D. The first P integrals go over the variables s_k^+, $k = 1, \ldots, P$ and are inserted in between the imaginary time propagators on the right side within the trace. The next N integrals over the variables s_k^+, $k = P + 1, \ldots, P + N$ are placed in between the real time propagators on the right of the operator $\hat{\Omega}$. The rest is inserted in between the propagators on the left of

$\hat{\Omega}$. The integration variables are labeled by s_k^-, $k = 1, \ldots, P$ and s_k^-, $k = P+1, \ldots, P+N$, respectively. The TCF can then be rewritten as

$$
C_{\Gamma\Omega}(N\Delta t) = \frac{1}{Z(\beta)} \text{Tr}_{\text{B}} \left[\int\limits_{-\infty}^{\infty} ds_0 \int\limits_{-\infty}^{\infty} ds_1^+ \cdots \int\limits_{-\infty}^{\infty} ds_P^+ \int\limits_{-\infty}^{\infty} ds_{P+1}^+ \cdots \int\limits_{-\infty}^{\infty} ds_{P+N}^+ \right.
$$

$$
\times \int\limits_{-\infty}^{\infty} ds_1^- \cdots \int\limits_{-\infty}^{\infty} ds_P^- \int\limits_{-\infty}^{\infty} ds_{P+1}^- \cdots \int\limits_{-\infty}^{\infty} ds_{P+N}^-
$$

$$
\times \left\langle s_0 \middle| e^{-\hat{H}\Delta\beta/\hbar} \middle| s_1^- \right\rangle \left\langle s_1^- \middle| e^{-\hat{H}\Delta\beta/\hbar} \middle| s_2^- \right\rangle \cdots \left\langle s_{P-1}^- \middle| e^{-\hat{H}\Delta\beta/\hbar} \middle| s_P^- \right\rangle
$$

$$
\times \left\langle s_P^- \middle| \hat{\Gamma} e^{i\hat{H}\Delta t/\hbar} \middle| s_{P+1}^- \right\rangle \left\langle s_{P+1}^- \middle| e^{i\hat{H}\Delta t/\hbar} \middle| s_{P+2}^- \right\rangle \cdots \left\langle s_{P+N-1}^- \middle| e^{i\hat{H}\Delta t/\hbar} \middle| s_{P+N-1}^- \right\rangle \left\langle s_{P+N}^- \middle| s_{P+N}^+ \right\rangle
$$

$$
\times \left\langle s_{P+N}^+ \middle| \hat{\Omega} e^{-i\hat{H}\Delta t/\hbar} \middle| s_{P+N-1}^+ \right\rangle \left\langle s_{P+N-1}^+ \middle| e^{-i\hat{H}\Delta t/\hbar} \middle| s_{P+N-2}^+ \right\rangle \cdots \left\langle s_{P+1}^+ \middle| e^{-i\hat{H}\Delta t/\hbar} \middle| s_P^+ \right\rangle
$$

$$
\left. \times \left\langle s_P^+ \middle| e^{-\hat{H}\Delta\beta/\hbar} \middle| s_{P-1}^+ \right\rangle \cdots \left\langle s_2^+ \middle| e^{-\hat{H}\Delta\beta/\hbar} \middle| s_1^+ \right\rangle \left\langle s_1^+ \middle| e^{-\hat{H}\Delta\beta/\hbar} \middle| s_0 \right\rangle \right] \ . \tag{4.98}
$$

Note that there are no closures inserted in between the system operators $\hat{\Gamma}$, $\hat{\Omega}$ and the propagators $e^{i\hat{H}\Delta t/\hbar}$, $e^{-i\hat{H}\Delta t/\hbar}$, respectively. This slightly reduces the number of integration variables and, thus, the effort for the numerical evaluation of the TCF. It is assumed that the products $\hat{\Gamma} e^{i\hat{H}\Delta t/\hbar}$ and $\hat{\Omega} e^{-i\hat{H}\Delta t/\hbar}$ propagate the system with an effective time step not larger than Δt, hence, the numerical stability remains unchanged. Note further that

$$
\int\limits_{-\infty}^{\infty} ds_{P+N}^+ \int\limits_{-\infty}^{\infty} ds_{P+N}^- \left\langle s_{P+N-1}^- \middle| e^{i\hat{H}\Delta t/\hbar} \middle| s_{P+N}^- \right\rangle \left\langle s_{P+N}^- \middle| s_{P+N}^+ \right\rangle \left\langle s_{P+N}^+ \middle| \hat{\Omega} e^{-i\hat{H}\Delta t/\hbar} \middle| s_{P+N-1}^+ \right\rangle =
$$

$$
\int\limits_{-\infty}^{\infty} ds \left\langle s_{P+N-1}^- \middle| e^{i\hat{H}\Delta t/\hbar} \middle| s \right\rangle \left\langle s \middle| \hat{\Omega} e^{-i\hat{H}\Delta t/\hbar} \middle| s_{P+N-1}^+ \right\rangle \ , \tag{4.99}
$$

which also reduces the number of integration variables by one. What follows now is very similar to Sec. 4.1.1. Therefore, the derivation steps are just commented on and the corresponding equations can be found in App. E.

In order to calculate the TCF numerically the integrals in Eq. (4.98) are replaced by discrete sums over the DVR states of the system (Sec. 4.1.2), see Eq. (E.3). In order to separate the bare system quantities from expressions that depend on the system-bath interaction, the

forward/backward time evolution operators are split according to Eq. (4.14). The same factorizations is applied to the imaginary time propagators, see Eq. (E.4). The error induced by the Trotter factorization is analogously proportional to $\Delta\beta^3$ [38] and, thus, dependent on the temperature. In a practical application the numerical parameter $\Delta\beta$ and, hence, P has to be determined by convergence. Performing the Trotter splitting according to Eq. (E.4) supplemented by inserting the respective closures reduce all system operators in the DVR basis to complex numbers. Thus, the trace over the bath's Hilbert space evaluates exclusively the bath-dependent operators $\hat{H}_{\mathrm{SB}}$. Therefore, each summand in Eq. (E.3) can be rearranged yielding Eq. (E.6). Here, the calculation of each summand can be divided into two mutually independent steps.

First, the value of each summand is determined by the bare system propagation in complex time along a grid point sequence $\tilde{s}_{i_0}, \tilde{s}_{i_1^+}, \ldots, \tilde{s}_{i_P^+}, \tilde{s}_{i_{P+1}^+}, \ldots, \tilde{s}_{i_{P+N-1}^+}, \tilde{s}_i, \tilde{s}_{i_0}, \tilde{s}_{i_1^-}, \ldots, \tilde{s}_{i_P^-}, \tilde{s}_{i_{P+1}^-} \ldots, \tilde{s}_{i_{P+N-1}^-}, \tilde{s}_i$. In analogy to Sec. 4.1.1 the coordinates are grouped into the new variable referred to as the *complex time* FBC

$$\tilde{\mathfrak{s}}^\pm \equiv \begin{pmatrix} \tilde{\mathfrak{s}}_0 & \tilde{\mathfrak{s}}_1^+ & \cdots & \tilde{\mathfrak{s}}_P^+ & \tilde{\mathfrak{s}}_{P+1}^+ & \cdots & \tilde{\mathfrak{s}}_{P+N-1}^+ \\ \tilde{\mathfrak{s}}_0 & \tilde{\mathfrak{s}}_1^- & \cdots & \tilde{\mathfrak{s}}_P^- & \tilde{\mathfrak{s}}_{P+1}^- & \cdots & \tilde{\mathfrak{s}}_{P+N-1}^- \end{pmatrix} = \begin{pmatrix} \tilde{s}_{i_0} & \tilde{s}_{i_1^+} & \cdots & \tilde{s}_{i_P^+} & \tilde{s}_{i_{P+1}^+} & \cdots & \tilde{s}_{i_{P+N-1}^+} \\ \tilde{s}_{i_0} & \tilde{s}_{i_1^-} & \cdots & \tilde{s}_{i_P^-} & \tilde{s}_{i_{P+1}^-} & \cdots & \tilde{s}_{i_{P+N-1}^-} \end{pmatrix}$$
$$(4.100)$$

with the *shared end point* $\tilde{s}_i$. The term forward-backward combination is adopted from Sec. 4.1.1. Here forward with respect to a complex time means the time evolution along the upper branch of the complex time contour $\tilde{\mathfrak{c}}_\chi$, whereas backward corresponds to the lower branch of $\tilde{\mathfrak{c}}_\chi$, see Fig. 3.4. Note that the end point $\tilde{s}_i$ is shared by the forward and backward part of the complex time FBC due to Eq. (4.99). As the result of the trace in the system's Hilbert space, also the first coordinate $\tilde{\mathfrak{s}}_0$ coincides in the forward and backward branches. This implies that here the path is indeed closed, not quasi-closed as in Sec. 3.2. As before, the end point is not included in the definition of $\tilde{\mathfrak{s}}^\pm$, since it is more convenient in order to formulate the iterative propagation scheme. A particular complex time FBC for $N = P = M = 3$ is depicted in Fig. 4.9, which is described in detail in App. E. By comparing Fig. 4.9 with Fig. 4.1, it becomes visible that the complex time propagation is very similar to the pure real time propagation, which is the consequence of splitting the Boltzmann operator, see Eq. (3.20).

Second, the summand is weighted by the *discrete complex time influence functional* $\tilde{\mathscr{F}}_{(0,P+N)}\left[\tilde{\mathfrak{s}}^\pm, \tilde{s}_i\right]$. Note that the subscript $(0, P+N)$ implies that the paths span P imaginary and N real time steps. A more detailed consideration is given in App. E. Similar to a time-
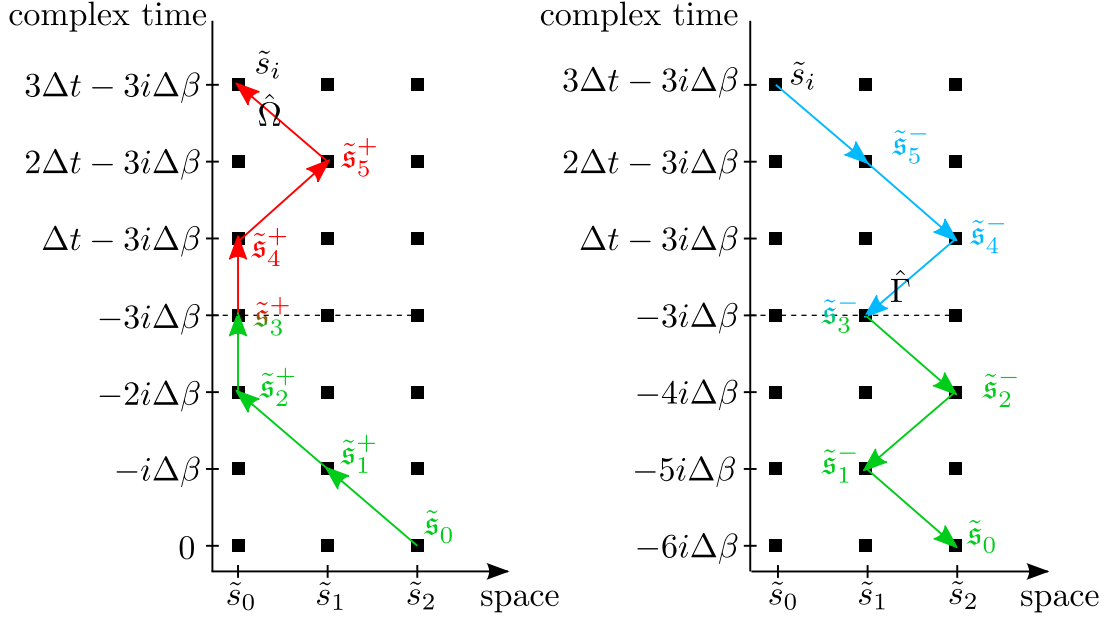
Figure 4.9.: **Propagation of the bare system in the complex time.** The forward/backward path is shown in the left/right panel, respectively

dependent observable, Eq. (4.34), the discrete TCF can be formulated for any $N > 0$ as a discrete PI

$$\tilde{C}_{\Gamma\Omega}(N\Delta t) = \frac{1}{Z(\beta)} \sum_{i=0}^{M-1} \sum_{\tilde{\mathfrak{s}}^{\pm} \in \underline{\mathbb{P}}_{P+N,M}} \tilde{\tilde{\mathscr{F}}}_{(0,P+N)} \left[\tilde{\mathfrak{s}}^{\pm}, \tilde{s}_i \right] \tilde{\mathscr{S}}_{(0,P+N)}^{\Gamma\Omega} \left[\tilde{\mathfrak{s}}^{\pm}, \tilde{s}_i \right] \quad , \tag{4.101}$$

where $\tilde{\mathscr{S}}_{(0,P+N)}^{\Gamma\Omega} \left[\tilde{\mathfrak{s}}^{\pm}, \tilde{s}_i \right]$, referred to as the *discrete complex time bare system part* of the discrete PI, represents the bare system as it is propagated in the complex time along the discrete paths $\tilde{\mathfrak{s}}^{\pm}$, according to the last four lines of Eq. (E.6), see also Figs. 3.5, 4.9. A detailed definition can be found in Eqs. (E.11, E.12). The set $\underline{\mathbb{P}}_{P+N,M}$ is a subset of $\mathbb{P}_{P+N,M} = (\mathbb{S}_M)^{2(P+N)}$ and it is defined as

$$\underline{\mathbb{P}}_{P+N,M} \equiv \left\{ \tilde{\mathfrak{s}}^{\pm} \in \mathbb{P}_{P+N,M} \, \middle| \, \tilde{\mathfrak{s}}_0^+ = \tilde{\mathfrak{s}}_0^- = \tilde{\mathfrak{s}}_0 \right\} \quad . \tag{4.102}$$

Note that due to the constraint $\tilde{\mathfrak{s}}_0^+ = \tilde{\mathfrak{s}}_0^- = \tilde{\mathfrak{s}}_0$, the number of elements $\underline{L}_{P+N,M} \equiv \left| \underline{\mathbb{P}}_{P+N,M} \right| = M^{2(P+N)-1}$. With the given definitions the discrete PI in Eq. (4.101) has the same form as its continuous counterpart given in Eq. (3.32). Again, the approximations employed in this

subsection provide the exact limit

$$\lim_{\Delta\beta,\Delta t\to 0, M\to\infty} \tilde{C}_{\Gamma\Omega}(N\Delta t) = C_{\Gamma\Omega}(t) \ . \tag{4.103}$$

Concerning the numerical applicability of Eq. (4.101), the same arguments hold as presented in the last paragraph of Sec. 4.1.1. A reasonable implementation is hindered by the number of FBCs $\underline{L}_{P+N,M}$ contributing to the PI. The amount of paths is very sensitive to the number of grid points M and it grows exponentially with propagation time according to $\underline{L}_{P+N,M} = M^{2(P+N)-1}$. The recipe to circumvent the first problem is already given by the employment of the DVR basis, see Sec. 4.1.2. The remaining task is to recast Eq. (4.101) into an iterative propagation scheme, which would circumvent the second problem. It is shown in the following subsection how exploiting the features of the MBO model helps to achieve this goal.

4.2.2. Iterative propagation of the TCF

As it was sketched in Sec. 4.1.3, the specific form of the interaction potential in the MBO model provides an analytical expression for the discrete real time influence functional $\tilde{F}_{(0,N)}\left[\tilde{\mathfrak{s}}^{\pm}, s_{\pm}\right]$. There, it was exploited that the bath consists of harmonic oscillators and the system is bilinearly coupled to the bath. Considering the results of the previous subsection, one notices that the discrete complex time influence functional $\tilde{\tilde{\mathscr{F}}}_{(0,P+N)}\left[\tilde{\mathfrak{s}}^{\pm}, \tilde{s}_i\right]$ has a similar structure to its real time counterpart, see Figs. 4.2,E.1 or Eqs. (4.25,E.7). Employing the same techniques as in Sec. 4.1.3, it is possible to express the discrete complex time influence functional as a closed expression [30]

$$\tilde{\tilde{\mathscr{F}}}_{(0,P+N)}\left[\tilde{\mathfrak{s}}^{\pm}, \tilde{s}_i\right] =$$
$$Z_{\mathrm{B}}(\beta)\exp\left\{-\frac{1}{\hbar}\sum_{k=0}^{P+N}\sum_{k'=0}^{k}\left(\eta_{k'k}^{++}\,\tilde{\mathfrak{s}}_{k'}^{+}\tilde{\mathfrak{s}}_{k}^{+} + \eta_{k'k}^{--}\,\tilde{\mathfrak{s}}_{k'}^{-}\tilde{\mathfrak{s}}_{k}^{-} + \eta_{k'k}^{-+}\,\tilde{\mathfrak{s}}_{k'}^{-}\tilde{\mathfrak{s}}_{k}^{+} + \eta_{k'k}^{+-}\,\tilde{\mathfrak{s}}_{k'}^{+}\tilde{\mathfrak{s}}_{k}^{-}\right)\right\} \ ,$$
$$\tag{4.104}$$

where $Z_{\mathrm{B}}(\beta)$ is the partition function of the isolated bath and $\tilde{\mathfrak{s}}_{P+N}^{\pm} \equiv \tilde{s}_i$. The *complex time memory coefficients* $\eta_{k'k}^{\pm\pm}$ and $\eta_{k'k}^{\pm\mp}$, given in App. B.2, depend on the *complex time bath response*

function

$$\mathscr{B}(\tau - \tau') \equiv \frac{1}{\pi} \int\limits_0^\infty \mathrm{d}\omega\, J(\omega) \frac{\cos\left(\omega\left(\tau - \tau' + i\beta\hbar/2\right)\right)}{\sinh\left(\beta\hbar\omega/2\right)} \quad . \tag{4.105}$$

Note that $\mathscr{B}(\tau - \tau')$ is formally identical to the real time bath response function $B(\tau - \tau')$ but here the argument consists of the complex times τ, τ' lying on the complex time contour $\mathfrak{c}_\chi$ as shown in Fig. 3.4. Equation (4.104) permits a similar interpretation as Eq. (4.53), though here the memory of the bath spans a complex time. In Sec. 4.1.3 it was claimed that $B(\tau - \tau')$ vanishes for a growing real time argument. This behavior was referred to as finite memory or finite correlation time. The argument of the *complex* time bath response function in Eq. (4.105) has a non-zero imaginary part causing an additional exponential decay in the imaginary direction of time. Since the imaginary time corresponds to temperature, this decay can be assigned to *thermal fluctuations* that destroy long correlation effects. Combining the decay in real time direction with the decay in imaginary time, one can suggest that there exists the following limit

$$\lim_{|\tau - \tau'| \to \infty} \mathscr{B}(\tau - \tau') = 0 \quad , \tag{4.106}$$

see also Fig. 4.10 for a special example. Note that the times τ, τ' lie on the complex time contour $\mathfrak{c}_\chi$. As a consequence of Eq. (4.106), the complex time memory coefficients $\eta_{k'k}^{\pm\pm}$ and $\eta_{k'k}^{\pm\mp}$ also tend to zero for $k \gg k'$. In the following it is thus assumed that coefficients with $k - k' > \kappa$ can be neglected without loss of accuracy in the numerical results. This assumption serves as the basis for an iterative propagation scheme, which is schematically derived in following paragraph with details given in App. E.1.

In analogy to Sec. 4.1.3 the discrete complex time influence functional can be written as a product of *complex time point-to-point influences*, see Eqs. (E.14,E.15). If the memory coefficients are neglected for $k - k' > \kappa$, then the corresponding complex time point-to-point influence acts like unity, thus, the double product in Eq. (E.15) can be truncated, see Eq. (E.17) and also Figs. 4.5,4.6. In the following it is assumed that it is sufficient to divide the imaginary time $-i\beta\hbar/2$ into $P = \kappa$ slices. This assumption can be justified by the fact, that the errors due to the Trotter factorization in real time and imaginary time behave identically, see Eqs. (4.14,E.4). One can claim that both approximations have the same quality if $\Delta t \approx \Delta\beta$, which is equivalent to $P \approx \kappa \cdot \beta\hbar/(2t_\kappa)$, where t_κ is the correlation time introduced in Sec. 4.1.4. For a typical temperature of 300K the imaginary time spans approximately $\beta\hbar/2 \approx 500\,\hbar/\mathrm{E_h}$, where $\mathrm{E_h}$ is
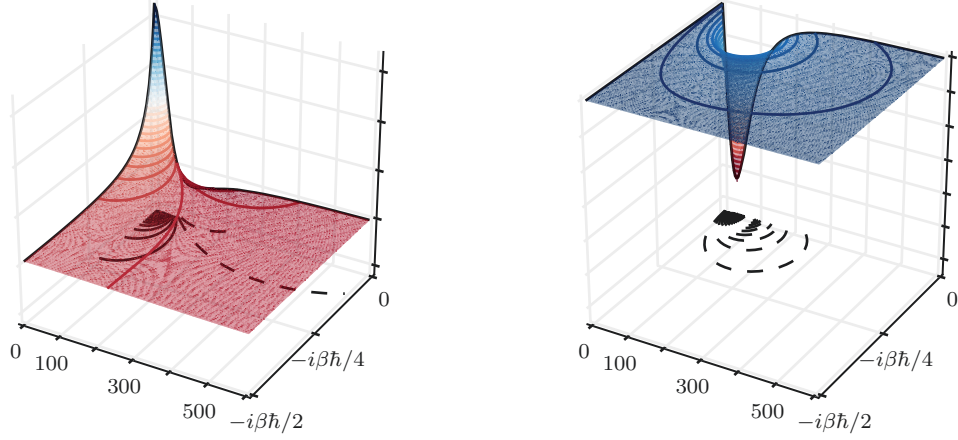
Figure 4.10.: **Complex time bath response function** for a spectral density of Ohmic type. The vertical axis in the left/right panel corresponds the real/imaginary part of $\mathscr{B}(\tau - \tau')$, respectively. The axis labeled with numbers measures the real part of the time difference $\tau - \tau'$ $[\hbar/\mathrm{E_h}]$, where $\mathrm{E_h}$ is the energy unit Hartree. The remaining axis takes account of the imaginary time.

the energy unit Hartree. Since in this thesis the focus is put on vibrational spectroscopy in solvents, a typical correlation time is about $t_\kappa \approx 12000\,\hbar/\mathrm{E_h}$ [39]. Therefore, in order to achieve an equal quality of the real and imaginary time discretization, it is absolutely sufficient to set $P = \kappa$. Of course, the assumption has to be individually ensured for the application to other SBCs at lower temperatures.

With the detailed derivation in App. E.1 at hand, the iterative propagation of the discrete TCF for any $N > 0$ can be formulated as follows. First, the time-dependent *discrete multi-time TCF functional* has to be propagated step by step to $N - \kappa$ via

$$\tilde{\mathscr{R}}\left[\tilde{\mathfrak{s}}^{\pm}; (N-\kappa)\Delta t\right] = \sum_{\tilde{\mathfrak{r}}^{\pm}\in\mathbb{P}_{\kappa,M}\left[\tilde{\mathfrak{s}}^{\pm}\right]} \mathscr{L}_{(N-1,N+\kappa)}\left[\tilde{\mathfrak{r}}^{\pm}, \tilde{\mathfrak{s}}^{\pm}\right] \tilde{\mathscr{R}}\left[\tilde{\mathfrak{r}}^{\pm}; (N-\kappa-1)\Delta t\right] \;, \qquad (4.107)$$

where the FBC $\tilde{\mathfrak{r}}^{\pm}$ and the set $\mathbb{P}_{\kappa,M}\left[\tilde{\mathfrak{s}}^{\pm}\right]$ have the same meaning as in Sec. 4.1.4 apart from the fact that $\tilde{\mathfrak{r}}^{\pm}$ spans complex time. Note that $\tilde{\mathscr{R}}\left[\tilde{\mathfrak{s}}^{\pm}; (N-\kappa)\Delta t\right]$ has a special initial condition taking the constraint $\tilde{\mathfrak{s}}_0^+ = \tilde{\mathfrak{s}}_0^- = \tilde{\mathfrak{s}}_0$ into account. The calculation of the discrete TCF itself

requires then the additional summation

$$\tilde{C}_{\Gamma\Omega}(N\Delta t) = \frac{1}{Z(\beta)} \sum_{i=0}^{M-1} \sum_{\tilde{\mathfrak{s}}^{\pm} \in \mathbb{P}_{\kappa,M}} \tilde{\mathscr{F}}_{(N,N+\kappa)} \left[\tilde{\mathfrak{s}}^{\pm}, \tilde{s}_i \right] \tilde{\mathscr{S}}^{\Gamma\Omega}_{(N,N+\kappa)} \left[\tilde{\mathfrak{s}}^{\pm}, \tilde{s}_i \right] \tilde{\mathscr{R}} \left[\tilde{\mathfrak{s}}^{\pm}; (N-\kappa)\Delta t \right] \quad .$$

$$(4.108)$$

As explained in detail in App. E.1, one can exploit the same features as presented in Secs. 4.1.5, 4.1.6 for the iterative propagation of the TCF, leading to a numerical scheme that provides the exact limit

$$\lim_{\theta,\Delta t \to 0, M, \kappa \to \infty} \tilde{C}_{\Gamma\Omega}(N\Delta t) = C_{\Gamma\Omega}(t) \quad . \tag{4.109}$$

Note that θ corresponds to the path filtering threshold and $\kappa \to \infty$ induces $\Delta\beta \to 0$ since it is assumed that $P = \kappa$.

5. Testing the methodology

5.1. Comparison to reference data

In order to verify the implementation, that is the main outcome of this thesis, its results are compared to published literature data.

5.1.1. Three-site electron transfer model

The first model system considered is adopted from Ref. [28]. The system Hamiltonian

$$\hat{H}_{\mathrm{s}} = \sum_{i=0}^{2} \varepsilon_i |\tilde{s}_i\rangle\langle\tilde{s}_i| + \sum_{i=0}^{1} V \cdot \left(|\tilde{s}_i\rangle\langle\tilde{s}_{i+1}| + |\tilde{s}_{i+1}\rangle\langle\tilde{s}_i| \right) \tag{5.1}$$

describes a three-site electron transfer, where only neighboring sites are interacting. The parameter $V \neq 0$ represents the strength of the coupling. Note that a site state is equivalent to a DVR state $|\tilde{s}_i\rangle$ and the values ε_i correspond to the diagonal of the Hamiltonian in the DVR basis, whereas the coupling V stands for off-diagonal terms. The MBO model is assumed, namely the system is bilinearly coupled to a set of harmonic oscillators, according to Eq. (4.44), with an Ohmic spectral density

$$J(\omega) = \frac{\pi}{2} \hbar \xi \omega \exp\left(-\omega/\omega_{\mathrm{c}}\right) \quad . \tag{5.2}$$

The observable of interest is the time evolution of the site populations $P_i(t)$, given that the electron is initially localized at the site with the highest energy, i.e.

$$\hat{\rho}_{\mathrm{s}}(0) = |\tilde{s}_0\rangle\langle\tilde{s}_0| \quad , \tag{5.3}$$

and

$$P_i(t) = \mathrm{Tr}_{\mathrm{s}} \left[\hat{\rho}_{\mathrm{s}}(t) |\tilde{s}_i\rangle\langle\tilde{s}_i| \right] \quad . \tag{5.4}$$

ε_0 [E$_\mathrm{h}$]	ε_1 [E$_\mathrm{h}$]	ε_2 [E$_\mathrm{h}$]	V [E$_\mathrm{h}$]	$\tilde{s}_0$ [bohr]	$\tilde{s}_1$ [bohr]	$\tilde{s}_2$ [bohr]
0.0	-1.33	-2.67	0.067	-1.0	0.0	1.0

(a) **System parameters.**

β [1/E$_\mathrm{h}$]	ξ [1]	ω_c [E$_\mathrm{h}/\hbar$]	M	Δt [$\hbar$/E$_\mathrm{h}$]	θ
0.72	0.1	1	3	0.3	10^{-5}

(b) **Bath specific and numerical parameters.**

Table 5.1.: **Simulation setup for the three-site electron transfer.**

The latter equation is evaluated as a discrete PI via the iterative scheme as presented in Sec. 4.1.1. The results of the current implementations for different correlation times, i.e. for different parameters κ are depicted in Fig. 5.1a. All other numerical parameters are given in Tab. 5.1. The calculated data is in excellent agreement with the results obtained by the authors of Ref. [28] as it can be seen by comparing panels a) and b) in Fig. 5.1.
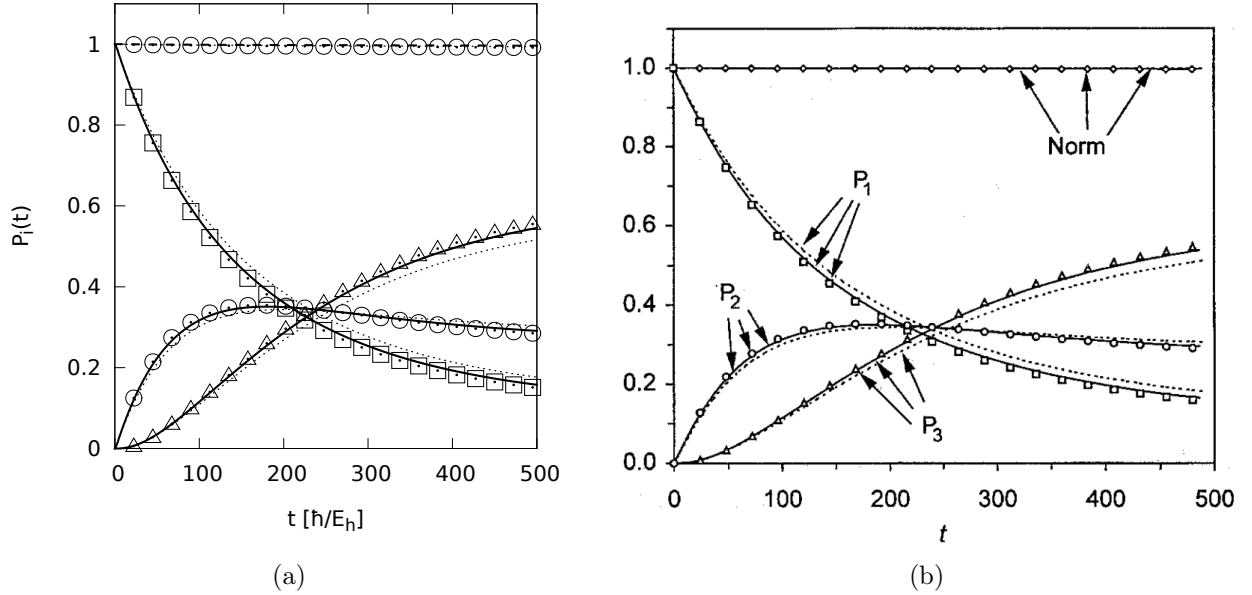

(a)

(b)

Figure 5.1.: **Time evolution of the site populations for different correlation times.** Panel a): Results of the current implementations. Panel b): Results directly taken from Ref. [28]. Dashed lines: $\kappa = 8$. Solid lines: $\kappa = 12$. Markers: $\kappa = 16$. The units in both panels coincide. Note that the indices of the populations in panel b) are shifted by one with respect to the numbering within this thesis. Note further that the data indicated by "Norm" is calculated via $\mathrm{Tr}_\mathrm{S}\left[\hat{\rho}_\mathrm{S}(t)\hat{1}_\mathrm{S}\right]$, where $\hat{1}_\mathrm{S} = \sum_{i=0}^{2} |\tilde{s}_i\rangle\langle\tilde{s}_i|$.

ε_0 [E$_\text{h}$]	ε_1 [E$_\text{h}$]	V [E$_\text{h}$]	$\tilde{s}_0$ [bohr]	$\tilde{s}_1$ [bohr]
0.0	1.0	1.0	-1.0	1.0

(a) **System parameters.**

β [1/E$_\text{h}$]	ξ [1]	ω_c [E$_\text{h}$/$\hbar$]	M	Δt [$\hbar$/E$_\text{h}$]	κ	θ
5.0	0.1	7.5	2	0.15	9	0.0

(b) **Bath specific and numerical parameters.**

Table 5.2.: **Simulation setup for the asymmetric two-level system.** Note that the threshold θ is set to zero, corresponding to an unfiltered set of paths.

5.1.2. Asymmetric two-level system

The second model is adopted from Ref. [26]. The Hamiltonian

$$\hat{H}_\text{s} = \sum_{i=0}^{1} \varepsilon_i |\tilde{s}_i\rangle\langle\tilde{s}_i| + V \cdot \left(|\tilde{s}_0\rangle\langle\tilde{s}_1| + |\tilde{s}_1\rangle\langle\tilde{s}_0| \right) \tag{5.5}$$

describes a two-level system with different site energies $\varepsilon_0 < \varepsilon_1$. Both sites are coupled due to the coupling parameter $V \neq 0$. In order to describe the interaction with the bath, the MBO model is employed. The bath's spectral density is again of Ohmic type, see Eq. (5.2). The initial condition for the system is set to

$$\hat{\rho}_\text{s}(0) = |\tilde{s}_1\rangle\langle\tilde{s}_1| \ , \tag{5.6}$$

meaning that the starting population is exclusively at the first site. The time evolution of two expectation values are considered: the population of the first site

$$P_1(t) = \text{Tr}_\text{s}\left[\hat{\rho}_\text{s}(t)|\tilde{s}_1\rangle\langle\tilde{s}_1| \right] \ . \tag{5.7}$$

and the expectation value of the system's position operator

$$\langle\hat{s}\rangle_t = \text{Tr}_\text{s}\left[\hat{\rho}_\text{s}(t)\hat{s} \right] \ . \tag{5.8}$$

The results are shown in Fig. 5.2a, where the numerical parameters are given in Tab. 5.2. Both simulated expectation values agree fine with the reference literature [26, 40] as it can be seen by comparing panels a) and b) in Fig. 5.2.
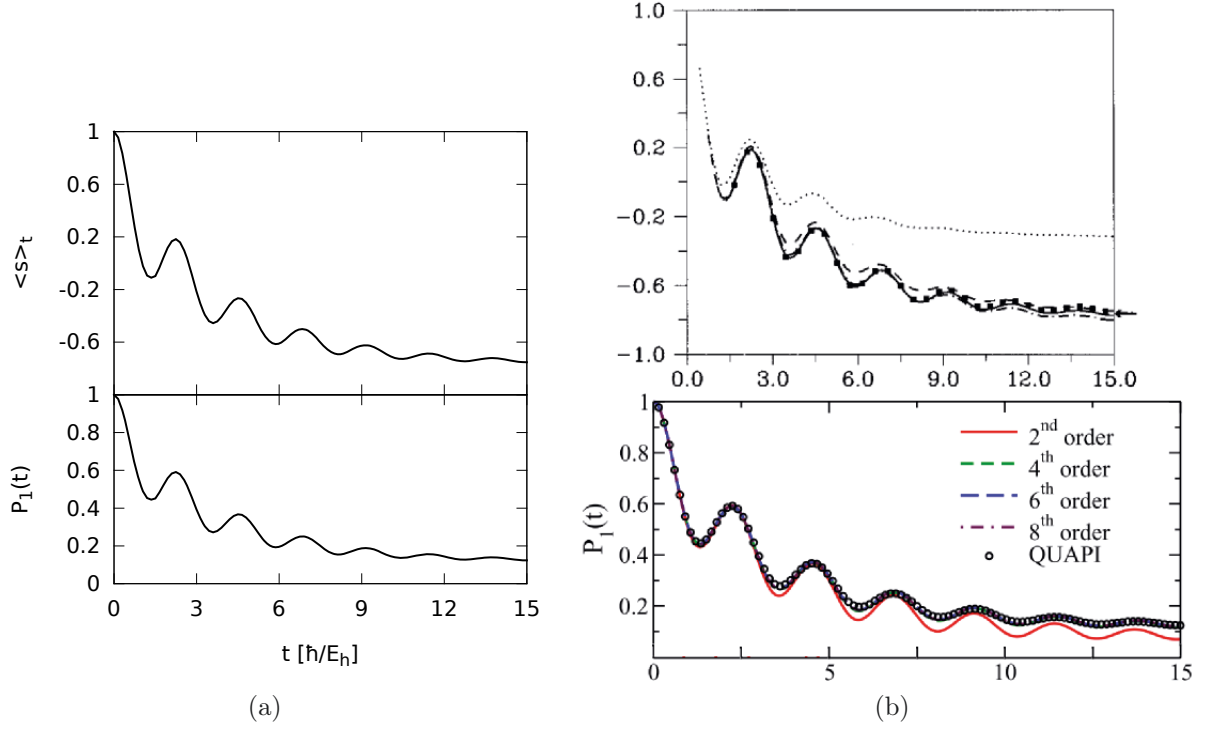
(a) (b)

Figure 5.2.: **Time-dependent expectation values of the two-level system.** Panel a): Results of the current implementation with $\kappa = 9$. Upper panel b): Results for the position expectation value directly taken from Ref. [26] with $\kappa = 1, 3, 5, 7$ and 9 (dotted, dashed, chain-dotted and solid lines and squares, respectively). Lower panel b): Results for the population $P_1(t)$ directly taken from Ref. [40]. Red, green, blue and purple curves are obtained with the hierarchy equation of motion (HEOM) methodology [41, 42, 43], where the purple curve correseponds to the highest accuracy. The data indicated by hollow circles is calculated via the discrete PI methodology presented in Ref. [26]. The units in the respective panels coincide.

5.1.3. The equilibrium TCF for a symmetric two-level system

In order to test the calculation of the TCF via the methodology presented in Sec. 4.2, a symmetric two-level system is considered. The obtained results are compared with the data presented in Ref. [29]. The corresponding Hamiltonian is identical to Eq. (5.5) if $\varepsilon_0 = \varepsilon_1 = 0$. Note that the system is equivalent to a two-level harmonic oscillator with a transition frequency $\omega = 2V/\hbar$. The frequencies of bath oscillators are again distributed according to the Ohmic

spectral density, see Eq. (5.2). The focus is put on the position auto-correlation function

$$\tilde{C}_{ss}(t) = \frac{1}{Z(\beta)}\mathrm{Tr}\left[\mathrm{e}^{-\beta\hat{H}}\hat{s}\,\hat{U}^{\dagger}(t)\hat{s}\,\hat{U}(t)\right]\;.$$ (5.9)

All numerical parameters are given in Tab. 5.3

ε_0 [E$_\mathrm{h}$]	ε_1 [E$_\mathrm{h}$]	V [E$_\mathrm{h}$]	$\tilde{s}_0$ [bohr]	$\tilde{s}_1$ [bohr]
0.0	0.0	1.0	-1.0	1.0

(a) **System parameters.**

β [1/E$_\mathrm{h}$]	ξ [1]	ω_c [E$_\mathrm{h}$/$\hbar$]	M	Δt [$\hbar$/E$_\mathrm{h}$]	$\Delta\beta$ [$\hbar$/E$_\mathrm{h}$]	κ	θ
1.0	0.2	7.5	2	0.1	1.0/12	6	0.0

(b) **Bath specific and numerical parameters.**

Table 5.3.: **Simulation setup for the symmetric two-level system.**

By comparing the results in Fig. 5.3a and the reference data from [29] in Fig. 5.3b one notices that the curves do agree only qualitatively. There is a small but noticeable quantitative discrepancy in the positions and the magnitudes of maxima and minima. Moreover, the imaginary part of $\tilde{C}_{ss}(t)$ in Fig. 5.3a has an unphysical kink at time $t = \kappa\Delta t$, not seen with the present figure scales. It remains unclear whether it is present in the reference data. Since the origin of the discrepancies is not understood yet, all following considerations are restricted to dynamics obtained by the propagation of the RDM.
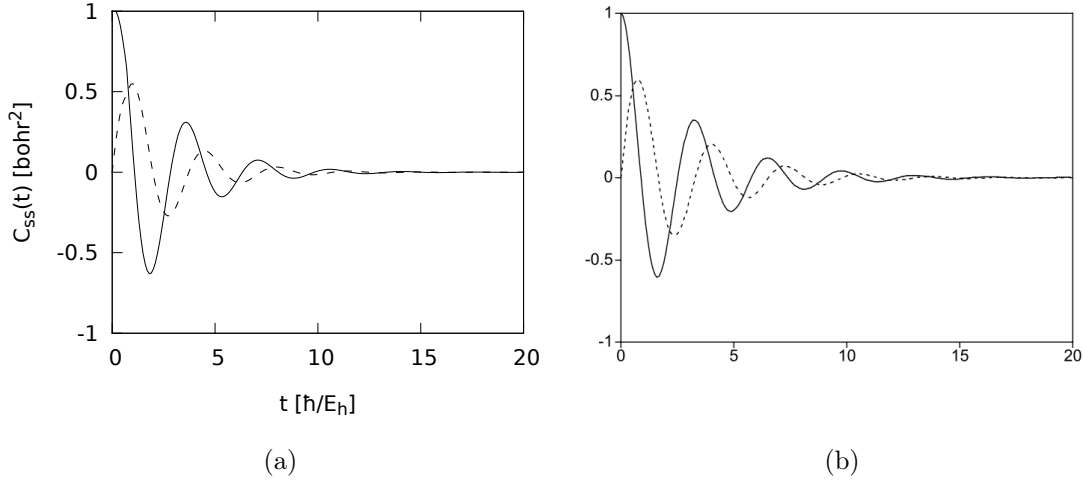
Figure 5.3.: **Equilibrium position auto-correlation function of a symmetric two-level system.** Panel a): Results of the current implementation. Panel b): Results for the position auto-correlation function directly taken from Ref. [29]. In both panels the solid/dashed line is the real/imaginary part of the TCF, respectively. The units coincide in both panels.

5.2. Failure of the discrete PI approach to vibrational systems in environment with realistic correlation times

The main goal of this thesis has been to provide a quantum methodology, applicable to realistic SBCs like vibrational systems in a liquid solvent. The obtained data should serve as a benchmark for other quantum methods or classical and quasi-classical approximations. Especially a quantitative benchmark for the artifacts induced by the curvature problem was desired as it was stated in the Introduction. Therefore, the following considerations are focused on the OH vibration of the HOD molecule in contact with a bath of H_2O molecules at ambient conditions. The OH bond has been chosen, since one expects here stronger quantum effects than for the OD bond, as the deuterium atom is heavier than the hydrogen one. Additionally the transition frequency of the system is similar to the transition frequencies of the H_2O molecules. Hence, potential resonances favor a significant influence of the bath onto the system's dynamics. As it was already mentioned in the Introduction, the MBO model provides the possibility to put quantum dynamics and (quasi-)classical approximations to it on equal footing, since the spec-

tral density, as the input of the MBO Hamiltonian, remains unchanged in all considerations. Thus, for the present purpose it is assumed that the the spectral density stemming from classical MD simulations of HOD in liquid H_2O [39] can be used to perform quantum simulations with the discrete PI formalism. It is noted in passing that the applicability of the MBO model to realistic systems was carefully investigated recently [39]. It was concluded that it is principally unable to describe a system if the system's potential is anharmonic. Importantly, the spectral densities parametrized under the assumption of effectively harmonic system cannot be transfered to the respective anharmonic case.

In this section it is shown that the successful PI description of the OH vibration in a water-like environment is unfortunately also inhibited by several obstacles. One problem of the discrete PI treatment of the OH vibration lies in the long correlation time resulting from the narrow spectral density of the bath, see Fig. 5.4. Another obstacle originates from the characteristics of the vibrational system itself, as it will be discussed below. For the simulations, that will be the basis for that discussion, the following parameters have been chosen. According to Ref. [39] the effective harmonic frequency of the OH vibration in liquid H_2O is $\omega_{OH} = 0.0165 \, E_h/\hbar \approx$ 3700cm^{-1}, where the qSPC/Fw force field model has been employed [15]. In order to carry out highly accurate classical MD simulations, the time step can be set to $\Delta t = 4.0 \, \hbar/E_h \approx 0.1 \, fs$ [39] and thus it is has been the initial choice for the time step in the discrete PI treatment as well. Test simulations have shown that the three lowest energy states are sufficient to describe the dynamics and thermodynamics of the OH bond at 300K. This means $M = 3$ grid points are required to discretize the space coordinate within the discrete PI framework, thanks to the DVR basis. If one would try to simulate the system dynamics numerically exactly via the iterative scheme (Sec. C.4), then the involved FBC segments have to span the correlation time $t_\kappa = 12000 \, \hbar/E_h \approx 300 \, fs$, see Fig. 5.4b. Hence, the corresponding parameter would be $\kappa = t_\kappa/\Delta t = 3000$. The resulting number of FBCs that contribute to the discrete PI in Eq. (4.81) *without path filtering* is $L_{\kappa,M} = 3^{8000} \approx 9 \cdot 10^{3816}$ according to Eq. (4.28). That would of course require numerical calculations that can not be handled within any finite time with any imaginable data storage. In the following section the performance of the path filtering, presented in Sec. 4.1.6, is investigated. The achieved reduction of the paths' number is rather spectacular though still insufficient in order to span the total correlation time for a typical vibrational system.
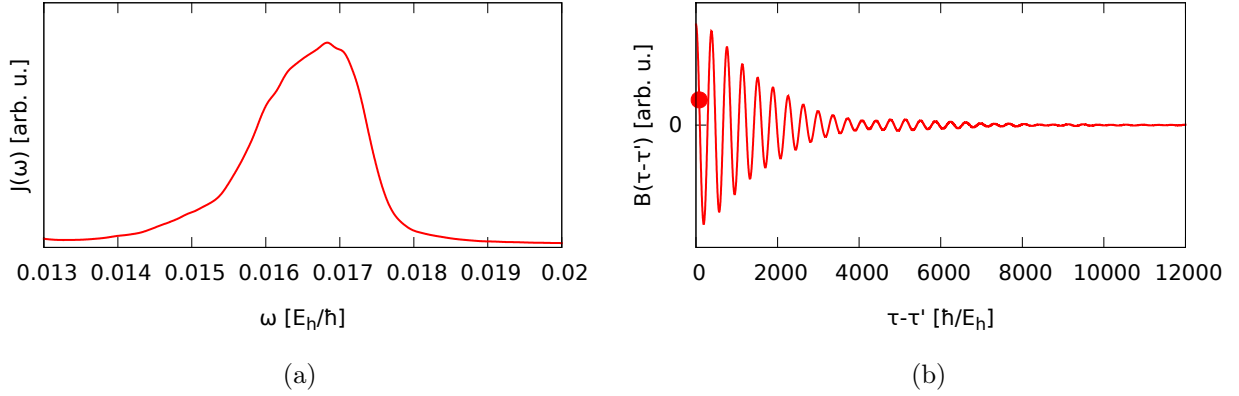
(a)

(b)

Figure 5.4.: **Spectral density and bath response function for HOD in** H_2O**.** Panel a): Spectral density in the vicinity of the OH vibration frequency $\omega_{\text{OH}} = 0,0165\,\text{E}_{\text{h}}/\hbar$. Note that it was shown in Ref. [39] that only this part of the spectral density has influence on the classical system's dynamics. Panel b): Corresponding bath response function. The filled circle indicates the correlation time $80\,\hbar/\text{E}_{\text{h}}$ for which the numerical results are obtained in the following subsection. The data for $J(\omega)$ is taken from Ref. [39].

5.2.1. The performance of the path filtering

Before proceeding to the numerical investigations for the path filtering, a word about the discrepancy between electron transfer and vibrational systems is appropriate. The general Hamiltonian in the DVR basis takes the matrix form

$$\hat{H}_{\text{S}} = \sum_{i=0}^{2} \varepsilon_i |\tilde{s}_i\rangle\langle\tilde{s}_i| + \sum_{i=0}^{2}\sum_{j=0}^{i-1} V_{ij} \cdot \left(|\tilde{s}_i\rangle\langle\tilde{s}_j| + |\tilde{s}_j\rangle\langle\tilde{s}_i| \right) \ , \tag{5.10}$$

which applies equally to electron transfer and vibrational problems. The difference between the two is contained in the magnitude of the coupling parameters V_{ij} that correspond to the off-diagonal elements of the Hamiltonian above. If one sets $V_{02} = V_{20} = 0$ and $V_{01} = V_{10} = -\alpha\varepsilon_0$, where α is fairly small, e.g., $\alpha = 10^{-2}$ or $\alpha = 10^{-1}$, one obtains a typical three-site electron transfer problem, where only the neighboring sites are interacting. The corresponding potential curves exhibit barriers depending on the magnitude of α in between the DVR grid points as depicted in Fig. 5.5. In contrast, if $V_{02} = V_{20} \approx 0.1\varepsilon_0$ and $V_{01} = V_{10} \approx -0.4\varepsilon_0$ the barriers vanish and the system corresponds to a harmonic oscillator $\hat{H}_{\text{S}} = \frac{\hat{p}^2}{2m} + \frac{1}{2}m\omega^2\hat{s}^2$, see black line therein. By increasing α further, e.g. up to 1.1 with $V_{02} = V_{20} = 0$, the potential energy curve

64

describes again a vibrational system, with the potential being a higher order polynomial, yellow line therein. In the following it is shown that the particular shape of the potential, or in other words the magnitude of the Hamiltonian's off-diagonal has an immense impact on the quality of the path filtering.

In order to probe the influence of the Hamiltonian's off-diagonal elements systematically, two electron transfer and two vibrational systems with the aforementioned parameters have been chosen.
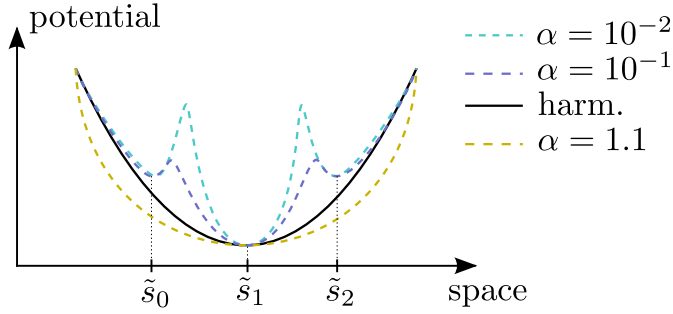

Figure 5.5.: **Potential energy curves for different coupling strengths α.** For explanation see text.

According to the considerations in the beginning of this section, the frequency of the harmonic oscillator is set to the effective harmonic frequency of the OH vibration of the HOD molecule, i.e. $\omega = \omega_{\text{OH}} = 0.0165 \, E_{\text{h}}/\hbar$. The corresponding mass is set to the reduced mass of the OH bond, thus $m = m_{\text{O}} m_{\text{H}}/(m_{\text{O}} + m_{\text{H}}) = 1740.9 \, m_{\text{e}}$, where m_{e} is the electron mass. The DVR states and the corresponding grid points for the harmonic oscillator are determined using the protocol in Sec. 4.1.2. The resulting diagonal elements ε_i of the Hamiltonian in the DVR basis and the grid points $\tilde{s}_i$, listed in Tab. 5.4, are used for all the systems studied. All systems are coupled to the same implicit bath that is described by spectral density adopted from Ref. [39], see Fig. 5.4. All other numerical parameters, given in Tab. 5.4, also coincide for the systems under investigation.

As it was stated above, an astronomical number of path segments would be required to obtain converged results with respect to the correlation time. One can strongly expect that even with path filtering the treatment of the total correlation time is not feasible. Therefore, all following numerical results are obtained by neglecting all non-local interactions that are separated by a time larger than $80 \, \hbar/E_{\text{h}}$, i.e. for $\Delta t = 4.0 \, \hbar/E_{\text{h}}$ such that $\kappa = 20$, marked with a filled circle in Fig. 5.4b. For each system the focus is put on the number of paths $L_{\kappa,M}^{\theta}$ that

have a path weight larger than the threshold θ, where θ is varied in the range $10^{-9} \ldots 10^{-5}$. Additionally, the convergence of the time-dependent position expectation value $\langle \hat{s} \rangle_t$ is investigated with respect to θ. The initial condition is in all cases set to $\hat{\rho}_s(0) = |\tilde{s}_0\rangle\langle\tilde{s}_0|$. It implies that the system is initially located at the coordinate $\tilde{s}_0$ or in other words the oscillators are displaced from the equilibrium by $\tilde{s}_0$.
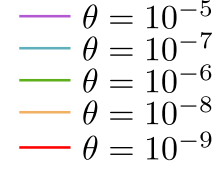
$$\theta = 10^{-5}$$
$$\theta = 10^{-7}$$
$$\theta = 10^{-6}$$
$$\theta = 10^{-8}$$
$$\theta = 10^{-9}$$

Figure 5.6.: **Legend for Figs. 5.7-5.9.**

ε_0 [E$_h$]	ε_1 [E$_h$]	ε_2 [E$_h$]	$\tilde{s}_0$ [bohr]	$\tilde{s}_1$ [bohr]	$\tilde{s}_1$ [bohr]	β [1/E$_h$]	M	Δt [$\hbar$/E$_h$]	κ
0.0275	0.0193	0.0275	-0.23	0.0	0.23	1052.58	3	4.0	20

Table 5.4.: **Simulation setup.** The grid-points are given by the DVR states of the harmonic oscillator. The value of β corresponds to a temperature of 300K.

The results of the simulations are visualized in Fig. 5.7, where the focus is first on the number of paths shown in the left panels of Fig. 5.7. Note the different ranges and logarithmic scaling of the y-axes. Overall, by comparing the black line representing the unfiltered exponential growth to the colored ones depicting the results of the filtering with various thresholds θ, one can see that the number of paths reduces dramatically if the filtering is employed. For the different systems and for all values of θ the path number increases with a similar functional form. It turns out that the number $L_{\kappa,M}^\theta$ can be best fitted to

$$L_{\kappa,M}^\theta = a\kappa^b \ , \tag{5.11}$$

where a and b are parameters which generally depend on M, Δt, θ and, of course, on the features of the system and the spectral density. The quality of the fit itself can be verified by considering Fig. 5.8 and the parameters' error behavior shown in Tab. 5.5. With the fit functions at hand, one is able to approximately predict the number of paths for arbitrary correlation time and a certain threshold as it is discussed later on.

Referring back to Fig. 5.7, it becomes visible that the number of paths increases rapidly with the value of α for a given threshold θ. For example in the case of the electron transfer system $\alpha = 10^{-2}$ and $\theta = 10^{-9}$ (panel 1, red curve) one has to take into account $2 \cdot 10^5$ path segments. Note that the curves for $\theta = 10^{-6}$, 10^{-7} and 10^{-8} are overlaying, which implies that the amount of paths with the weights in the range $10^{-8} \ldots 10^{-6}$ is negligible. For $\alpha = 10^{-1}$, panel 2 therein, the number has increased already to $3 \cdot 10^6$ with the same threshold (red curve). Again the

curves for $\theta = 10^{-6}$, 10^{-7} as well as for $\theta = 10^{-8}$, 10^{-9} are overlaying for the same reasons as in the previous case. Switching to the vibrational systems, for the harmonic oscillator with $\theta = 10^{-9}$ the set of paths contains $7 \cdot 10^8$ path segments, i.e. two orders of magnitude more than for the worst electron transfer case considered, see panel 3, red curve. The local computer resources were not sufficient to simulate the corresponding dynamics due to the unavailability of the required memory. The resumption of this behavior can be seen in the example of $\alpha = 1.1$ with $\theta = 10^{-6}$, where using this considerably large threshold resulted in $2 \cdot 10^8$ path segments that contribute significantly to the discrete PI (panel 4, turquoise curve). Here, the dynamics could not be simulated due to the same reasons as for the harmonic oscillator.

The right panels of Fig. 5.7 are dedicated to the convergence behavior of the position expectation value $\langle \hat{s} \rangle_t$; other expectation values exhibit similar trends (data not shown). For illustration, the difference $\langle \hat{s} \rangle_t^{\theta} - \langle \hat{s} \rangle_t^{\theta^*}$ is plotted, where $\langle \hat{s} \rangle_t^{\theta}$ is the expectation value simulated with the threshold θ. Here θ^* denotes the lowest threshold within $10^{-9} \ldots 10^{-5}$ that has been employed in the dynamical simulations. One notices that the speed of convergence decreases with the increase of the coupling parameter α. For the system with the smallest inter-site coupling $\alpha = 10^{-2}$, panel 1a therein, the convergence with respect to the threshold is already sufficient for $\theta = 10^{-6}$. In the case $\alpha = 10^{-1}$, panel 2a, dynamics simulated with $\theta = 10^{-5}$ were unstable and for $\theta = 10^{-6}$, 10^{-7} the data remained unconverged; here the curves for $\theta = 10^{-6}$ and $\theta = 10^{-7}$ are overlaying. The dynamics for the harmonic oscillator for all thresholds $\theta > 10^{-8}$ turn out to be unstable, see panel 3a. Unfortunately there is no dynamical data available for $\theta = 10^{-9}$ due to the aforementioned reasons. Therefore, one can not state that the results for $\theta = 10^{-8}$ are converged with respect to the threshold but it is natural to expect that they are not. For the strongest coupling with $\alpha = 1.1$ the local computer resources were only able to handle dynamics for $\theta = 10^{-5}$. Here, the results are also not physically reasonable due to numerical instabilities.

To summarize, the quality of the path filtering is very low for vibrational systems ($\alpha \geq 0.4$) in comparison to typical electron transfer systems ($\alpha \ll 0.4$). The number of path segments required to obtain converged results grows with the coupling parameter α and, moreover, the speed of convergence decreases.
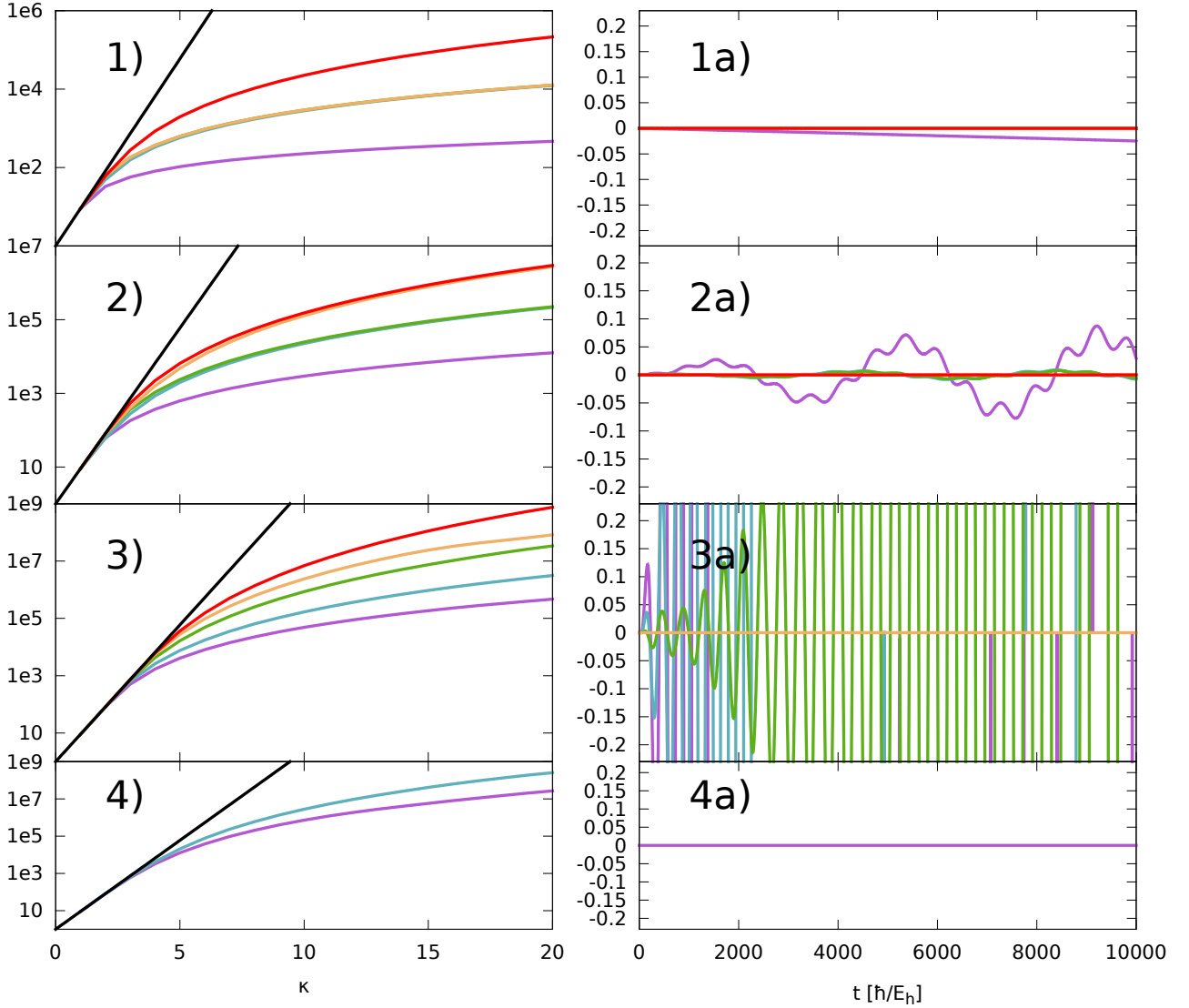
Figure 5.7.: **The quality of the path filtering depending on α.** Panels 1), 1a); 2), 2a); 3), 3a); and 4), 4a) correspond to $\alpha = 10^{-2}$; $\alpha = 10^{-1}$; harmonic oscillator and $\alpha = 1.1$, respectively. The colors stand for various thresholds as shown in Fig. 5.6. The left panels illustrate the behavior of the number of paths $L^{\theta}_{\kappa,M}$ with the correlation time κ. The black line represents the exponential growth, $M^{2\kappa}$, that corresponds to the unfiltered number of paths. The convergence behavior of the difference $\langle \hat{s} \rangle^{\theta}_t - \langle \hat{s} \rangle^{\theta^*}_t$ is depicted in the right panels. For 1) and 2) $\theta^* = 10^{-9}$ and for the harmonic oscillator $\theta^* = 10^{-8}$. For 4) only with $\theta = 10^{-5}$ dynamics could be calculated.

The reason for the observed behavior is contained already in the structure of Eq. (4.81). As it

was stated in Sec. 4.1.1, each summand of the PI consists of three mutually independent factors. For all considered systems the initial condition, the spectral density and, hence, the influence functional are the same. What remains is the discrete bare system part, defined in Eq. (4.29). The value of each summand therein is mainly determined by a product of the probability amplitudes $\langle \tilde{s}_i | e^{\pm i \hat{H}_S \Delta t / \hbar} | \tilde{s}_j \rangle$. Hence, a path segment has a small weight if it contains a pair of subsequent coordinates $\tilde{s}_i$, $\tilde{s}_j$ that are connected by a small probability amplitude. Considering again Fig. 5.5, it is foreseen that in the case of the smallest coupling constant $\alpha = 10^{-2}$ the probability for the system to go from $\tilde{s}_0$ to $\tilde{s}_1$ is very small due to the high barriers between the coordinates. All FBC segments that contain the factors $\langle \tilde{s}_1 | e^{\pm i \hat{H}_S \Delta t / \hbar} | \tilde{s}_0 \rangle$ several times have consequently a small path weight and can be filtered out. It is worth mentioning that the FBCs containing this factor only once cannot be filtered out as they are responsible for the transfer and the dynamics in their absence would be artificial. In contrast, the harmonic oscillator is free to go from $\tilde{s}_0$ to $\tilde{s}_1$. Hence, the probability amplitude for that transition is rather high and paths containing the sequence $\tilde{s}_0$, $\tilde{s}_1$ can not be filtered out without the loss of dynamical information. To rephrase, there are no physical reasons for the amplitudes to be small in the absence of the barriers. One can conclude that, the larger the coupling between the sites of the system is, the worse is the quality of the path filtering. Or, in other words, the larger the probability amplitude for the transition between two different coordinates of the discretized system space is, the more paths are important for the dynamics.

All presented considerations were restricted to path segments that span the very short time of $80\,\hbar/E_h$, since there were neither time nor resources to investigate longer correlation times. In order to estimate if there are any resources available that can treat the total correlation time of $12000\,\hbar/E_h$, one can employ the fit function introduced in Eq. (5.11). Since the relative fit errors for the exponent b are very small, the fit functions are considered as reliable for large values of κ. The fourth column of Tab. 5.5 contains the estimate of the path number for the various systems studied. If one focuses on the harmonic oscillator, then the prediction reads $1.7 \cdot 10^{23}$. Let us assume one has formulated the optimal algorithm based on the methodology presented in Sec. 4.2, where optimal means that there is no unnecessary memory storage. The only quantity that has to be stored is the multi-time reduced density vector $\tilde{\mathbf{R}}\left((N - \kappa)\Delta t\right) \in \mathbb{C}^{L_{\kappa,M}^{\theta}}$, since it depends on its previous time step counterpart and, thus, it can not be recalculated. Each element of $\tilde{\mathbf{R}}\left((N - \kappa)\Delta t\right)$ is a complex number (16 Byte with double precision) and the number of elements is $L_{\kappa,M}^{\theta} = 1.7 \cdot 10^{23}$. The vector $\tilde{\mathbf{R}}\left((N - \kappa)\Delta t\right)$ would require a storage of $1.7 \cdot 10^{23} \cdot 16\,\text{Byte} = 2.72 \cdot 10^{12}\,\text{TB}$. For comparison, in 2013 the total data contained in the world

wide web was estimated to occupy $4 \cdot 10^9$ TB [44]. With these numbers at hand, it becomes apparent that there is no possibility to achieve converged results for the OH vibration in a bath of H_2O molecules via the discrete iterative PI methodology and the simulation setup given in this subsection. This eventually implies, that either the methodology has to be reformulated or approximations invoked.

In the following subsection it is discussed how the size of the time step influences the growth of paths' number and the convergence of results.
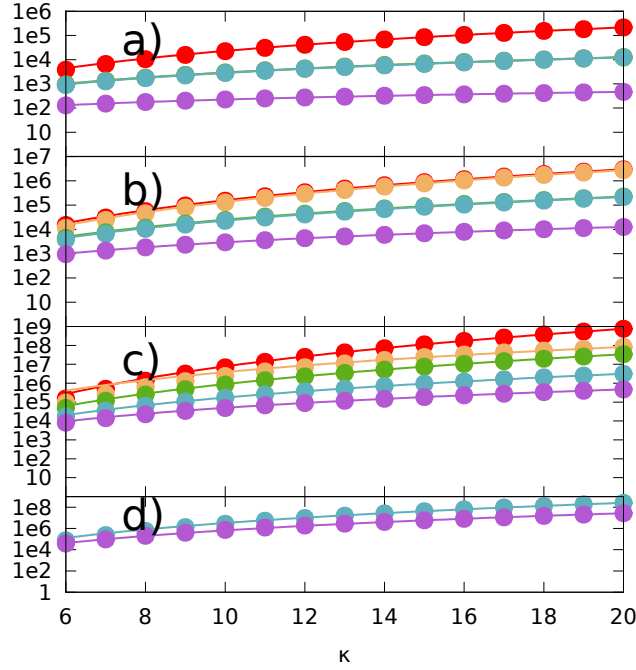

Figure 5.8.: **Fitting the number of paths.** The y-axes are referred to the number of paths. See Fig. 5.6 for color code.

α	θ	a	$\Delta a/a$	b	$\Delta b/b$	$L^{\theta}_{3000,M}$
10^{-2}	10^{-6}	20.3	2.30%	2.14	0.38%	570320642
10^{-1}	10^{-8}	6.10	2.61%	4.35	0.21%	7.8e+15
harm.	10^{-9}	1.96	3.32%	6.60	0.17%	1.7e+23
1.1	10^{-6}	1.61	7.64%	6.31	0.41%	1.4e+22

Table 5.5.: **Fitting results.** The value of θ corresponds to converged results for $\alpha = 10^{-2}$, 10^{-1}. For the harmonic oscillator and $\alpha = 1.1$ the value of θ corresponds to the highest accuracy that was possible with local computer resources in the given time.

5.2.2. The quality of filtering for different sizes of time steps

As it was stated in the previous subsection, one of the main problems of the discrete PI treatment of the OH vibration is the long correlation time of the bath. From a numerical point of view, the origin of this problem lies in the ratio $t_\kappa/\Delta t = \kappa = 3000$. That means a discrete path that spans the total correlation time contains three thousand coordinates and, thus, there exist numerous possibilities to construct that path on the time-space grid. Since the correlation time t_κ is set by nature and, hence, fixed, one can change the value of κ only by varying the time step Δt. Therefore, in this subsection the focus is put on the impact of the time step on the convergence behavior and the number of paths. The considered system is the three-level harmonic oscillator coupled to the spectral density as it is was used in the previous subsection. All numerical parameters are taken from Tab. 5.4 except from Δt and κ which are varied such that $\kappa\Delta t = 80.0\,\hbar/\mathrm{E_h}$.

The results of the simulations are visualized in Fig. 5.9. The number of paths that span a time $80.0\,\hbar/\mathrm{E_h}$ and that have a weight larger than a fixed threshold θ decreases with an increasing size of the time step. For example, if $\Delta t = 10.0$ and $\theta = 10^{-8}$, see panel 3 therein, then a number of $\approx 5 \cdot 10^6$ paths contribute significantly to the discrete PI, whereas for $\Delta t = 2.0$ and $\theta = 10^{-8}$, panel 2, more than 10^8 paths have to be taken into account. Noticeably the speed of convergence improves with an increasing size of the time step as is shown in the right panels of Fig. 5.9. For $\Delta t = 10.0$ one can see already an acceptable convergence for $\theta = 10^{-8}$, whereas for $\Delta t = 2.0$ the dynamics obtained with $\theta = 10^{-8}$ are unstable. Therefore, the solution to overcome the obstacles presented in the previous subsection seems the choice of a larger time step, where of course the maximal reasonable time step has to be determined by convergence. Unfortunately, the maximization of the time step circumvents the numerical problems only virtually. That becomes clear by considering the predictions of the fit function in Eq. 5.11, see Tab. 5.6. It turns out that the number of FBC segments that span the total correlation time would be $6.6 \cdot 10^{30}$, where it is assumed that the results are fully converged with $\Delta t = 10.0$ and $\theta = 10^{-9}$. The resulting numerical effort is of course unfeasible by any means. For shorter time steps the predictions of the fit functions seem to be advantageous. But since the dynamics obtained with $\Delta t = 0.5$ and $\Delta t = 2.0$ and the investigated thresholds are not stable, one can not state the numbers given the ninth column of Tab. 5.6 corresponds to converged results.
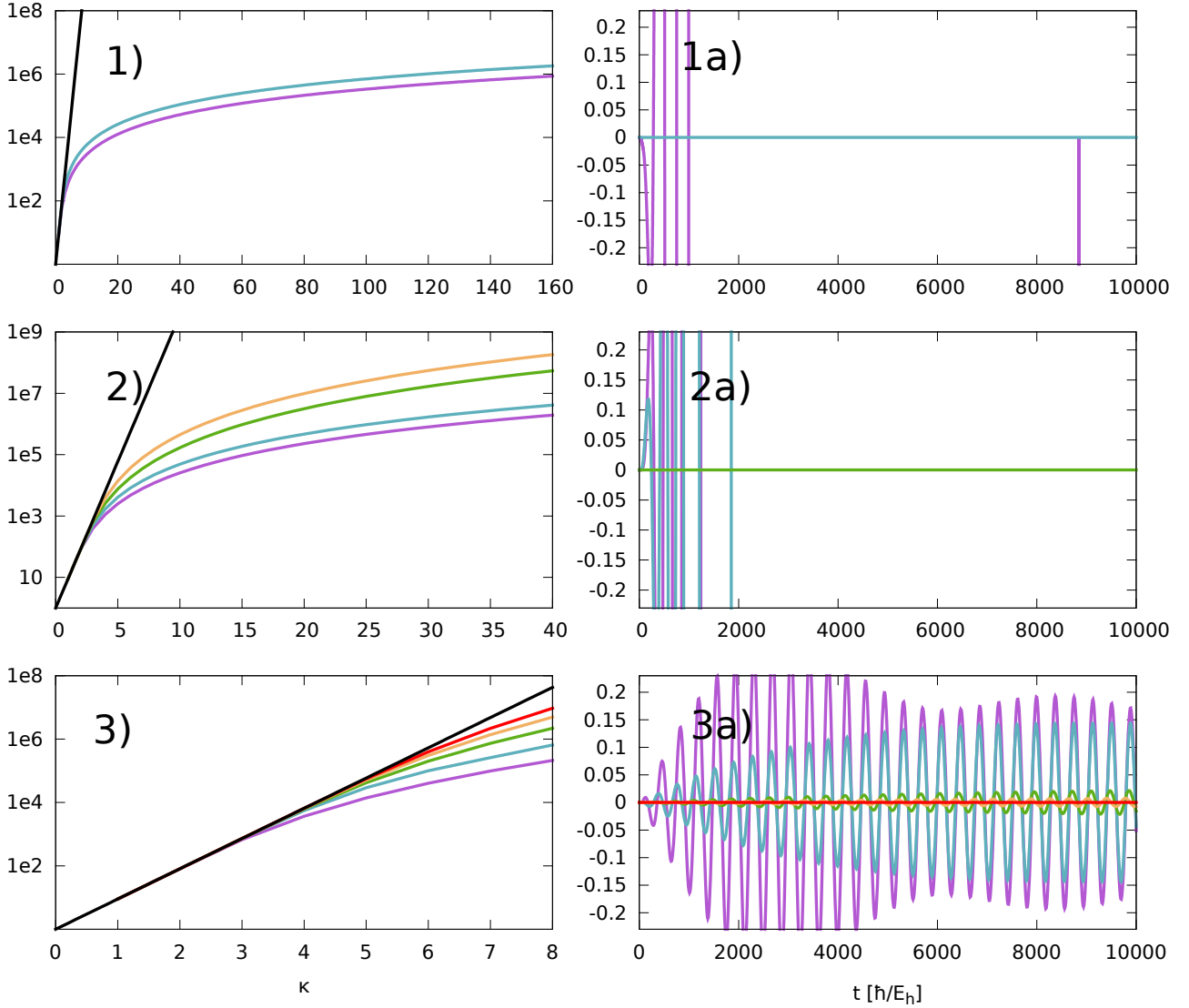
Figure 5.9.: **The quality of the path filtering depending on** Δt**.** Panels 1), 1a); 2), 2a) and 3), 3a) correspond to $\Delta t = 0.5$; $\Delta t = 2.0$ and $\Delta t = 10.0$, respectively. The colors correspond to different thresholds as shown in Fig. 5.6. The left panels show the number of paths $L_{\kappa,M}^{\theta}$. The black line represents the exponential $M^{2\kappa}$ that corresponds to the unfiltered number of paths. The right panels show the convergence behavior of the position expectation value. The difference $\langle \hat{s} \rangle_t^{\theta} - \langle \hat{s} \rangle_t^{\theta^*}$ is plotted, where $\langle \hat{s} \rangle_t^{\theta}$ is the expectation value calculated with the threshold θ. The value of θ^* corresponds to the lowest threshold within $\left(10^{-9}, 10^{-5}\right)$ for that dynamics were calculated. For 1), 2) and 3) $\theta^* = 10^{-6}$, $\theta^* = 10^{-7}$ and $\theta^* = 10^{-9}$ whereas for the harmonic oscillator $\theta^* = 10^{-8}$. For 4) only with $\theta = 10^{-5}$ numerical results could be obtained.

$\Delta t\ [\hbar/\mathrm{E_h}]$	κ	θ	a	$\Delta a/a$	b	$\Delta b/b$	κ_{tot}	$L^{\theta}_{\kappa_{\mathrm{tot}},M}$
0.5	160	10^{-6}	64.43	0.19%	2.02	0.020%	24000	$4.5 \cdot 10^{10}$
2.0	40	10^{-8}	35.72	1.35%	4.19	0.090%	6000	$2.4 \cdot 10^{17}$
10.0	8	10^{-9}	0.0012	1.53%	10.96	0.067%	1200	$6.6 \cdot 10^{30}$

Table 5.6.: **Fitting results.** The parameter κ_{tot} is set such that $\kappa_{\mathrm{tot}}\Delta t = 12000\,\hbar/\mathrm{E_h}$, which corresponds to the total correlation time of the H_2O bath. The value of θ corresponds to converged results for $\Delta t = 10.0$. For $\Delta t = 2.0$ and $\Delta t = 0.5$ the value of θ corresponds to the highest accuracy that was possible with local computer resources in the given time.

Since the result of the PI for the given correlation time should not depend on the time step, the decrease of the time step (increase of κ) ultimately leads to an increase of the paths' number and, hence, to the decrease of the average contribution of a single path. Thus the absolute value of the threshold has to be decreased accordingly. Not doing so leads to loosing the important paths and unstable unphysical dynamics, as was shown above. Hence, the advantage suggested by the predictions of the fit functions in Tab. 5.6 is only virtual.

6. Conclusion & Outlook

The goal of this thesis has been to understand and implement the path integral (PI) formalism in order to provide precise benchmarks for the typical molecular systems probed by means of infrared vibrational spectroscopy. The promising features of this formalism lie in the absence of any approximations apart from necessary numerics. The iterative calculation of the real time and the complex time PI as introduced by the research group of Nancy Makri, appeared as a suitable methodology to obtain numerically exact quantum dynamics for a system coupled to a non-Markovian macroscopic bath.

After a brief introduction, the theoretical basis have been provided in the second chapter. With the separation of a system-bath complex (SBC) into small subsystem S and a bath B, one is able to formulate reduced dynamics. The corresponding time-dependent expectation values and the equilibrium time-correlation functions (TCFs) can be used to understand experimental results in terms of microscopic dynamics. In the third chapter, the continuous PI framework has been established. It has been presented that the time evolution of the reduced density operator can be expressed as an integral over forward and backward paths available to the system. As an important quantity, the so-called influence functional has been put forward, which contains the complete influence of the bath onto the system implicitly. The second section of this chapter has been devoted to TCFs. In terms of PIs, the TCF is an integral not only over paths the system follows forward and backward in time but additionally over paths that span imaginary time stemming from the Boltzmann operator and, thus, corresponding to the temperature.

In the fourth chapter, the focus has been on the numerical evaluation of the PI formalism, where I have chosen most attractive and powerful algorithms to be adopted the corresponding literature of the last two and a half decades. A gross effort has been put into the understanding and unifying the terminology connected to the discrete treatment of PIs. In the first section of the fourth chapter, the derivation of time evolution of the reduced density matrix (RDM) as a discrete PI corresponding to global propagation has been presented. The peculiarity of this thesis is the concise and practical formulation of the PI in terms of discrete forward-backward

combinations of paths (FBCs). In order to optimize the spatial discretization the discrete variable representation (DVR) has been utilized. The famous MBO model that sets the grounds for quantum-classical comparison and leads to analytical expressions for the non-local influence functional has been discussed. If the bath has a finite correlation time, then the non-local character of the influence functional is also finite. It is this finiteness that theoretically allows one to recast the discrete PI into an iterative propagation scheme that circumvents the exponential growth of the effort connected to a global propagation. In order to reduce the numerical effort further, the concept of the path filtering has been employed. The described propagation scheme for the RDM has been then implemented. The corresponding source code is kept general and requires as input only the numerical parameters, an arbitrary system Hamiltonian in a matrix or functional form as well as an arbitrary spectral density as raw data. In the second part of the fourth chapter, the same line of reasoning has led to an iterative propagation scheme of the TCF. The resulting algorithms have been also implemented.

In the first section of the fifth chapter the self-implemented algorithms have been tested against published literature data. For the RDM propagation, an excellent agreement with the references could be found. Unfortunately, the results for the TCF are not fully reliable. The data agree qualitatively but not quantitatively with the reference one. Moreover, the imaginary part of the TCF exhibits unphysical kinks and the responsible error could not be found yet. The second section of the fifth chapter has been focused on the applicability of the discrete PI formalism to electron transfer and vibrational systems coupled to a bath with a realistic correlation time for a liquid solvent. It has turned out that the discrete PI formalism does not provide a feasible methodology to simulate quantum dynamics for the latter, while it is perfectly suitable for the former. This is the central conclusion of the thesis. The reason has been traced down to the magnitude of the off-diagonal elements of the Hamiltonian matrix in the DVR basis. With an increasing magnitude, the amount of paths that contribute significantly to the discrete PI exceeds available computer resources by far. In the case of small off-diagonal elements, which corresponds to a typical electron transfer problem, the growth of the path number is much more moderate. In the last part of the fifth chapter it has been confirmed, that in the case of the harmonic oscillator the variation of the time step size can not circumvent an unfeasible amount of paths.

The outcome of this thesis opened more questions than solved. In order to proceed further one should consider. First, the error within the iterative TCF propagation has to be located and eliminated. Second, despite the failure for vibrational systems interacting with realistic

baths, it still can enjoy application to electron transfer problems, which are common targets in our group. Therefore the code can for sure be optimized. For example, a more user-friendly interface for input parameters can be implemented in order make the code accessible for others. Also an alternative storage of the paths as single numbers, where each coordinate is represented as a digit, would noticeably reduce the amount of memory storage. Additionally some part of the propagation could be carried out globally on each time step, to reduce the memory usage further. Third, the current implementation is serial and, since PI techniques are tailored for parallel computation, a suitable CPU and/or GPU parallelization is desired. Last but not least, in order to extend the applicability to electron transfer problems, the comparison to results obtained via, e.g., the hierarchy equations of motion (HEOM) [41, 42, 43] would provide an indication of advantages and disadvantages of the discrete PI methodology.

Finally, it can be concluded that the discrete PI formalism has the charm to serve as methodology that produces numerically exact quantum dynamics. Unfortunately, it fails to provide the vibrational infrared spectra for a system solvated in a bath with correlation time typical for a liquid environment. The reason for the failure appears to be an intrinsic feature of vibrational systems in general. Thus, it is not expected that the corresponding numerical obstacles can be circumvented within this framework, and a suitable reformulation or a reasonable approximation are prospected.

A. Derivation of path integrals

In this part of the appendix it is shown that

$$\left\langle s \left| \exp\left\{ \lambda\left(\hat{p}^2/(2m) + \hat{V}(\hat{s}) \right) \right\} \right| s_0 \right\rangle \equiv \int_{s_0}^{s} \mathrm{D}^\lambda \mathfrak{s}(\tau) \, \exp\left\{ S^\lambda[\mathfrak{s}(\tau)] \right\}, \tag{A.1}$$

where

$$S^{\mp it/\hbar}[\mathfrak{s}(\tau)] = \pm\frac{i}{\hbar} A_{(0,t)}[\mathfrak{s}(\tau)] = \pm\frac{i}{\hbar} \int_0^t \mathrm{d}\tau \left[\frac{1}{2}m\dot{\mathfrak{s}}^2(\tau) - V\left(\mathfrak{s}(\tau) \right) \right] \tag{A.2}$$

contains the classical action with the measure

$$\int_{s_0}^{s} \mathrm{D}^{\mp it/\hbar}\mathfrak{s}(\tau) = \int_{s_0}^{s} \mathrm{D}_{(0,t)}\mathfrak{s}(\tau) \tag{A.3}$$

and

$$S^{-\beta}[\mathfrak{s}(\tau)] = -\frac{1}{\hbar} E_{(0,\beta\hbar)}[\mathfrak{s}(\tau)] = -\frac{1}{\hbar} \int_0^{\beta\hbar} \mathrm{d}\tau \left[\frac{1}{2}m\dot{\mathfrak{s}}^2(\tau) + V\left(\mathfrak{s}(\tau) \right) \right] \tag{A.4}$$

contains the Euclidian action with the measure

$$\int_{s_0}^{s} \mathrm{D}^{-\beta}\mathfrak{s}(\tau) = \int_{s_0}^{s} \mathrm{D}_{(0,\beta\hbar)}\mathfrak{s}(\tau) \tag{A.5}$$

Following [37] the first step of derivation employs the Trotter theorem

$$\exp\left\{ \lambda(\hat{A} + \hat{B}) \right\} = \lim_{P\to\infty} \left[\mathrm{e}^{\frac{\lambda}{2P}\hat{B}} \mathrm{e}^{\frac{\lambda}{P}\hat{A}} \mathrm{e}^{\frac{\lambda}{2P}\hat{B}} \right]^P, \tag{A.6}$$

A. Derivation of path integrals

where $\hat{A}$ and $\hat{B}$ are operators which do not commute in general and λ is a complex number and P is integer. Substituting this theorem into Eq. () with $\hat{A} = \hat{p}^2/(2m)$, $\hat{B} = \hat{V}(\hat{s})$ yields

$$\left\langle s \left| \exp\left\{ \lambda\left(\hat{p}^2/(2m) + \hat{V}(\hat{s})\right)\right\}\right| s_0 \right\rangle =$$

$$\lim_{P\to\infty} \left\langle s \left| \left[\exp\left\{\frac{\lambda}{2P}\hat{V}(\hat{s})\right\} \exp\left\{\frac{\lambda}{2mP}\hat{p}^2\right\} \exp\left\{\frac{\lambda}{2P}\hat{V}(\hat{s})\right\}\right]^P \right| s_0 \right\rangle$$

With the definition

$$\hat{\Omega}_P^\lambda := \exp\left\{\frac{\lambda}{2P}\hat{V}(\hat{s})\right\} \exp\left\{\frac{\lambda}{2mP}\hat{p}^2\right\} \exp\left\{\frac{\lambda}{2P}\hat{V}(\hat{s})\right\} \tag{A.7}$$

one can reformulate

$$\left\langle s \left| \exp\left\{ \lambda\left(\hat{p}^2/(2m) + \hat{V}(\hat{s})\right)\right\}\right| s_0 \right\rangle = \lim_{P\to\infty} \langle s| \underbrace{\hat{\Omega}_P^\lambda \cdot \hat{\Omega}_P^\lambda \cdots \hat{\Omega}_P^\lambda}_{P\,\text{times}} |s_0\rangle \,. \tag{A.8}$$

An insertion of $P-1$ closures

$$\hat{1} = \int_{-\infty}^{\infty} \mathrm{d}s_i\, |s_i\rangle\langle s_i| \tag{A.9}$$

between each $\hat{\Omega}_P^\lambda$ yields

$$\left\langle s \left| \exp\left\{ \lambda\left(\hat{p}^2/(2m) + \hat{V}(\hat{s})\right)\right\}\right| s_0 \right\rangle = \lim_{P\to\infty} \int_{-\infty}^{\infty} \mathrm{d}s_1 \cdots \int_{-\infty}^{\infty} \mathrm{d}s_{P-1} \prod_{i=0}^{P-1} \langle s_{i+1}| \hat{\Omega}_P^\lambda |s_i\rangle \,, \quad s_P \equiv s. \tag{A.10}$$

The quantities $\langle s_{i+1}| \hat{\Omega}_P^\lambda |s_i\rangle$ can be further evaluated since $\hat{s}|s_i\rangle = s_i|s_i\rangle$

$$\langle s_{i+1}| \hat{\Omega}_P^\lambda |s_i\rangle = \exp\left\{\frac{\lambda}{2P}V(s_{i+1})\right\} \langle s_{i+1}| \exp\left\{\frac{\lambda}{2mP}\hat{p}^2\right\} |s_i\rangle \exp\left\{\frac{\lambda}{2P}V(s_i)\right\} \,, \tag{A.11}$$

78

A. Derivation of path integrals

where $V(s)$ is the classical correspondence of $\hat{V}(\hat{s})$ evaluated at the position s. By inserting a closure of momentum eigenstates

$$\hat{1} = \int\limits_{-\infty}^{\infty} \mathrm{d}p \, |p\rangle \langle p| \,, \quad \hat{p} \, |p\rangle = p \, |p\rangle \tag{A.12}$$

Eq. (A.11) becomes

$$\langle s_{i+1}| \, \hat{\Omega}_P^\lambda \, |s_i\rangle = \exp\left\{\frac{\lambda}{2P}\left(V(s_{i+1}) + V(s_i)\right)\right\} \int\limits_{-\infty}^{\infty} \mathrm{d}p \, \langle s_{i+1}| \, p\rangle \exp\left\{\frac{\lambda}{2mP}p^2\right\} \langle p \, |s_i\rangle \,, \tag{A.13}$$

here $\langle s| \, p\rangle$ is nothing else than the momentum eigenstate in coordinate presentation namely the wavefunction

$$\langle s| \, p\rangle = \frac{1}{\sqrt{2\pi\hbar}} \mathrm{e}^{ips/\hbar}. \tag{A.14}$$

With Eq. (A.14) one finds

$$\langle s_{i+1}| \, \hat{\Omega}_P^\lambda \, |s_i\rangle = \exp\left\{\frac{\lambda}{2P}\left(V(s_{i+1}) + V(s_i)\right)\right\} \frac{1}{2\pi\hbar} \int\limits_{-\infty}^{\infty} \mathrm{d}p \, \exp\left\{\frac{\lambda}{2mP}p^2\right\} \exp\left\{\frac{ip\left(s_{i+1} - s_i\right)}{\hbar}\right\}. \tag{A.15}$$

The momentum integral can be carried out analytically for $\Re(\lambda) < 0$

$$\langle s_{i+1}| \, \hat{\Omega}_P^\lambda \, |s_i\rangle = \left(-\frac{mP}{2\pi\lambda\hbar^2}\right)^{1/2} \exp\left\{\frac{\lambda}{2P}\left(V(s_{i+1}) + V(s_i)\right)\right\} \exp\left\{\frac{mP}{2\lambda\hbar^2}\left(s_i - s_{i+1}\right)^2\right\}. \tag{A.16}$$

Inserting this result in Eq. (A.10) and performing the product, one gets

$$\left\langle s \left| \exp\left\{\lambda\left(\hat{p}^2/(2m) + \hat{V}(\hat{s})\right)\right\} \right| s_0 \right\rangle = \lim_{P\to\infty} \int\limits_{-\infty}^{\infty} \mathrm{d}s_1 \cdots \int\limits_{-\infty}^{\infty} \mathrm{d}s_{P-1}$$

$$\times \left(-\frac{mP}{2\pi\lambda\hbar^2}\right)^{P/2} \exp\left\{\frac{\lambda}{2P}\left(V(s) + V(s_0)\right)\right\}$$

$$\times \exp\left\{\frac{mP}{2\lambda\hbar^2}\sum_{i=0}^{P-1}\left(s_i - s_{i+1}\right)^2 + \frac{\lambda}{P}\sum_{i=1}^{P-1}V(s_i)\right\}. \tag{A.17}$$

A. Derivation of path integrals

With the definitions $l = \mathfrak{Re}(\lambda) + \mathfrak{Im}(\lambda)$ and $\Delta = l/P$ the latter equation can be written as

$$
\left\langle s \left| \exp\left\{ \lambda \left(\hat{p}^2/(2m) + \hat{V}(\hat{s}) \right) \right\} \right| s_0 \right\rangle = \lim_{P \to \infty} \int_{-\infty}^{\infty} \mathrm{d}s_1 \cdots \int_{-\infty}^{\infty} \mathrm{d}s_{P-1}
$$

$$
\times \left(-\frac{ml}{2\pi\Delta\hbar^2\lambda} \right)^{P/2} \exp\left\{ \frac{\lambda}{l}\frac{\Delta}{2} \left(V(s) + V(s_0) \right) \right\}
$$

$$
\times \exp\left\{ \frac{m\Delta}{2}\frac{l}{\lambda} \sum_{i=0}^{P-1} \left(\frac{s_i - s_{i+1}}{\Delta} \right)^2 + \frac{\lambda}{l}\Delta \sum_{i=1}^{P-1} V(s_i) \right\} \tag{A.18}
$$

Note that the limit $P \to \infty$ also induces $\Delta \to 0$. If one thinks of the coordinates s_i as values of a continuous function $\mathfrak{s}(i\Delta) = s_i$ then in the limit the difference $s_i - s_{i+1}$ vanishes and $i\Delta$ gets a continuous variable $\tau \in (0, l)$ thus

$$
\lim_{P \to \infty} \frac{s_i - s_{i+1}}{\Delta} = \dot{\mathfrak{s}}(\tau). \tag{A.19}
$$

Additionally the sums can be formulated as integrals

$$
\lim_{P \to \infty} \left\{ \sum_{i=1}^{P-1} V(s_i)\Delta + \frac{\Delta}{2} \left(V(s) + V(s_0) \right) \right\} = \int_0^l \mathrm{d}\tau V(\mathfrak{s}(\tau)) \tag{A.20}
$$

$$
\lim_{P \to \infty} \frac{m}{2} \sum_{i=0}^{P-1} \left(\frac{s_i - s_{i+1}}{\Delta} \right)^2 \Delta = \int_0^l \mathrm{d}\tau \frac{m}{2}\dot{\mathfrak{s}}^2(\tau). \tag{A.21}
$$

The integration variables s_i get infinitely close in the limit but they always span the interval $(0, l)$ where the points $s_0 = \mathfrak{s}(0)$, $s = \mathfrak{s}(l)$ are fixed and all points in between are varied from $-\infty$ to ∞. Thus one can think of the integral as a "scanning" and summation over all possible continuous functions that connect s_0 and s within l. With this interpretation one can recast the integration measure such that it is now a *functional* integration over all continuous function $\mathfrak{s}(\tau)$ that span the interval $(0, l)$ with boundaries $s(0) = s_0$, $\mathfrak{s}(l) = s$. Such an integration shall be denoted by

$$
\int_{s_0}^{s} \mathrm{D}_{(0,l)}\mathfrak{s}(\tau). \tag{A.22}
$$

A. Derivation of path integrals

Now one can formulate the equivalence

$$\left\langle s \left| \exp\left\{ \lambda \left(\hat{p}^2/(2m) + \hat{V}(\hat{s}) \right) \right\} \right| s_0 \right\rangle = \int_{s_0}^{s} D_{(0,l)}\mathfrak{s}(\tau) \, \exp\left\{ \frac{\lambda}{l} \int_0^l d\tau \left[\left(\frac{l}{\lambda}\right)^2 \frac{1}{2} m\dot{\mathfrak{s}}^2(\tau) + V(\mathfrak{s}(\tau)) \right] \right\}.$$
(A.23)

That means for $\lambda = -\beta$ with the substitution $\tau \to -\hbar\tau$

$$\left\langle s \left| \exp\left\{ -\beta \left(\hat{p}^2/(2m) + \hat{V}(\hat{s}) \right) \right\} \right| s_0 \right\rangle = \int_{s_0}^{s} D_{(0,\beta\hbar)}\mathfrak{s}(\tau) \, \exp\left\{ -\frac{1}{\hbar} \int_0^{\beta\hbar} d\tau \left[\frac{1}{2} m\dot{\mathfrak{s}}^2(\tau) + V(\mathfrak{s}(\tau)) \right] \right\}$$
(A.24)

and for $\lambda = \mp it/\hbar$ with the substitution $\tau \to \mp\hbar\tau$

$$\left\langle s \left| \exp\left\{ \mp it/\hbar \left(\hat{p}^2/(2m) + \hat{V}(\hat{s}) \right) \right\} \right| s_0 \right\rangle = \int_{s_0}^{s} D_{(0,t)}\mathfrak{s}(\tau) \, \exp\left\{ \pm\frac{i}{\hbar} \int_0^{t} d\tau \left[\frac{1}{2} m\dot{\mathfrak{s}}^2(\tau) - V(\mathfrak{s}(\tau)) \right] \right\}.$$
(A.25)

B. Memory coefficients of the discrete influence functional

B.1. Real time propagation

The memory coefficients for the global propagation scheme in Eqs. (4.54,4.55) can be given explicitly as [28]

$$
\eta_{k'k} = \frac{2}{\pi} \int\limits_{-\infty}^{\infty} d\omega \frac{J(\omega)e^{\beta\hbar\omega/2}}{\omega^2 \sinh(\beta\hbar\omega/2)} \sin^2(\omega\Delta t/2)e^{-i\omega\Delta t(k-k')}, \quad 0 < k' < k < N \ , \tag{B.1}
$$

$$
\eta_{00} = \eta_{NN} = \frac{1}{2\pi} \int\limits_{-\infty}^{\infty} d\omega \frac{J(\omega)e^{\beta\hbar\omega/2}}{\omega^2 \sinh(\beta\hbar\omega/2)} \left(1 - e^{-i\omega\Delta t/2}\right) \ , \tag{B.2}
$$

$$
\eta_{0N} = \frac{2}{\pi} \int\limits_{-\infty}^{\infty} d\omega \frac{J(\omega)e^{\beta\hbar\omega/2}}{\omega^2 \sinh(\beta\hbar\omega/2)} \sin^2(\omega\Delta t/4)e^{-i\omega(t-\Delta t/2)} \ , \tag{B.3}
$$

$$
\eta_{0k} = \frac{2}{\pi} \int\limits_{-\infty}^{\infty} d\omega \frac{J(\omega)e^{\beta\hbar\omega/2}}{\omega^2 \sinh(\beta\hbar\omega/2)} \sin(\omega\Delta t/4) \sin(\omega\Delta t/2)e^{-i\omega(k\Delta t-\Delta t/4)} \ , \quad 0 < k < N \ , \tag{B.4}
$$

$$
\eta_{k'N} = \frac{2}{\pi} \int\limits_{-\infty}^{\infty} d\omega \frac{J(\omega)e^{\beta\hbar\omega/2}}{\omega^2 \sinh(\beta\hbar\omega/2)} \sin(\omega\Delta t/4) \sin(\omega\Delta t/2)e^{-i\omega(t-k'\Delta t-\Delta t/4)} \ , \quad 0 < k < N \ , \tag{B.5}
$$

$$
\eta_{kk} = \frac{1}{2\pi} \int\limits_{-\infty}^{\infty} d\omega \frac{J(\omega)e^{\beta\hbar\omega/2}}{\omega^2 \sinh(\beta\hbar\omega/2)} \left(1 - e^{-i\omega\Delta t}\right) \ , \quad 0 < k < N \ . \tag{B.6}
$$

B. Memory coefficients of the discrete influence functional

Note that η_{N0}, η_{k0} and η_{Nk} depend on the absolute values of k or N, respectively, since $t = N\Delta t$.

For the iterative propagation scheme the coefficients $\eta_{k'+N-\kappa,k+N-\kappa}$ appear in Eq. (4.73), where $k, k' = 0, \ldots, \kappa$. That means for $N > \kappa$ and if $k = \kappa$ the following coefficient has to be evaluated

$$
\eta_{k'+N-\kappa,k+N-\kappa} = \eta_{k'+N-\kappa,N} = \frac{2}{\pi} \int\limits_{-\infty}^{\infty} d\omega \frac{J(\omega)e^{\beta\hbar\omega/2}}{\omega^2 \sinh(\beta\hbar\omega/2)} \sin(\omega\Delta t/4)\sin(\omega\Delta t/2)
$$
$$
\times e^{-i\omega(t-(k'+N-\kappa)\Delta t-\Delta t/4)} \tag{B.7}
$$
$$
= \frac{2}{\pi} \int\limits_{-\infty}^{\infty} d\omega \frac{J(\omega)e^{\beta\hbar\omega/2}}{\omega^2 \sinh(\beta\hbar\omega/2)} \sin(\omega\Delta t/4)\sin(\omega\Delta t/2)
$$
$$
\times e^{-i\omega((\kappa-k')\Delta t-\Delta t/4)} \quad, \tag{B.8}
$$

since $t = N\Delta t$. The coefficient depends on k, which is in each iterative step in the range $0, \ldots, \kappa$. Note that if $N > \kappa$ the coefficients η_{N0}, η_{k0} do not enter the iterative scheme any more. Therefore, one can define the coefficients $\eta_{k'k}^{\text{mid-fin}}$ as discussed in Sec. 4.1.5 as

$$
\eta_{k'k}^{\text{mid-fin}} = \frac{2}{\pi} \int\limits_{-\infty}^{\infty} d\omega \frac{J(\omega)e^{\beta\hbar\omega/2}}{\omega^2 \sinh(\beta\hbar\omega/2)} \sin^2(\omega\Delta t/2)e^{-i\omega\Delta t(k-k')} \quad, \quad 0 \le k' < k < \kappa \tag{B.9}
$$

$$
\eta_{\kappa\kappa}^{\text{mid-fin}} = \frac{1}{2\pi} \int\limits_{-\infty}^{\infty} d\omega \frac{J(\omega)e^{\beta\hbar\omega/2}}{\omega^2 \sinh(\beta\hbar\omega/2)} \left(1 - e^{-i\omega\Delta t/2}\right) \quad, \tag{B.10}
$$

$$
\eta_{k'\kappa}^{\text{mid-fin}} = \frac{2}{\pi} \int\limits_{-\infty}^{\infty} d\omega \frac{J(\omega)e^{\beta\hbar\omega/2}}{\omega^2 \sinh(\beta\hbar\omega/2)} \sin(\omega\Delta t/4)\sin(\omega\Delta t/2)e^{-i\omega((\kappa-k')\Delta t-\Delta t/4)} \quad, 0 \le k' < \kappa \tag{B.11}
$$

$$
\eta_{kk}^{\text{mid-fin}} = \frac{1}{2\pi} \int\limits_{-\infty}^{\infty} d\omega \frac{J(\omega)e^{\beta\hbar\omega/2}}{\omega^2 \sinh(\beta\hbar\omega/2)} \left(1 - e^{-i\omega\Delta t}\right) \quad, \quad 0 \le k < \kappa \quad. \tag{B.12}
$$

Since κ is constant and k, k' are always in the range $0, \ldots, \kappa$ the coefficients $\eta_{k'k}^{\text{mid-fin}}$ do not change during the iteration.

For the case $N \le \kappa$ the coefficients $\eta_{k'k}^{\text{init-fin}}$ coincide with $\eta_{k'k}$ corresponding to the global propagation scheme. The coefficients corresponding to the lambda propagator read as

$$\eta_{0k}^{\mathrm{mid}} = \frac{2}{\pi} \int\limits_{-\infty}^{\infty} \mathrm{d}\omega \frac{J(\omega)\mathrm{e}^{\beta\hbar\omega/2}}{\omega^2 \sinh(\beta\hbar\omega/2)} \sin^2(\omega\Delta t/2)\mathrm{e}^{i\omega k\Delta t}, \quad 0 \le k \le \kappa \tag{B.13}$$

and

$$\eta_{00}^{\mathrm{init\text{-}mid}} = \frac{1}{2\pi} \int\limits_{-\infty}^{\infty} \mathrm{d}\omega \frac{J(\omega)\mathrm{e}^{\beta\hbar\omega/2}}{\omega^2 \sinh(\beta\hbar\omega/2)} \left(1 - \mathrm{e}^{-i\omega\Delta t/2}\right) , \tag{B.14}$$

$$\eta_{0k}^{\mathrm{init\text{-}mid}} = \frac{2}{\pi} \int\limits_{-\infty}^{\infty} \mathrm{d}\omega \frac{J(\omega)\mathrm{e}^{\beta\hbar\omega/2}}{\omega^2 \sinh(\beta\hbar\omega/2)} \sin(\omega\Delta t/4)\sin(\omega\Delta t/2)\mathrm{e}^{-i\omega(k\Delta t - \Delta t/4)} , \quad 0 < k \le \kappa . \tag{B.15}$$

B.2. Complex time propagation

The complex time memory coefficients for the global propagation scheme in Eq. (4.104) read as

$$\eta_{k'k}^{++} = \left(\eta_{k'k}^{--}\right)^* = \int\limits_{\tau_k}^{\tau_{k+1}} \mathrm{d}\tau \int\limits_{\tau_{k'}}^{\tau_{k'+1}} \mathrm{d}\tau' \mathscr{B}(\tau - \tau'), \quad k \ne k' \tag{B.16}$$

$$\eta_{kk}^{++} = \left(\eta_{kk}^{--}\right)^* = \int\limits_{\tau_k}^{\tau_{k+1}} \mathrm{d}\tau \left(\int\limits_{\tau_k}^{\tau_{k+1}} \mathrm{d}\tau' \mathscr{B}(\tau - \tau') + i\pi \int\limits_{0}^{\infty} \mathrm{d}\omega \frac{J(\omega)}{\omega} \right) \tag{B.17}$$

$$\eta_{k'k}^{+-} = \left(\eta_{k'k}^{-+}\right)^* = \int\limits_{\tau_k^* - i\beta\hbar}^{\tau_{k+1}^* - i\beta\hbar} \mathrm{d}\tau \int\limits_{\tau_{k'}}^{\tau_{k'+1}} \mathrm{d}\tau' \mathscr{B}(\tau - \tau'), \quad k \ne k' \tag{B.18}$$

$$\eta_{kk}^{+-} = \left(\eta_{kk}^{-+}\right)^* = \int\limits_{\tau_k^* - i\beta\hbar}^{\tau_{k+1}^* - i\beta\hbar} \mathrm{d}\tau \left(\int\limits_{\tau_k}^{\tau_{k+1}} \mathrm{d}\tau' \mathscr{B}(\tau - \tau') + i\pi \int\limits_{0}^{\infty} \mathrm{d}\omega \frac{J(\omega)}{\omega} \right) . \tag{B.19}$$

B. Memory coefficients of the discrete influence functional

The complex times

$$
\tau_k = \begin{cases}
0 \, , & k = 0 \\
-i\left(k - \frac{1}{2}\right)\Delta\beta \, , & k = 1, \ldots, P \\
\left(k - P - \frac{1}{2}\right)\Delta t - i\beta\hbar/2 \, , & k = P+1, \ldots, P+N \\
N\Delta t - i\beta\hbar/2 \, , & k = P+N+1 \; .
\end{cases}
\tag{B.20}
$$

are given by the complex time forward propagation of the bath within Eq. (E.7), see also the upper panel of Fig. E.1. Closed expressions are given in Ref. [30] and read as

$$
\eta_{k'k}^{++} = \left(\eta_{k'k}^{--}\right)^* = \frac{2}{\pi}\int\limits_{-\infty}^{\infty} d\omega \frac{J(\omega)}{\omega^2}\frac{\sin(\omega(\tau_{k+1} - \tau_k)/2)}{\sinh(\beta\hbar\omega/2)}
$$
$$
\times \sin(\omega(\tau_{k'+1} - \tau_{k'})/2)
$$
$$
\times \cos(\omega(\tau_{k+1} + \tau_k - \tau_{k'+1} - \tau_{k'} + i\beta\hbar)/2) \; ,
\tag{B.21}
$$

$$
\eta_{kk}^{++} = \left(\eta_{kk}^{--}\right)^* = \frac{1}{\pi}\int\limits_{-\infty}^{\infty} d\omega \frac{J(\omega)}{\omega^2}\frac{\sin(\omega(\tau_{k+1} - \tau_k)/2)}{\sinh(\beta\hbar\omega/2)}
$$
$$
\times \sin(\omega(\tau_{k+1} - \tau_k + i\beta\hbar)/2) \; ,
\tag{B.22}
$$

$$
\eta_{k'k}^{+-} = \left(\eta_{k'k}^{-+}\right)^* = \frac{2}{\pi}\int\limits_{-\infty}^{\infty} d\omega \frac{J(\omega)}{\omega^2}\frac{\sin(\omega(\tau_{k+1} - \tau_k)/2)}{\sinh(\beta\hbar\omega/2)}
$$
$$
\times \sin(\omega(\tau_{k'}^* - \tau_{k'+1}^*)/2)
$$
$$
\times \cos(\omega(\tau_{k'+1}^* + \tau_{k'}^* - \tau_{k+1} - \tau_k - i\beta\hbar)/2) \; ,
\tag{B.23}
$$

B. Memory coefficients of the discrete influence functional

$$\eta_{kk}^{+-} = \left(\eta_{kk}^{-+}\right)^* = \frac{2}{\pi} \int\limits_{-\infty}^{\infty} d\omega \frac{J(\omega)}{\omega^2} \frac{\sin(\omega(\tau_{k+1} - \tau_k)/2)}{\sinh(\beta\hbar\omega/2)}$$
$$\times \sin(\omega(\tau_k^* - \tau_{k+1}^*)/2)$$
$$\times \cos(\omega(\tau_{k+1}^* + \tau_k^* - \tau_{k+1} - \tau_k - i\beta\hbar)/2) \ , \tag{B.24}$$

If $N > \kappa$ the coefficients used for the iterative scheme read as

$$\eta_{k+N, k+N}^{++} = \left(\eta_{k+N, k+N}^{--}\right)^* = \frac{1}{\pi} \int\limits_{-\infty}^{\infty} d\omega \frac{J(\omega)}{\omega^2} \frac{\sin(\omega\Delta t/2)}{\sinh(\beta\hbar\omega/2)}$$
$$\times \sin(\omega(i\beta\hbar + \Delta t)/2) \ , \quad 0 \leq k < \kappa \tag{B.25}$$

$$\eta_{k'+N, k+N}^{++} = \left(\eta_{k'+N, k+N}^{--}\right)^* = \frac{2}{\pi} \int\limits_{-\infty}^{\infty} d\omega \frac{J(\omega)}{\omega^2} \frac{\sin^2(\omega\Delta t/2)}{\sinh(\beta\hbar\omega/2)}$$
$$\times \cos(\omega((k'-k)\Delta t - i\beta\hbar/2)) \ , \quad 0 \leq k' < k < \kappa \tag{B.26}$$

$$\eta_{k'+N, \kappa+N}^{++} = \left(\eta_{k'+N, \kappa+N}^{--}\right)^* = \frac{2}{\pi} \int\limits_{-\infty}^{\infty} d\omega \frac{J(\omega)}{\omega^2} \frac{\sin(\omega\Delta t/4)}{\sinh(\beta\hbar\omega/2)}$$
$$\times \sin(\omega\Delta t/2)$$
$$\times \cos(\omega((\kappa - k' - 1/4)\Delta t + i\beta\hbar/2)) \ , \quad 0 \leq k' < \kappa \tag{B.27}$$

$$\eta_{\kappa+N, \kappa+N}^{++} = \left(\eta_{\kappa+N, \kappa+N}^{--}\right)^* = \frac{1}{\pi} \int\limits_{-\infty}^{\infty} d\omega \frac{J(\omega)}{\omega^2} \frac{\sin(\omega\Delta t/4)}{\sinh(\beta\hbar\omega/2)}$$
$$\times \sin(\omega(i\beta\hbar + \Delta t/2)/2) \ , \tag{B.28}$$

B. Memory coefficients of the discrete influence functional

$$\eta_{k+N,\,k+N}^{+-} = \left(\eta_{k+N,\,k+N}^{-+}\right)^* = -\frac{1}{\pi}\int\limits_{-\infty}^{\infty}\mathrm{d}\omega\,\frac{J(\omega)}{\omega^2}\sin^2(\omega\Delta t/2)\coth(\beta\hbar\omega/2)\ ,\quad 0\le k<\kappa$$

$$\eta_{k'+N,k+N}^{+-} = \left(\eta_{k'+N,k+N}^{-+}\right)^* = -\frac{2}{\pi}\int\limits_{-\infty}^{\infty}\mathrm{d}\omega\,\frac{J(\omega)}{\omega^2}\frac{\sin^2(\omega\Delta t/2)}{\sinh(\beta\hbar\omega/2)}$$
$$\times\cos(\omega((k'-k)\Delta t+i\beta\hbar/2))\ ,\quad 0\le k'<k<\kappa\qquad(\text{B.29})$$

$$\eta_{k'+N,\kappa+N}^{+-} = \left(\eta_{k'+N,\kappa+N}^{-+}\right)^* = -\frac{2}{\pi}\int\limits_{-\infty}^{\infty}\mathrm{d}\omega\,\frac{J(\omega)}{\omega^2}\frac{\sin(\omega\Delta t/4)}{\sinh(\beta\hbar\omega/2)}$$
$$\times\sin(\omega\Delta t/2)$$
$$\times\cos(\omega((\kappa-k'-1/4)\Delta t-i\beta\hbar/2))\ ,\quad 0\le k'<\kappa\qquad(\text{B.30})$$

$$\eta_{\kappa+N,\,\kappa+N}^{+-} = \left(\eta_{\kappa+N,\,\kappa+N}^{-+}\right)^* = -\frac{1}{\pi}\int\limits_{-\infty}^{\infty}\mathrm{d}\omega\,\frac{J(\omega)}{\omega^2}\sin^2(\omega\Delta t/4)\coth(\beta\hbar\omega/2)\ .$$

Note that all coefficients do not depend on the global time step N, thus one can define the coefficients $\eta_{k'k}^{\pm\pm,\text{mid-fin}} = \eta_{k'+N,k+N}^{\pm\pm}$ and $\eta_{k'k}^{\pm\mp,\text{mid-fin}} = \eta_{k'+N,k+N}^{\pm\mp}$ where $k,k'=0,\dots,\kappa$ according to the last equations. The coefficients for the complex time lambda propagator read as $\eta_{0k}^{\pm\pm,\text{mid}} = \eta_{0k}^{\pm\pm,\text{mid-fin}}$ and $\eta_{0k}^{\pm\mp,\text{mid}} = \eta_{0k}^{\pm\mp,\text{mid-fin}}$ for $k=0,\dots,\kappa-1$ and

$$\eta_{0,\kappa}^{\text{mid},++} = \left(\eta_{k'+N,k+N}^{\text{mid},--}\right)^* = \frac{2}{\pi}\int\limits_{-\infty}^{\infty}\mathrm{d}\omega\,\frac{J(\omega)}{\omega^2}\frac{\sin^2(\omega\Delta t/2)}{\sinh(\beta\hbar\omega/2)}$$
$$\times\cos(\omega(-\kappa\Delta t-i\beta\hbar/2))\ ,\qquad(\text{B.31})$$

$$\eta_{0,\kappa}^{\text{mid},+-} = \left(\eta_{k'+N,k+N}^{\text{mid},-+}\right)^* = -\frac{2}{\pi}\int\limits_{-\infty}^{\infty}\mathrm{d}\omega\,\frac{J(\omega)}{\omega^2}\frac{\sin^2(\omega\Delta t/2)}{\sinh(\beta\hbar\omega/2)}$$
$$\times\cos(\omega(-\kappa\Delta t+i\beta\hbar/2))\ .\qquad(\text{B.32})$$

C. Algorithms

For a numerical treatment the FBCs are enumerated and are labled by $\tilde{\mathfrak{s}}^{l,\pm}$. The set $\mathbb{P}^{\theta}_{\kappa,M}$ can then be considered as an array, who's elements are the FBCs.

C.1. Global propagation of the first steps

The first κ propagation steps employ a global propagation. At the beginning of the propagation all convergence parameters Δt, M, κ and θ are set to proper values. Within each step the set $\mathbb{P}^{\theta}_{\kappa,M}$ is build up successively. The pseudo code is as follows:

Algorithm C.1

\# *** first step: $N = 1$ ***
$\mathbb{P}^{\theta}_{1,M} = \{\emptyset\}$, $l = 0$ \# initialize set of paths and number of FBCs
for $i = 0, \dots M - 1$ do   \# go over all possible end points of the forward path
   for $j = 0, \dots M - 1$ do   \# go over all possible end points of the backward path
     $l \to l + 1$ \# increment number of FBCs
     $\tilde{\mathfrak{s}}^{l,\pm} \equiv \begin{pmatrix} s_i \\ s_j \end{pmatrix}$ \# construct new FBC with index l
     $\mathbb{P}^{\theta}_{1,M} \to \left\{ \mathbb{P}^{\theta}_{1,M}, \tilde{\mathfrak{s}}^{l,\pm} \right\}$ \# accept new FBC in the set
   done
done
$L = l$ \# total number of FBCs

\# calculate RDM
for $i = 0, \dots M - 1$ do   \# go over all possible end points of the forward path
   for $j = 0, \dots M - 1$ do   \# go over all possible end points of the backward path
     $\rho^{M}_{\mathrm{s},i,j}(\Delta t) = \sum_{l=1}^{L} \tilde{F}^{\text{init-fin}}_{(0,1)} \left[\tilde{\mathfrak{s}}^{l,\pm}, s_i, s_j \right] \tilde{S}_{(0,1)} \left[\tilde{\mathfrak{s}}^{l,\pm}, s_i, s_j \right] \tilde{R} \left[\tilde{\mathfrak{s}}^{l,\pm}, 0 \right]$
     done
   done
done

Algorithm C.2

*** next steps: $N = 2, \ldots, \kappa$ ***
for $N = 2, \ldots, \kappa$
    $\mathbb{P}^{\theta}_{N,M} = \{\emptyset\}$, $l' = 0$ # initialize set of paths and number of FBCs
    for $l = 1, \ldots L$ do   # sum over all FBCs of the previous time step
        for $i = 0, \ldots M - 1$ do   # go over all possible end points of the forward path
            for $j = 0, \ldots M - 1$ do   # go over all possible end points of the backward path
$$\tilde{\mathfrak{p}}^{\pm} \equiv \left(\tilde{\mathfrak{s}}^{l,\pm}, \begin{array}{c} s_i \\ s_j \end{array} \right) \text{ with } \tilde{\mathfrak{s}}^{l,\pm} \in \mathbb{P}^{\theta}_{N-1,M} \quad \text{# construct a new temporary FBC}$$
                if $w_{N-1}\left[\tilde{\mathfrak{p}}^{\pm}\right] > \theta$ # check path weight of temporary FBC
                $l' \to l' + 1$ # increment number of FBCs
                $\tilde{\mathfrak{s}}^{l',\pm} \equiv \tilde{\mathfrak{p}}^{\pm}$ # new member of the set is indicated by l'
                $\mathbb{P}^{\theta}_{N,M} \to \left\{ \mathbb{P}^{\theta}_{N,M}, \tilde{\mathfrak{s}}^{l',\pm} \right\}$ # accept new FBC in the set
            end if
            done
        done
    done
    $L = l'$ # new total number of FBCs

calculate RDM
    for $i = 0, \ldots M - 1$ do   # go over all possible end points of the forward path
        for $j = 0, \ldots M - 1$ do   # go over all possible end points of the backward path
$$\rho^{M}_{s,i,j}(N\Delta t) = \sum_{l=1}^{L} \tilde{F}^{\text{init-fin}}_{(0,N)}\left[\tilde{\mathfrak{s}}^{l,\pm}, s_i, s_j\right] \tilde{S}_{(0,N)}\left[\tilde{\mathfrak{s}}^{l,\pm}, s_i, s_j\right] \tilde{R}\left[\tilde{\mathfrak{s}}^{l,\pm}, 0\right]$$
        done
    done
done

Note that at the end of this propagation the set $\mathbb{P}^{\theta}_{\kappa,M}$ consisting of L elements is fully determined and can be used for the iterative procedure.

C.2. Binning of the FBCs by their path weights

This section is a kind of preparation of the following section, which is focused on the lambda propagator. An efficient way to calculate this propagator utilizes a histogram of the FBCs binned by their path weights. This method is especially adopted from Ref. [31]. The goal of this section is to create a histogram, which can be used to set up the lambda propagator reasonably.

The indices $l = 1, \ldots, L$ of all FBCs in $\mathbb{P}^{\theta}_{\kappa,M}$ are distributed over n_{bins} with respect to the path weight $w_{\kappa-1}\left[\tilde{\mathfrak{s}}^{l,\pm}\right]$. Each bin $\mathbb{B}_i$, $i = 0, \ldots, n_{\text{bins}} - 1$ is then a set of integer numbers, where each number number is the index of a particular FBC. The resulting histogram spans the total interval $\left[w_{\text{min}} \equiv \min_{\mathbb{P}^{\theta}_{\kappa,M}}\left\{w_{\kappa-1}\left[\tilde{\mathfrak{s}}^{\pm}\right]\right\}, w_{\text{max}} \equiv \max_{\mathbb{P}^{\theta}_{\kappa,M}}\left\{w_{\kappa-1}\left[\tilde{\mathfrak{s}}^{\pm}\right]\right\}\right]$. The goal is to fill up all bins approximately equally, since this provides the most efficient calculation of the lambda propagator, see Sec. C.3 and Sec. C.4. It can be seen that the majority of FBCs have very small weights. Consequently, an equidistant slicing of the histogram would fail to distribute the number of FBCs per bin equally. A much more efficient interval spacing is presented in this thesis. The function $g(w)$ that assigns a particular FBC $\tilde{\mathfrak{s}}^{\pm} \in \mathbb{P}^{\theta}_{\kappa,M}$ with the path weight $w = w_{\kappa-1}\left[\tilde{\mathfrak{s}}^{\pm}\right]$ to a bin index i is as follows

$$g(w) \equiv (n_{\text{bins}} - 1) \sqrt[b]{\left(\frac{w - w_{\text{min}}}{w_{\text{max}} - w_{\text{min}}}\right)}, \quad i = \underline{g(w)} \tag{C.1}$$

where $b > 1$ is an arbitrary integer and $\underline{\;\cdot\;}$ denotes the floor function. The result of this function are bins with an index-dependent width

$$\Delta w_i = \frac{(i+1)^b - i^b}{(n_{\text{bins}} - 1)^b}, \tag{C.2}$$

which is much more narrow for small i than in the case of equidistant spacing, where $\Delta w = 1/(n_{\text{bins}} - 1)$. The parameter b has to be chosen properly for given setup. With these definitions at hand one can formulate the following algorithm for creating the histogram

---

Algorithm C.3

---

for $i = 0, \ldots, n_{\text{bins}} - 1$
  $\mathbb{B}_i = \{\emptyset\}$ # initialize all bins as empty sets
done

for $l = 1, \ldots, L$ do   # go over all FBCs in $\mathbb{P}^{\theta}_{\kappa,M}$
  $w \equiv w_{\kappa-1}\left[\tilde{\mathfrak{s}}^{l,\pm}\right]$ # calculate path weight of the l-th FBC
  $i \equiv g(w)$ # determine the corresponding bin
  $\mathbb{B}_i \rightarrow \{\mathbb{B}_i, l\}$ # put FBC index into the bin
done

C.3. Preparation for the lambda propagator

In order to calculate the RDM for time steps $N > \kappa$ the discrete multi-time reduced density functional is propagated via Eq. (4.78). The goal is now to recast the propagation as

$$\tilde{R}\left[\tilde{\mathfrak{s}}^{l,\pm};\,(k+1)\Delta t\right] = \sum_{p\in\mathbb{I}_l} \Lambda_{(k,k+\kappa)}\left[\tilde{\mathfrak{s}}^{p,\pm},\,\tilde{\mathfrak{s}}^{l,\pm}\right]\cdot\tilde{R}\left[\tilde{\mathfrak{s}}^{p,\pm};\,k\Delta t\right]\quad,\tag{C.3}$$

where $\tilde{\mathfrak{s}}^{l,\pm}$ *and* $\tilde{\mathfrak{s}}^{p,\pm}$ are in $\mathbb{P}^{\theta}_{\kappa,M}$. By doing this, one is able to evaluate Eq. (C.3) without the explicit storage of the subset $\mathbb{P}^{\theta}_{\kappa,M}\left[\tilde{\mathfrak{s}}^{l,\pm}\right]$. It is sufficient to know the set of indices $\mathbb{I}_l$ of FBCs in $\mathbb{P}^{\theta}_{\kappa,M}$ that are possible histories of the particular FBC $\tilde{\mathfrak{s}}^{l,\pm}$. The evaluation of Eq. (C.3) then remains remains exclusively in the set $\mathbb{P}^{\theta}_{\kappa,M}$. How this set of indices is determined in the following algorithm:

Algorithm C.4

*** determine set of indices $\mathbb{I}_l$ ***
for $l = 1,\ldots,L$ do   # go over all FBCs in $\mathbb{P}^{\theta}_{\kappa,M}$
  $\mathbb{I}_l = \{\emptyset\}$ # initialize set as empty set
  for $i = 0,\ldots M-1$ do   # go over all possible histories of $\tilde{\mathfrak{s}}^{l,+}$
    for $j = 0,\ldots M-1$ do   # go over all possible histories of $\tilde{\mathfrak{s}}^{l,-}$
      $\tilde{\mathfrak{p}}^{\pm} \equiv \begin{pmatrix} s_i & \tilde{\mathfrak{s}}^+_0 & \cdots & \tilde{\mathfrak{s}}^+_{\kappa-2} \\ s_j & \tilde{\mathfrak{s}}^-_0 & \cdots & \tilde{\mathfrak{s}}^-_{\kappa-2} \end{pmatrix}$ # define temporary FBC
      $w \equiv w_{\kappa-1}\left[\tilde{\mathfrak{p}}^{\pm}\right]$ # calculate weight of temporary FBC
      if $w_{\kappa-1}\left[\tilde{\mathfrak{p}}^{\pm}\right] > \theta$ # has $\tilde{\mathfrak{p}}^{\pm}$ a sufficient weight?
        $k \equiv g(w)$ # determine bin of $\tilde{\mathfrak{p}}^{\pm}$
        for $p \in \mathbb{B}_k$ do   # go over all indices in the bin
          if $\tilde{\mathfrak{p}}^{\pm} = \tilde{\mathfrak{s}}^{p,\pm}$ # compare temporary FBC with FBCs in the bin
            $\mathbb{I}_l = \{\mathbb{I}_l,\,p\}$ # collect the indices of all history FBCs of $\tilde{\mathfrak{s}}^{l,\pm}$
            break for loop
          end if
        done
      end if
    done
  done
done

C.4. The iterative propagation

This subsection describes the ongoing propagation for the time steps $N = \kappa + 1, \ldots, \infty$. In order to avoid redundant recalculations the following *time-independent* quantities are defined. The *propagator matrix* $\check{P} \in \mathbb{C}^{M^2 \times L}$ with elements $P_{iM+j,l}$ and the *lambda array* consisting of elements Λ_{lp}. Additionally the time-dependent *multi-time reduced density vector* $\boldsymbol{R}(N\Delta t) \in \mathbb{C}^L$ with elements $R_l(N\Delta t)$ and a temporary vector $\boldsymbol{Y} \in \mathbb{C}^L$ with elements Y_l are defined. The algorithm is as follows

---

Algorithm C.5

*** first iterative step: $N = \kappa + 1$ ***
for $l = 1, \ldots, L$ do   # go over all FBCs in $\mathbb{P}^{\theta}_{\kappa,M}$

    $Y_l = \left\langle \tilde{\sigma}_0^{l,+} \left| \hat{\rho}_{\mathrm{s}}(0) \right| \tilde{\sigma}_0^{l,-} \right\rangle$ # initialize temporary vector with initial condition

    $R_l(0) = 0$ # initialize multi-time reduced density vector

done

propagate multi-time reduced density vector by one time step
for $l = 1, \ldots, L$ do   # go over all FBCs in $\mathbb{P}^{\theta}_{\kappa,M}$

    for $p \in \mathbb{I}_l$ do   # go over all possible histories of $\tilde{\mathfrak{s}}^{l,\pm}$

        $R_l(\Delta t) \rightarrow R_l(\Delta t) + \Lambda^{\text{init-mid}} \left[\tilde{\mathfrak{s}}^{p,\pm}, \tilde{\mathfrak{s}}^{l,\pm} \right] \cdot Y_p$ # calculate new multi-time reduced density vector

    done

done

set up propagator matrix
for $l = 1, \ldots, L$ do   # go over all FBCs in $\mathbb{P}^{\theta}_{\kappa,M}$

    for $i = 0, \ldots M - 1$ do   # go over all possible end points of the forward path

        for $j = 0, \ldots M - 1$ do   # go over all end points of the backward path

            $P_{iM+j,l} \equiv \tilde{F}^{\text{mid-fin}}_{(0,\kappa)} \left[\tilde{\mathfrak{s}}^{l,\pm}, s_i, s_j \right] \tilde{S}_{(0,\kappa)} \left[\tilde{\mathfrak{s}}^{l,\pm}, s_i, s_j \right]$

        done

    done

done

calculate RDM
for $i = 0, \ldots M - 1$ do   # go over all possible end points of the forward path

    for $j = 0, \ldots M - 1$ do   # go over all possible end points of the backward path

        $\rho^M_{\mathrm{s},i,j}((\kappa + 1)\Delta t) = \sum_{l=1}^{L} P_{iM+j,l} R_l(\Delta t)$

    done

done

Algorithm C.6

$\#$ *** following iterative steps: $N = \kappa + 2, \ldots, \infty$ ***

$\#$ set up lambda array
for $l = 1, \ldots, L$ do
 for $p \in \mathbb{I}_l$ do
  $\Lambda_{lp} \equiv \Lambda^{\text{mid}} \left[\tilde{\mathfrak{s}}^{p,\pm}, \tilde{\mathfrak{s}}^{l,\pm} \right]$
 done
done

$\#$ ongoing iterative propagation
for $N = \kappa + 2, \ldots \infty$ do
 for $l = 1, \ldots, L$ do $\#$ go over all FBCs in $\mathbb{P}^{\theta}_{\kappa, M}$
  $Y_l = R_l((N - \kappa - 1)\Delta t)$ $\#$ initialize temporary vector
  $R_l((N - \kappa)\Delta t) = 0$ $\#$ initialize multi-time reduced density vector
 done
 for $l = 1, \ldots, L$ do $\#$ go over all FBCs in $\mathbb{P}^{\theta}_{\kappa, M}$
  for $p \in \mathbb{I}_l$ do $\#$ go over all possible histories of $\tilde{\mathfrak{s}}^{l,\pm}$
   $R_l((N - \kappa)\Delta t) \to R_l((N - \kappa)\Delta t) + \Lambda_{lp} \cdot Y_p$ $\#$ calculate new multi-time reduced density vector
  done
 done
$\#$ calculate RDM
 for $i = 0, \ldots M - 1$ do $\#$ go over all possible end points of the forward path
  for $j = 0, \ldots M - 1$ do $\#$ go over all possible end points of the backward path
   $\rho^M_{\text{s},i,j}(N\Delta t) = \sum_{l=1}^{L} P_{iM+j,l} R_l((N - \kappa)\Delta t)$
  done
 done
done

D. The discrete TCF for $N = 0$

For the special case $N = 0$ the calculation of the TCF corresponds to a pure imaginary time propagation. In order to derive an expression that can be treated numerically, the TCF can be rewritten as

$$C_{\Gamma\Omega}(0) \equiv \frac{1}{Z(\beta)} \mathrm{Tr} \left[\underbrace{\mathrm{e}^{-\hat{H}\Delta\beta/\hbar} \cdots \mathrm{e}^{-\hat{H}\Delta\beta/\hbar}}_{P \text{ times}} \hat{\Gamma}\hat{\Omega} \underbrace{\mathrm{e}^{-\hat{H}\Delta\beta/\hbar} \cdots \mathrm{e}^{-\hat{H}\Delta\beta/\hbar}}_{P \text{ times}} \right] .$$

$$\equiv \frac{1}{Z(\beta)} \mathrm{Tr}_\mathrm{B} \left[\int_{-\infty}^{\infty} \mathrm{d}s_0 \int_{-\infty}^{\infty} \mathrm{d}s_1^+ \cdots \int_{-\infty}^{\infty} \mathrm{d}s_{P-1}^+ \int_{-\infty}^{\infty} \mathrm{d}s^+ \int_{-\infty}^{\infty} \mathrm{d}s_1^- \cdots \int_{-\infty}^{\infty} \mathrm{d}s_{P-1}^- \int_{-\infty}^{\infty} \mathrm{d}s^- \right.$$

$$\times \left\langle s_0 \right| \mathrm{e}^{-\hat{H}\Delta\beta/\hbar} \left| s_1^- \right\rangle \left\langle s_1^- \right| \mathrm{e}^{-\hat{H}\Delta\beta/\hbar} \left| s_2^- \right\rangle \cdots \left\langle s_{P-2}^- \right| \mathrm{e}^{-\hat{H}\Delta\beta/\hbar} \left| s_{P-1}^- \right\rangle \left\langle s_{P-1}^- \right| \mathrm{e}^{-\hat{H}\Delta\beta/\hbar} \left| s^- \right\rangle$$

$$\times \left\langle s^- \right| \hat{\Gamma}\hat{\Omega} \left| s^+ \right\rangle \left\langle s^+ \right| \mathrm{e}^{-\hat{H}\Delta\beta/\hbar} \left| s_{P-1}^+ \right\rangle \cdots \left\langle s_2^+ \right| \mathrm{e}^{-\hat{H}\Delta\beta/\hbar} \left| s_1^+ \right\rangle \left\langle s_1^+ \right| \mathrm{e}^{-\hat{H}\Delta\beta/\hbar} \left| s_0 \right\rangle , \quad \text{(D.1)}$$

where spatial closures have been inserted in between the imaginary time propagators. After replacing the continuous integrals by sums over the DVR states, the discrete TCF takes the form

$$\tilde{C}_{\Gamma\Omega}(0) \equiv \frac{1}{Z(\beta)} \mathrm{Tr}_\mathrm{B} \left[\sum_{i_0=0}^{M-1} \sum_{i_1^+=0}^{M-1} \cdots \sum_{i_{P-1}^+=0}^{M-1} \sum_{i^+=0}^{M-1} \sum_{i_1^-=0}^{M-1} \cdots \sum_{i_{P-1}^-=0}^{M-1} \sum_{i^-=0}^{M-1} \right.$$

$$\left\langle \tilde{s}_{i_0} \right| \mathrm{e}^{-\hat{H}\Delta\beta/\hbar} \left| \tilde{s}_{i_1^-} \right\rangle \left\langle \tilde{s}_{i_1^-} \right| \mathrm{e}^{-\hat{H}\Delta\beta/\hbar} \left| \tilde{s}_{i_2^-} \right\rangle \cdots \left\langle \tilde{s}_{i_{P-1}^-} \right| \mathrm{e}^{-\hat{H}\Delta\beta/\hbar} \left| \tilde{s}_{i^-} \right\rangle \left\langle \tilde{s}_{i^-} \right| \hat{\Gamma}\hat{\Omega} \left| \tilde{s}_{i^+} \right\rangle$$

$$\times \left\langle \tilde{s}_{i^+} \right| \mathrm{e}^{-\hat{H}\Delta\beta/\hbar} \left| \tilde{s}_{i_{P-1}^+} \right\rangle \cdots \left\langle \tilde{s}_{i_2^+} \right| \mathrm{e}^{-\hat{H}\Delta\beta/\hbar} \left| \tilde{s}_{i_1^+} \right\rangle \left\langle \tilde{s}_{i_1^+} \right| \mathrm{e}^{-\hat{H}\Delta\beta/\hbar} \left| \tilde{s}_{i_0} \right\rangle \right] . \quad \text{(D.2)}$$

D. The discrete TCF for $N = 0$

Employing the Trotter factorization in Eq. (E.4) and separating bare system parts from system-bath dependent quantities leads to

$$
\tilde{C}_{\Gamma\Omega}(0) = \frac{1}{Z(\beta)} \sum_{i_0=0}^{M-1} \sum_{i_1^+=0}^{M-1} \cdots \sum_{i_{N+P-1}^+=0}^{M-1} \sum_{i_1^-=0}^{M-1} \cdots \sum_{i_{N+P-1}^-=0}^{M-1} \sum_{i=0}^{M-1}
$$

$$
f\left(\tilde{s}_i, \tilde{s}_{i_1^+}, \cdots, \tilde{s}_{i_{P-1}^+}, \tilde{s}_{i^+} \tilde{s}_{i_1^-}, \ldots, \tilde{s}_{i_{P-1}^-}, \tilde{s}_{i^-}\right)
$$

$$
\times \left\langle \tilde{s}_{i_0} \left| e^{-\hat{H}_S \Delta\beta/\hbar} \right| \tilde{s}_{i_1^-} \right\rangle \left\langle \tilde{s}_{i_1^-} \left| e^{-\hat{H}_S \Delta\beta/\hbar} \right| \tilde{s}_{i_2^-} \right\rangle \cdots \left\langle \tilde{s}_{i_{P-1}^-} \left| e^{-\hat{H}_S \Delta\beta/\hbar} \right| \tilde{s}_{i^-} \right\rangle
$$

$$
\times \left\langle \tilde{s}_{i^-} \left| \hat{\Gamma}\hat{\Omega} \right| \tilde{s}_{i^+} \right\rangle \left\langle \tilde{s}_{i^+} \left| e^{-\hat{H}_S \Delta\beta/\hbar} \right| \tilde{s}_{i_{P-1}^+} \right\rangle \cdots \left\langle \tilde{s}_{i_2^+} \left| e^{-\hat{H}_S \Delta\beta/\hbar} \right| \tilde{s}_{i_1^+} \right\rangle \left\langle \tilde{s}_{i_1^+} \left| e^{-\hat{H}_S \Delta\beta/\hbar} \right| \tilde{s}_{i_0} \right\rangle , \quad \text{(D.3)}
$$

where

$$
f\left(\tilde{s}_0, \tilde{s}_1^+, \cdots, \tilde{s}_{P-1}^+, \tilde{s}^+, \tilde{s}_1^-, \ldots, \tilde{s}_{P-1}^-, \tilde{s}^-\right) \equiv
$$

$$
\text{Tr}_B \left[e^{-\hat{H}_{SB}(\tilde{s}_0)\Delta\beta/(2\hbar)} e^{-\hat{H}_{SB}(\tilde{s}_1^-)\Delta\beta/\hbar} \cdots e^{-\hat{H}_{SB}(\tilde{s}_{P-1}^-)\Delta\beta/\hbar} e^{-\hat{H}_{SB}(\tilde{s}^-)\Delta\beta/(2\hbar)} \right.
$$

$$
\left. \times e^{-\hat{H}_{SB}(\tilde{s}^+)\Delta\beta/(2\hbar)} e^{-\hat{H}_{SB}(\tilde{s}_{P-1}^+)\Delta\beta/\hbar} \cdots e^{-\hat{H}_{SB}(\tilde{s}_1^+)\Delta\beta/\hbar} e^{-\hat{H}_{SB}(\tilde{s}_0)\Delta\beta/(2\hbar)} \right] \quad \text{(D.4)}
$$

contains the the influence from the bath onto the system. The sequence of coordinates $\tilde{s}_{i_0}, \tilde{s}_{i_1^+}, \ldots, \tilde{s}_{i_{P-1}^+}, \tilde{s}_{i^+}, \tilde{s}_{i_1^-}, \ldots, \tilde{s}_{i_{P-1}^-}, \tilde{s}_{i^-}$ is now replaced by an *imaginary time FBC*

$$
\tilde{\mathfrak{s}}^\pm \equiv \begin{pmatrix} \tilde{\mathfrak{s}}_0 & \tilde{\mathfrak{s}}_1^+ & \cdots & \tilde{\mathfrak{s}}_{P-1}^+ \\ \tilde{\mathfrak{s}}_0 & \tilde{\mathfrak{s}}_1^- & \cdots & \tilde{\mathfrak{s}}_{P-1}^- \end{pmatrix} = \begin{pmatrix} \tilde{s}_{i_0} & \tilde{s}_{i_1^+} & \cdots & \tilde{s}_{i_{P-1}^+} \\ \tilde{s}_{i_0} & \tilde{s}_{i_1^-} & \cdots & \tilde{s}_{i_{P-1}^-} \end{pmatrix} \quad \text{(D.5)}
$$

with end points $\tilde{s}_{i^+}, \tilde{s}_{i^-}$. Note that in contrast to the expression for $\tilde{C}_{\Gamma\Omega}(N\Delta t)$, where $N > 0$, the endpoints do not necessarily coincide. With the definition of the imaginary time FBC, the TCF for $N = 0$ can be written as a discrete PI

$$
\tilde{C}_{\Gamma\Omega}(0) = \frac{1}{Z(\beta)} \sum_{i^\pm=0}^{M-1} \sum_{\tilde{\mathfrak{s}}^\pm \in \mathbb{P}_{P,M}} \tilde{\mathscr{F}}_{(0,P)} \left[\tilde{\mathfrak{s}}^\pm, \tilde{s}_{i^\pm}\right] \tilde{\mathscr{S}}_{(0,P)}^{\Gamma\Omega} \left[\tilde{\mathfrak{s}}^\pm, \tilde{s}_{i^\pm}\right] , \quad \text{(D.6)}
$$

where

$$
\tilde{\mathscr{S}}_{(0,P)}^{\Gamma\Omega} \left[\tilde{\mathfrak{s}}^\pm, \tilde{s}_{i^\pm}\right] \equiv \prod_{k=0}^{P-1} \tilde{\mathscr{S}}_{(k,k+1)}^{\Gamma\Omega} \left(\tilde{\mathfrak{s}}_k^\pm, \tilde{\mathfrak{s}}_{k+1}^\pm\right) , \quad \text{(D.7)}
$$

is the *discrete imaginary time bare system part* of the PI. The quantity $\tilde{\mathscr{S}}^{\Gamma\Omega}_{(0,P)}\left[\tilde{\mathfrak{s}}^\pm, \tilde{s}_{i^\pm}\right]$ is a product of *imaginary time bare system point-to-point propagators*

$$\tilde{\mathscr{S}}_{(k,k+1)}\left(\tilde{\mathfrak{s}}_k^\pm, \tilde{\mathfrak{s}}_{k+1}^\pm\right) \equiv \begin{cases} \left\langle\underline{\tilde{\mathfrak{s}}_k^-}\left|\mathrm{e}^{-\hat{H}_\mathrm{S}\Delta\beta/\hbar}\right|\underline{\tilde{\mathfrak{s}}_{k+1}^-}\right\rangle\left\langle\underline{\tilde{\mathfrak{s}}_{k+1}^+}\left|\mathrm{e}^{-\hat{H}_\mathrm{S}\Delta\beta/\hbar}\right|\underline{\tilde{\mathfrak{s}}_k^+}\right\rangle, & 0 \leq k \leq P-1 \\ \left\langle\underline{\tilde{s}_{i^-}}\left|\hat{\Gamma}\hat{\Omega}\right|\underline{\tilde{s}_{i^-}}\right\rangle, & k = P \end{cases} \tag{D.8}$$

The influence of the bath is contained in the *discrete imaginary time influence functional*

$$\tilde{\mathscr{F}}_{(0,P)}\left[\tilde{\mathfrak{s}}^\pm, \tilde{s}_{i^\pm}\right] \equiv f\left(\tilde{\mathfrak{s}}_0, \tilde{\mathfrak{s}}_1^+, \ldots, \tilde{\mathfrak{s}}_P^+, \tilde{s}_{i^+}, \tilde{\mathfrak{s}}_1^-, \ldots, \tilde{\mathfrak{s}}_P^-, \tilde{s}_{i^-}\right). \tag{D.9}$$

Note that $\sum_{i^\pm=0}^{M-1} \equiv \sum_{i^+=0}^{M-1}\sum_{i^-=0}^{M-1}$ is a two-fold sum over the end points and the set $\mathbb{P}_{P,M}$ is defined in Eq. (4.102).

E. Numerical treatment of the TCF

Analogously to Sec. 4.1.1, the integrals in Eq. (4.98) are replaced by sums over M grid points $\tilde{s}_i \in \mathbb{S}_M$

$$\int_{-\infty}^{\infty} \mathrm{d}s_k^{\pm} \left| s_k^{\pm} \right\rangle \left\langle s_k^{\pm} \right| \rightarrow \sum_{i_k^{\pm}=0}^{M-1} \left| \underline{\tilde{s}_{i_k^{\pm}}} \right\rangle \left\langle \underline{\tilde{s}_{i_k^{\pm}}} \right| \tag{E.1}$$

and also

$$\int_{-\infty}^{\infty} \mathrm{d}s_0 \left\langle s_0 \right| \cdot \left| s_0 \right\rangle \rightarrow \sum_{i_0=0}^{M-1} \left\langle \underline{\tilde{s}_{i_0}} \right| \cdot \left| \underline{\tilde{s}_{i_0}} \right\rangle \;, \tag{E.2}$$

where the states $\left| \underline{\tilde{s}_i} \right\rangle$ form the DVR basis according to Sec. 4.1.2. The result is the *discrete TFC*

$$\tilde{C}_{\Gamma\Omega}(N\Delta t) \equiv \frac{1}{Z(\beta)} \mathrm{Tr}_{\mathrm{B}} \left[\sum_{i_0=0}^{M-1} \sum_{i_1^+=0}^{M-1} \cdots \sum_{i_{N+P-1}^+=0}^{M-1} \sum_{i_1^-=0}^{M-1} \cdots \sum_{i_{N+P-1}^-=0}^{M-1} \sum_{i=0}^{M-1} \right.$$

$$\left\langle \underline{\tilde{s}_{i_0}} \right| \mathrm{e}^{-\hat{H}\Delta\beta/\hbar} \left| \underline{\tilde{s}_{i_1^-}} \right\rangle \left\langle \underline{\tilde{s}_{i_1^-}} \right| \mathrm{e}^{-\hat{H}\Delta\beta/\hbar} \left| \underline{\tilde{s}_{i_2^-}} \right\rangle \cdots \left\langle \underline{\tilde{s}_{i_{P-1}^-}} \right| \mathrm{e}^{-\hat{H}\Delta\beta/\hbar} \left| \underline{\tilde{s}_{i_P^-}} \right\rangle$$

$$\times \left\langle \underline{\tilde{s}_{i_P^-}} \right| \hat{\Gamma} \mathrm{e}^{i\hat{H}\Delta t/\hbar} \left| \underline{\tilde{s}_{i_{P+1}^-}} \right\rangle \left\langle \underline{\tilde{s}_{i_{P+1}^-}} \right| \mathrm{e}^{i\hat{H}\Delta t/\hbar} \left| \underline{\tilde{s}_{i_{P+2}^-}} \right\rangle \cdots \left\langle \underline{\tilde{s}_{i_{P+N-1}^-}} \right| \mathrm{e}^{i\hat{H}\Delta t/\hbar} \left| \underline{\tilde{s}_i} \right\rangle$$

$$\times \left\langle \underline{\tilde{s}_i} \right| \hat{\Omega} \mathrm{e}^{-i\hat{H}\Delta t/\hbar} \left| \underline{\tilde{s}_{i_{P+N-1}^+}} \right\rangle \left\langle \underline{\tilde{s}_{i_{P+N-1}^+}} \right| \mathrm{e}^{-i\hat{H}\Delta t/\hbar} \left| \underline{\tilde{s}_{i_{P+N-2}^+}} \right\rangle \cdots \left\langle \underline{\tilde{s}_{i_{P+1}^+}} \right| \mathrm{e}^{-i\hat{H}\Delta t/\hbar} \left| \underline{\tilde{s}_{i_P^+}} \right\rangle$$

$$\left. \times \left\langle \underline{\tilde{s}_{i_P^+}} \right| \mathrm{e}^{-\hat{H}\Delta\beta/\hbar} \left| \underline{\tilde{s}_{i_{P-1}^+}} \right\rangle \cdots \left\langle \underline{\tilde{s}_{i_2^+}} \right| \mathrm{e}^{-\hat{H}\Delta\beta/\hbar} \left| \underline{\tilde{s}_{i_1^+}} \right\rangle \left\langle \underline{\tilde{s}_{i_1^+}} \right| \mathrm{e}^{-\hat{H}\Delta\beta/\hbar} \left| \underline{\tilde{s}_{i_0}} \right\rangle \right] \;. \tag{E.3}$$

The application of the Trotter factorization

$$\exp\left\{ -\frac{1}{\hbar} \hat{H} \Delta\beta \right\} \approx \exp\left\{ -\frac{1}{2\hbar} \hat{H}_{\mathrm{SB}} \Delta\beta \right\} \exp\left\{ -\frac{1}{\hbar} \hat{H}_{\mathrm{S}} \Delta\beta \right\} \exp\left\{ -\frac{1}{2\hbar} \hat{H}_{\mathrm{SB}} \Delta\beta \right\} \tag{E.4}$$

leads to the approximation

$$\left\langle \tilde{s}_{i_{k+2}^+} \middle| \mathrm{e}^{-\hat{H}\Delta\beta/\hbar} \middle| \tilde{s}_{i_{k+1}^+} \right\rangle \left\langle \tilde{s}_{i_{k+1}^+} \middle| \mathrm{e}^{-\hat{H}\Delta\beta/\hbar} \middle| \tilde{s}_{i_k^+} \right\rangle \approx$$

$$\exp\left\{ -\frac{1}{2\hbar} \hat{H}_{\mathrm{SB}}\left(\tilde{s}_{i_{k+2}^+}\right)\Delta\beta \right\} \exp\left\{ -\frac{1}{\hbar} \hat{H}_{\mathrm{SB}}\left(\tilde{s}_{i_{k+1}^+}\right)\Delta\beta \right\} \exp\left\{ -\frac{1}{2\hbar} \hat{H}_{\mathrm{SB}}\left(\tilde{s}_{i_k^+}\right)\Delta\beta \right\}$$

$$\times \left\langle \tilde{s}_{i_{k+2}^+} \middle| \mathrm{e}^{-\hat{H}_{\mathrm{S}}\Delta\beta/\hbar} \middle| \tilde{s}_{i_{k+1}^+} \right\rangle \left\langle \tilde{s}_{i_{k+1}^+} \middle| \mathrm{e}^{-\hat{H}_{\mathrm{S}}\Delta\beta/\hbar} \middle| \tilde{s}_{i_k^+} \right\rangle \;, \quad \text{(E.5)}$$

which is transferable to quantities involving the states labeled by $\left| \tilde{s}_{i_k^-} \right\rangle$. After the separation of bare system parts and system-bath depending quantities, the discrete TCF becomes

$$\tilde{C}_{\Gamma\Omega}(N\Delta t) = \frac{1}{Z(\beta)} \sum_{i_0=0}^{M-1} \sum_{i_1^+=0}^{M-1} \cdots \sum_{i_{N+P-1}^+=0}^{M-1} \sum_{i_1^-=0}^{M-1} \cdots \sum_{i_{N+P-1}^-=0}^{M-1} \sum_{i=0}^{M-1}$$

$$f\left(\tilde{s}_{i_0}, \tilde{s}_{i_1^+}, \cdots, \tilde{s}_{i_{P+N-1}^+}, \tilde{s}_{i_1^-}, \ldots, \tilde{s}_{i_{P+N-1}^-}, \tilde{s}_i \right)$$

$$\times \left\langle \tilde{s}_{i_0} \middle| \mathrm{e}^{-\hat{H}_{\mathrm{S}}\Delta\beta/\hbar} \middle| \tilde{s}_{i_1^-} \right\rangle \left\langle \tilde{s}_{i_1^-} \middle| \mathrm{e}^{-\hat{H}_{\mathrm{S}}\Delta\beta/\hbar} \middle| \tilde{s}_{i_2^-} \right\rangle \cdots \left\langle \tilde{s}_{i_{P-1}^-} \middle| \mathrm{e}^{-\hat{H}_{\mathrm{S}}\Delta\beta/\hbar} \middle| \tilde{s}_{i_P^-} \right\rangle$$

$$\times \left\langle \tilde{s}_{i_P^-} \middle| \hat{\Gamma}\mathrm{e}^{i\hat{H}_{\mathrm{S}}\Delta t/\hbar} \middle| \tilde{s}_{i_{P+1}^-} \right\rangle \left\langle \tilde{s}_{i_{P+1}^-} \middle| \mathrm{e}^{i\hat{H}_{\mathrm{S}}\Delta t/\hbar} \middle| \tilde{s}_{i_{P+2}^-} \right\rangle \cdots \left\langle \tilde{s}_{i_{P+N-1}^-} \middle| \mathrm{e}^{i\hat{H}_{\mathrm{S}}\Delta t/\hbar} \middle| \tilde{s}_i \right\rangle$$

$$\times \left\langle \tilde{s}_i \middle| \hat{\Omega}\mathrm{e}^{-i\hat{H}_{\mathrm{S}}\Delta t/\hbar} \middle| \tilde{s}_{i_{P+N-1}^+} \right\rangle \left\langle \tilde{s}_{i_{P+N-1}^+} \middle| \mathrm{e}^{-i\hat{H}_{\mathrm{S}}\Delta t/\hbar} \middle| \tilde{s}_{i_{P+N-2}^+} \right\rangle \cdots \left\langle \tilde{s}_{i_{P+1}^+} \middle| \mathrm{e}^{-i\hat{H}_{\mathrm{S}}\Delta t/\hbar} \middle| \tilde{s}_{i_P^+} \right\rangle$$

$$\times \left\langle \tilde{s}_{i_P^+} \middle| \mathrm{e}^{-\hat{H}_{\mathrm{S}}\Delta\beta/\hbar} \middle| \tilde{s}_{i_{P-1}^+} \right\rangle \cdots \left\langle \tilde{s}_{i_2^+} \middle| \mathrm{e}^{-\hat{H}_{\mathrm{S}}\Delta\beta/\hbar} \middle| \tilde{s}_{i_1^+} \right\rangle \left\langle \tilde{s}_{i_1^+} \middle| \mathrm{e}^{-\hat{H}_{\mathrm{S}}\Delta\beta/\hbar} \middle| \tilde{s}_{i_0} \right\rangle \;, \quad \text{(E.6)}$$

where the system-bath interaction is implicitly contained in the multi-dimensional function

$$f\left(\tilde{s}_0, \tilde{s}_1^+, \cdots, \tilde{s}_{P+N-1}^+, \tilde{s}_1^-, \ldots, \tilde{s}_{P+N-1}^-, \tilde{s}_i \right) \equiv$$

$$\mathrm{Tr}_{\mathrm{B}}\left[\mathrm{e}^{-\hat{H}_{\mathrm{SB}}(\tilde{s}_0)\Delta\beta/(2\hbar)} \mathrm{e}^{-\hat{H}_{\mathrm{SB}}(\tilde{s}_1^-)\Delta\beta/\hbar} \cdots \mathrm{e}^{-\hat{H}_{\mathrm{SB}}(\tilde{s}_{P-1}^-)\Delta\beta/\hbar} \mathrm{e}^{-\hat{H}_{\mathrm{SB}}(\tilde{s}_P^-)\Delta\beta/(2\hbar)} \right.$$

$$\times \mathrm{e}^{i\hat{H}_{\mathrm{SB}}(\tilde{s}_P^-)\Delta t/(2\hbar)} \mathrm{e}^{i\hat{H}_{\mathrm{SB}}(\tilde{s}_{P+1}^-)\Delta t/\hbar} \cdots \mathrm{e}^{i\hat{H}_{\mathrm{SB}}(\tilde{s}_{P+N-1}^-)\Delta t/\hbar} \mathrm{e}^{i\hat{H}_{\mathrm{SB}}(\tilde{s}_i)\Delta t/(2\hbar)}$$

$$\times \mathrm{e}^{-i\hat{H}_{\mathrm{SB}}(\tilde{s}_i)\Delta t/(2\hbar)} \mathrm{e}^{-i\hat{H}_{\mathrm{SB}}(\tilde{s}_{P+N-1}^+)\Delta t/\hbar} \cdots \mathrm{e}^{-i\hat{H}_{\mathrm{SB}}(\tilde{s}_{P+1}^+)\Delta t/\hbar} \mathrm{e}^{-i\hat{H}_{\mathrm{SB}}(\tilde{s}_P^+)\Delta t/(2\hbar)}$$

$$\left. \times \mathrm{e}^{-\hat{H}_{\mathrm{SB}}(\tilde{s}_P^+)\Delta\beta/(2\hbar)} \mathrm{e}^{-\hat{H}_{\mathrm{SB}}(\tilde{s}_{P-1}^+)\Delta\beta/\hbar} \cdots \mathrm{e}^{-\hat{H}_{\mathrm{SB}}(\tilde{s}_1^+)\Delta\beta/\hbar} \mathrm{e}^{-\hat{H}_{\mathrm{SB}}(\tilde{s}_0)\Delta\beta/(2\hbar)} \right] \;, \quad \text{(E.7)}$$

which will be later defined as the discrete complex time influence functional. In analogy to Sec. 4.1.1 the grid point sequence $\tilde{s}_{i_0}, \tilde{s}_{i_1^+}, \ldots, \tilde{s}_{i_P^+}, \tilde{s}_{i_{P+1}^+}, \ldots, \tilde{s}_{i_{P+N-1}^+}, \tilde{s}_{i_1^-}, \ldots, \tilde{s}_{i_P^-}, \tilde{s}_{i_{P+1}^-} \ldots, \tilde{s}_{i_{P+N-1}^-}, \tilde{s}_i$

is within this thesis substituted by a *complex time* FBC, which is defined as

$$
\tilde{\mathfrak{s}}^{\pm} \equiv \begin{pmatrix} \tilde{\mathfrak{s}}_0 & \tilde{\mathfrak{s}}_1^+ & \cdots & \tilde{\mathfrak{s}}_P^+ & \tilde{\mathfrak{s}}_{P+1}^+ & \cdots & \tilde{\mathfrak{s}}_{P+N-1}^+ \\ \tilde{\mathfrak{s}}_0 & \tilde{\mathfrak{s}}_1^- & \cdots & \tilde{\mathfrak{s}}_P^- & \tilde{\mathfrak{s}}_{P+1}^- & \cdots & \tilde{\mathfrak{s}}_{P+N-1}^- \end{pmatrix} = \begin{pmatrix} \tilde{s}_{i_0} & \tilde{s}_{i_1^+} & \cdots & \tilde{s}_{i_P^+} & \tilde{s}_{i_{P+1}^+} & \cdots & \tilde{s}_{i_{P+N-1}^+} \\ \tilde{s}_{i_0} & \tilde{s}_{i_1^-} & \cdots & \tilde{s}_{i_P^-} & \tilde{s}_{i_{P+1}^-} & \cdots & \tilde{s}_{i_{P+N-1}^-} \end{pmatrix}
$$
(E.8)

with the *shared end point* $\tilde{s}_i$. The motivation for this substitution is according to Sec. 4.1.1. Note that Eq. (E.6) has to be read from the right to the left. If one considers the special case $N = P = M = 3$ and the particular summand σ, where the indices are fixed to $i_0 = 2$, $i_1^+ = 1$, $i_2^+ = 0$, $i_3^+ = 0$, $i_4^+ = 0$, $i_5^+ = 1$, $i_1^- = 1$, $i_2^- = 2$, $i_3^- = 1$, $i_4^- = 2$, $i_5^- = 1$ and $i = 0$, then two independent operations have to be performed.

First, the *bare* system is propagated stepwise in imaginary time starting at time zero and following the *discrete imaginary time path* $\tilde{\mathfrak{s}}_{\mathrm{im}}^+ \equiv \left(\tilde{\mathfrak{s}}_0, \tilde{\mathfrak{s}}_1^+, \tilde{\mathfrak{s}}_2^+, \tilde{\mathfrak{s}}_3^+ \right) \equiv \left(\tilde{s}_{i_0}, \tilde{s}_{i_1^+}, \tilde{s}_{i_2^+}, \tilde{s}_{i_3^+} \right) = \left(\tilde{s}_2, \tilde{s}_1, \tilde{s}_0, \tilde{s}_0 \right)$, see Fig. 4.9. The propagation ends at time $-3i\Delta\beta$. In the fifth line of Eq. (E.6) follows a propagation forward in the real time, where system follows the *discrete real time forward path* $\tilde{\mathfrak{s}}_{\mathrm{re}}^+ \equiv \left(\tilde{\mathfrak{s}}_4^+, \tilde{\mathfrak{s}}_5^+ \right) \equiv \left(\tilde{s}_{i_4^+}, \tilde{s}_{i_5^+} \right) = \left(\tilde{s}_0, \tilde{s}_1 \right)$. Within the last step, where the system is propagated to the shared end point $\tilde{s}_i = \tilde{s}_0$ at the particular complex time $\chi \equiv 3\Delta t - 3i\Delta\beta$, the time propagator $\mathrm{e}^{-i\hat{H}_{\mathrm{S}}\Delta t/\hbar}$ is multiplied by the operator $\hat{\Omega}$. Note that it is assumed that the multiplication does not change the effective size of the time step and, hence, the numerical stability is not affected. One can now attach the real time path to the imaginary time path and define the *discrete complex time forward path* $\tilde{\mathfrak{s}}^+ \equiv \left(\tilde{\mathfrak{s}}_{\mathrm{im}}^+, \tilde{\mathfrak{s}}_{\mathrm{re}}^+ \right)$. Here, forward with respect to a complex time is referred to a propagation, where the time argument changes as labeled on the vertical axis in Fig. 4.9. In other words, a complex time forward path spans the upper half of the complex time contour as depicted in Fig. 3.4. The fourth line in Eq. (E.6) represents a propagation of the bare system backward in the real time. Here, the system starts at the end point of the forward propagation $\tilde{s}_0$. Afterwards it follows *reversely* the *real time backward path* $\tilde{\mathfrak{s}}_{\mathrm{re}}^- \equiv \left(\tilde{\mathfrak{s}}_4^-, \tilde{\mathfrak{s}}_5^- \right) \equiv \left(\tilde{s}_{i_4^-}, \tilde{s}_{i_5^-} \right) = \left(\tilde{s}_2, \tilde{s}_1 \right)$. Within the last step backward in real time the system is propagated to the pure imaginary time $-3i\Delta\beta$. Here, the propagator $\mathrm{e}^{i\hat{H}_{\mathrm{S}}\Delta t/\hbar}$ is multiplied by the operator $\hat{\Gamma}$. It is assumed that the multiplication does not affect the numerical stability. What follows in the third line of Eq. (E.6), is the resumption of the pure imaginary time propagation of the sixth line. The system it follows *reversely* the coordinates of the discrete imaginary time path defined as $\tilde{\mathfrak{s}}_{\mathrm{im}}^- \equiv \left(\tilde{\mathfrak{s}}_0, \tilde{\mathfrak{s}}_1^-, \tilde{\mathfrak{s}}_2^-, \tilde{\mathfrak{s}}_3^- \right) \equiv \left(\tilde{s}_{i_0}, \tilde{s}_{i_1^-}, \tilde{s}_{i_2^-}, \tilde{s}_{i_3^-} \right) = \left(\tilde{s}_2, \tilde{s}_1, \tilde{s}_2, \tilde{s}_1 \right)$. The bare system propagation ends at the time $-6i\Delta\beta = -i\beta\hbar$. Attaching the path $\tilde{\mathfrak{s}}_{\mathrm{re}}^-$ to $\tilde{\mathfrak{s}}_{\mathrm{im}}^-$ creates the *discrete complex time backward path* $\tilde{\mathfrak{s}}^- \equiv \left(\tilde{\mathfrak{s}}_{\mathrm{im}}^-, \tilde{\mathfrak{s}}_{\mathrm{re}}^- \right)$. Here, the backward direction in

the complex time is defined by lower half of the complex time contour in Fig. 3.4. To conclude, according to the last four lines in Eq. (E.6), the first task in order to calculate the particular summand σ requires the propagation of the bare system along the FBC

$$
\tilde{\mathfrak{s}}^{\pm} \equiv \begin{pmatrix} \tilde{\mathfrak{s}}_0 & \tilde{\mathfrak{s}}_1^+ & \tilde{\mathfrak{s}}_2^+ & \tilde{\mathfrak{s}}_3^+ & \tilde{\mathfrak{s}}_4^+ & \tilde{\mathfrak{s}}_5^+ \\ \tilde{\mathfrak{s}}_0 & \tilde{\mathfrak{s}}_1^- & \tilde{\mathfrak{s}}_2^- & \tilde{\mathfrak{s}}_3^- & \tilde{\mathfrak{s}}_4^- & \tilde{\mathfrak{s}}_5^- \end{pmatrix} = \begin{pmatrix} \tilde{s}_2 & \tilde{s}_1 & \tilde{s}_0 & \tilde{s}_0 & \tilde{s}_0 & \tilde{s}_1 \\ \tilde{s}_2 & \tilde{s}_1 & \tilde{s}_2 & \tilde{s}_1 & \tilde{s}_2 & \tilde{s}_1 \end{pmatrix} .
\tag{E.9}
$$

with the shared end point $\tilde{s}_i = \tilde{s}_0$.

Second, the multi-dimensional function f appearing in the first line of Eq. (E.6) has to be evaluated. According to Eq. (E.7), f represents

$$
f \left(\tilde{s}_2, \tilde{s}_1, \tilde{s}_0, \tilde{s}_0, \tilde{s}_0, \tilde{s}_1, \tilde{s}_1, \tilde{s}_2, \tilde{s}_1, \tilde{s}_2, \tilde{s}_1, \tilde{s}_0 \right) =
$$
$$
f \left(\tilde{\mathfrak{s}}_0, \tilde{\mathfrak{s}}_1^+, \tilde{\mathfrak{s}}_2^+, \tilde{\mathfrak{s}}_3^+, \tilde{\mathfrak{s}}_4^+, \tilde{\mathfrak{s}}_5^+, \tilde{\mathfrak{s}}_1^-, \tilde{\mathfrak{s}}_2^-, \tilde{\mathfrak{s}}_3^-, \tilde{\mathfrak{s}}_4^-, \tilde{\mathfrak{s}}_5^-, \tilde{s}_i \right) =
$$
$$
\mathrm{Tr}_{\mathrm{B}} \left[\mathrm{e}^{-\hat{H}_{\mathrm{SB}}(\tilde{\mathfrak{s}}_0)\Delta\beta/(2\hbar)} \mathrm{e}^{-\hat{H}_{\mathrm{SB}}(\tilde{\mathfrak{s}}_1^-)\Delta\beta/\hbar} \mathrm{e}^{-\hat{H}_{\mathrm{SB}}(\tilde{\mathfrak{s}}_2^-)\Delta\beta/\hbar} \mathrm{e}^{-\hat{H}_{\mathrm{SB}}(\tilde{\mathfrak{s}}_3^-)\Delta\beta/(2\hbar)} \right.
$$
$$
\times \mathrm{e}^{i\hat{H}_{\mathrm{SB}}(\tilde{\mathfrak{s}}_3^-)\Delta t/(2\hbar)} \mathrm{e}^{i\hat{H}_{\mathrm{SB}}(\tilde{\mathfrak{s}}_4^-)\Delta t/\hbar} \mathrm{e}^{i\hat{H}_{\mathrm{SB}}(\tilde{\mathfrak{s}}_5^-)\Delta t/\hbar} \mathrm{e}^{i\hat{H}_{\mathrm{SB}}(\tilde{s}_i)\Delta t/(2\hbar)}
$$
$$
\times \mathrm{e}^{-i\hat{H}_{\mathrm{SB}}(\tilde{s}_i)\Delta t/(2\hbar)} \mathrm{e}^{-i\hat{H}_{\mathrm{SB}}(\tilde{\mathfrak{s}}_5^+)\Delta t/\hbar} \mathrm{e}^{-i\hat{H}_{\mathrm{SB}}(\tilde{\mathfrak{s}}_4^+)\Delta t/\hbar} \mathrm{e}^{-i\hat{H}_{\mathrm{SB}}(\tilde{\mathfrak{s}}_3^+)\Delta t/(2\hbar)}
$$
$$
\left. \times \mathrm{e}^{-\hat{H}_{\mathrm{SB}}(\tilde{\mathfrak{s}}_3^+)\Delta\beta/(2\hbar)} \mathrm{e}^{-\hat{H}_{\mathrm{SB}}(\tilde{\mathfrak{s}}_2^+)\Delta\beta/\hbar} \mathrm{e}^{-\hat{H}_{\mathrm{SB}}(\tilde{\mathfrak{s}}_1^+)\Delta\beta/\hbar} \mathrm{e}^{-\hat{H}_{\mathrm{SB}}(\tilde{\mathfrak{s}}_0)\Delta\beta/(2\hbar)} \right] .
\tag{E.10}
$$

Following the same line of reasoning as for Eq. (4.25), the expression within the trace in Eq. (E.10) can be interpreted as a certain propagation of the bath. In contrast to Sec. 4.1.1 the bath is here propagated in the complex time. Within the propagation the bath experiences the interaction potential that parametrically depends on the coordinates of the discrete complex time paths $\tilde{\mathfrak{s}}^+, \tilde{\mathfrak{s}}^-$ and the shared end point $\tilde{s}_i$. The interaction potential is kept constant during the propagation steps and can therefore be described by an operator-like step function, as shown in Fig. E.1. The trace evaluates then the integral over all initial and final states the bath could have had within the propagation, see Eq. (4.25). Therefore, the second conclusion is as follows, after σ is determined by the bare system propagation along the CFBC $\tilde{\mathfrak{s}}^{\pm}$, the summand is weighted by the function f. The value of f in turn takes account of the mutual interaction between system and bath if the system follows $\tilde{\mathfrak{s}}^{\pm}$. In order to calculate all other summands that contribute to the discrete TCF in Eq. (E.6) the indices $i_0, i_k^{\pm}$, $k = 1, \ldots, 5$ are varying. The sum over the index i and, hence, the sum over shared end points $\tilde{s}_i$ is treated individually in the following. Each summand represents a particular FBC, which is a combinatoric sequence
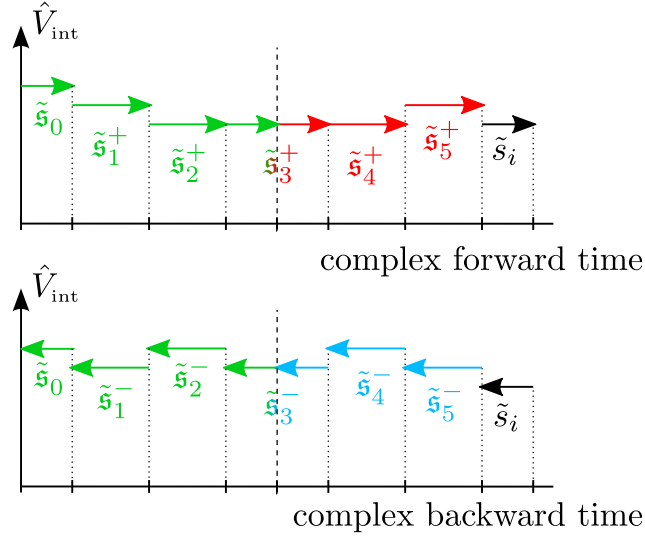
Figure E.1.: **Interaction potential experienced by the bath.** The forward/backward evolution in the complex time is shown in the upper/lower panel, respectively. The marked times on the *complex forward time* axis read from the left to the right as 0, $-i\Delta\beta/2$, $-3i\Delta\beta/2$, $-5i\Delta\beta/2$, $-3i\Delta\beta$, $\Delta t/2 - 3i\Delta\beta$, $3\Delta t/2 - 3i\Delta\beta$, $5\Delta t/2 - 3i\Delta\beta$, $3\Delta t - 3i\Delta\beta$. The marked times on the *complex backward time* axis read from the left to the right as $-6i\Delta\beta$, $-11i\Delta\beta/2$, $-9i\Delta\beta/2$, $-7i\Delta\beta/2$, $-3i\Delta\beta$, $\Delta t/2 - 3i\Delta\beta$, $3\Delta t/2 - 3i\Delta\beta$, $5\Delta t/2 - 3i\Delta\beta$, $3\Delta t - 3i\Delta\beta$. The vertical axis is referred to the "strength" of the system-bath interaction.

of $2(P + N) = 12$ grid points, where the discrete complex time forward and backward path must share the same initial coordinate as the result of the trace, i.e. $\tilde{\mathfrak{s}}_0^+ = \tilde{\mathfrak{s}}_0^- = \tilde{\mathfrak{s}}_0$.

In analogy to Sec. 4.1.1, for any N and P the $2(P + N)$-fold sum in Eq. (E.6) is replaced by one sum over all FBCs that can be constructed upon $2(P+N)$ grid points, where $\tilde{\mathfrak{s}}_0^+ = \tilde{\mathfrak{s}}_0^- = \tilde{\mathfrak{s}}_0$, see Eq. (4.101). Each summand consists of two mutually independent quantities.

First, the discrete complex time bare system part

$$\tilde{\mathscr{S}}_{(0,P+N)}^{\Gamma\Omega}\left[\tilde{\mathbf{s}}^{\pm}, \tilde{s}_i\right] \equiv \prod_{k=0}^{P+N-1} \tilde{\mathscr{S}}_{(k,k+1)}^{\Gamma\Omega}\left(\tilde{\mathfrak{s}}_k^{\pm}, \tilde{\mathfrak{s}}_{k+1}^{\pm}\right) \quad , \tag{E.11}$$

with the *complex time bare system point-to-point propagator*

$$\mathscr{S}^{\Gamma\Omega}_{(k,k+1)}\left(\tilde{\mathfrak{s}}^{\pm}_k, \tilde{\mathfrak{s}}^{\pm}_{k+1}\right) \equiv \begin{cases} \left\langle\tilde{\mathfrak{s}}^{-}_k\right|e^{-\hat{H}_S\Delta\beta/\hbar}\left|\tilde{\mathfrak{s}}^{-}_{k+1}\right\rangle\left\langle\tilde{\mathfrak{s}}^{+}_{k+1}\right|e^{-\hat{H}_S\Delta\beta/\hbar}\left|\tilde{\mathfrak{s}}^{+}_k\right\rangle, & 0 \leq k \leq P-1 \\ \left\langle\tilde{\mathfrak{s}}^{-}_P\right|\hat{\Gamma}e^{i\hat{H}_S\Delta t/\hbar}\left|\tilde{\mathfrak{s}}^{-}_{P+1}\right\rangle\left\langle\tilde{\mathfrak{s}}^{+}_{P+1}\right|e^{-i\hat{H}_S\Delta t/\hbar}\left|\tilde{\mathfrak{s}}^{+}_P\right\rangle, & k = P \\ \left\langle\tilde{\mathfrak{s}}^{-}_k\right|e^{i\hat{H}_S\Delta t/\hbar}\left|\tilde{\mathfrak{s}}^{-}_{k+1}\right\rangle\left\langle\tilde{\mathfrak{s}}^{+}_{k+1}\right|e^{-i\hat{H}_S\Delta t/\hbar}\left|\tilde{\mathfrak{s}}^{+}_k\right\rangle, & P+1 \leq k \leq P+N-2 \\ \left\langle\tilde{\mathfrak{s}}^{-}_{P+N-1}\right|e^{i\hat{H}_S\Delta t/\hbar}\left|\tilde{s}_i\right\rangle\left\langle\tilde{s}_i\right|\hat{\Omega}e^{-i\hat{H}_S\Delta t/\hbar}\left|\tilde{\mathfrak{s}}^{+}_{P+N-1}\right\rangle, & k = P+N-1 \ , \end{cases}$$

(E.12)

where $\tilde{\mathfrak{s}}^{+}_0 = \tilde{\mathfrak{s}}^{-}_0 = \tilde{\mathfrak{s}}_0$.

Second, the summand is weighted by *discrete complex time influence functional* defined for $N > 0$ as

$$\tilde{\mathscr{F}}_{(0,P+N)}\left[\tilde{\mathfrak{s}}^{\pm}, \tilde{s}_i\right] \equiv$$
$$f\left(\tilde{\mathfrak{s}}_0, \tilde{\mathfrak{s}}^{+}_1, \ldots, \tilde{\mathfrak{s}}^{+}_P, \tilde{\mathfrak{s}}^{+}_{P+1}, \ldots, \tilde{\mathfrak{s}}^{+}_{P+N-1}, \tilde{\mathfrak{s}}^{-}_1, \ldots, \tilde{\mathfrak{s}}^{-}_P, \tilde{\mathfrak{s}}^{-}_{P+1} \ldots, \tilde{\mathfrak{s}}^{-}_{P+N-1}, \tilde{s}_i\right) \ , \quad \text{(E.13)}$$

which contains implicitly the influence of the bath due to the interaction with the system if it follows the FBC $\tilde{\mathfrak{s}}^{\pm}$.

E.1. Iterative propagation of the TCF

In order to derive an iterative scheme for the propagation of the TCF, the discrete complex time influence functional is written as a product of *complex time point-to-point influences*

$$\tilde{\mathscr{F}}_{(0,P+N)}\left[\tilde{\mathfrak{s}}^{\pm}, \tilde{s}_i\right] = Z_B(\beta)\prod_{k=0}^{P+N}\prod_{k'=0}^{k}\tilde{\mathscr{F}}_{(k',k)}\left(\tilde{\mathfrak{s}}^{\pm}_{k'}, \tilde{\mathfrak{s}}^{\pm}_k\right)$$

(E.14)

or equivalently

$$\tilde{\mathscr{F}}_{(0,P+N)}\left[\tilde{\mathfrak{s}}^{\pm}, \tilde{s}_i\right] = Z_B(\beta)\prod_{k'=0}^{P+N}\prod_{k=k'}^{P+N}\tilde{\mathscr{F}}_{(k',k)}\left(\tilde{\mathfrak{s}}^{\pm}_{k'}, \tilde{\mathfrak{s}}^{\pm}_k\right) \ ,$$

(E.15)

where

$$\tilde{\mathscr{F}}_{(k',k)}\left(\tilde{\mathfrak{s}}^{\pm}_{k'}, \tilde{\mathfrak{s}}^{\pm}_k\right) = \exp\left\{-\frac{1}{\hbar}\left(\eta^{++}_{k'k}\tilde{\mathfrak{s}}^{+}_{k'}\tilde{\mathfrak{s}}^{+}_k + \eta^{--}_{k'k}\tilde{\mathfrak{s}}^{-}_{k'}\tilde{\mathfrak{s}}^{-}_k + \eta^{-+}_{k'k}\tilde{\mathfrak{s}}^{-}_{k'}\tilde{\mathfrak{s}}^{+}_k + \eta^{+-}_{k'k}\tilde{\mathfrak{s}}^{+}_{k'}\tilde{\mathfrak{s}}^{-}_k\right)\right\} \ .$$

(E.16)

In case of a finite memory the double product in Eq. (E.15) can be truncated

$$\tilde{\mathscr{F}}_{(0,P+N)}\left[\tilde{\mathfrak{s}}^{\pm}, \tilde{s}_i\right] = Z_{\mathrm{B}}(\beta) \prod_{k'=0}^{P+N} \prod_{k=k'}^{\min\{P+N, k'+\kappa\}} \tilde{\mathscr{F}}_{(k',k)}\left(\tilde{\mathfrak{s}}_{k'}^{\pm}, \tilde{\mathfrak{s}}_{k}^{\pm}\right) \ . \tag{E.17}$$

In order to make the following derivation more transparent, let us restrict ourselves at first to the case where $N = 1$, $P = \kappa = 3$. The sum over FBCs in Eq. (4.101) is unfolded back into the form of Eq. (E.6). With the definition of $\tilde{\mathscr{S}}_{(0,N-iP)}\left[\tilde{\mathfrak{s}}^{\pm}, \tilde{s}_i\right]$ in Eqs. (E.11, E.12) and $\tilde{\mathscr{F}}_{(0,P+N)}\left[\tilde{\mathfrak{s}}^{\pm}, \tilde{s}_i\right]$ in Eq. (E.17) the discrete TCF can then be calculated via

$$\tilde{C}_{\Gamma\Omega}(\Delta t) = \frac{1}{Z(\beta)} \sum_{i_0^+=0}^{M-1} \sum_{i_1^+=0}^{M-1} \sum_{i_2^+=0}^{M-1} \sum_{i_3^+=0}^{M-1} \sum_{i_0^-=0}^{M-1} \sum_{i_1^-=0}^{M-1} \sum_{i_2^-=0}^{M-1} \sum_{i_3^-=0}^{M-1} \sum_{i=0}^{M-1}$$
$$Z_{\mathrm{B}}(\beta) \left(\prod_{k'=0}^{4} \prod_{k=k'}^{\min\{4,k'+3\}} \tilde{\mathscr{F}}_{(k',k)}\left(\tilde{s}_{i_{k'}^\pm}, \tilde{s}_{i_k^\pm}\right)\right) \left(\prod_{k=0}^{3} \tilde{\mathscr{S}}_{(k,k+1)}\left(\tilde{s}_{i_k^\pm}, \tilde{s}_{i_{k+1}^\pm}\right)\right) \delta_{i_0^+, i_0^-} \ , \tag{E.18}$$

where $\tilde{s}_{i_4^\pm} \equiv \tilde{s}_i$. Note that the Kronecker delta takes account of the fact that the complex time forward and backward paths have the same beginning point as the result of the trace in Eq. (4.94). All quantities depending on the indices i_0^+, i_0^- and, thus, $k, k' = 0$ can be grouped with the following result

$$\tilde{C}_{\Gamma\Omega}(\Delta t) = \frac{1}{Z(\beta)} \sum_{i_1^+=0}^{M-1} \sum_{i_2^+=0}^{M-1} \sum_{i_3^+=0}^{M-1} \sum_{i_1^-=0}^{M-1} \sum_{i_2^-=0}^{M-1} \sum_{i_3^-=0}^{M-1} \sum_{i=0}^{M-1}$$
$$Z_{\mathrm{B}}(\beta) \left(\prod_{k'=1}^{4} \prod_{k=k'}^{\min\{4,k'+3\}} \tilde{\mathscr{F}}_{(k',k)}\left(\tilde{s}_{i_{k'}^\pm}, \tilde{s}_{i_k^\pm}\right)\right) \left(\prod_{k=1}^{3} \tilde{\mathscr{S}}_{(k,k+1)}\left(\tilde{s}_{i_k^\pm}, \tilde{s}_{i_{k+1}^\pm}\right)\right)$$
$$\times \sum_{i_0^+=0}^{M-1} \sum_{i_0^-=0}^{M-1} \left(\prod_{k=0}^{\min\{4,3\}} \tilde{\mathscr{F}}_{(0,k)}\left(\tilde{s}_{i_0}, \tilde{s}_{i_k^\pm}\right)\right) \tilde{\mathscr{S}}_{(0,1)}\left(\tilde{s}_{i_0}, \tilde{s}_{i_1^\pm}\right) \delta_{i_0^+, i_0^-} \ . \tag{E.19}$$

E. Numerical treatment of the TCF

The last line of Eq. (E.19) defines the new quantity

$$r\big(\tilde{s}_{i_1^\pm},\, \tilde{s}_{i_2^\pm},\, \tilde{s}_{i_3^\pm};\, -2\Delta t\big) \equiv \sum_{i_0^+=0}^{M-1}\sum_{i_0^-=0}^{M-1} \left(\prod_{k=0}^{\min\{4,3\}} \tilde{\mathscr{F}}_{(0,k)}\big(\tilde{s}_{i_0},\, \tilde{s}_{i_k^\pm}\big) \right) \tilde{\mathscr{S}}_{(0,1)}\big(\tilde{s}_{i_0},\, \tilde{s}_{i_1^\pm}\big)\, \delta_{i_0^+,i_0^-}\ , \quad (\text{E.20})$$

where $-2 = (N-\kappa)$. Keeping the last two equations in mind, one can now focus on the case $N=2$. According to Eqs. (E.6,E.11,E.17) the discrete TCF is calculated via

$$\tilde{C}_{\Gamma\Omega}(2\Delta t) = \frac{1}{Z(\beta)} \sum_{i_2^+=0}^{M-1}\sum_{i_3^+=0}^{M-1}\sum_{i_4^+=0}^{M-1}\sum_{i_2^-=0}^{M-1}\sum_{i_3^-=0}^{M-1}\sum_{i_4^-=0}^{M-1}\sum_{i=0}^{M-1}$$

$$\times\, Z_{\mathrm{B}}(\beta) \left(\prod_{k'=2}^{5} \prod_{k=k'}^{\min\{5,k'+3\}} \tilde{\mathscr{F}}_{(k',k)}\big(\tilde{s}_{i_{k'}^\pm},\, \tilde{s}_{i_k^\pm}\big) \right) \left(\prod_{k=2}^{4} \tilde{\mathscr{S}}_{(k,k+1)}\big(\tilde{s}_{i_k^\pm},\, \tilde{s}_{i_{k+1}^\pm}\big) \right)$$

$$\times \sum_{i_1^+=0}^{M-1}\sum_{i_1^-=0}^{M-1} \left(\prod_{k=1}^{\min\{5,4\}} \tilde{\mathscr{F}}_{(1,k)}\big(\tilde{s}_{i_1^\pm},\, \tilde{s}_{i_k^\pm}\big) \right) \tilde{\mathscr{S}}_{(1,2)}\big(\tilde{s}_{i_1^\pm},\, \tilde{s}_{i_2^\pm}\big) \cdot r\big(\tilde{s}_{i_1^\pm},\, \tilde{s}_{i_2^\pm},\, \tilde{s}_{i_3^\pm};\, -2\Delta t\big)\ ,$$

$$(\text{E.21})$$

where all quantities depending on $\tilde{s}_{i_1^\pm}$ and $k,\ k'=1$ are grouped and the definition of $r\big(\tilde{s}_{i_1^\pm},\, \tilde{s}_{i_2^\pm},\, \tilde{s}_{i_3^\pm};\, -2\Delta t\big)$ is inserted. Equation (E.21) is identical to Eq. (E.19) if one would shift the indices $k,\ k'$ by one and replace $r\big(\tilde{s}_{i_1^\pm},\, \tilde{s}_{i_2^\pm},\, \tilde{s}_{i_3^\pm};\, \Delta t\big)$ by $\delta_{i_0^+,i_0^-}$. It is straight forward to apply the presented concept to arbitrary $N>0$ and κ. The result is an iterative propagation scheme consisting of two subsequent calculations for each propagation step. First, the quantity r has to be propagated via

$$r\big(\tilde{s}_{i_N^\pm},\, \ldots,\, \tilde{s}_{i_{N+\kappa-1}^\pm};\, (N-\kappa)\Delta t\big) \equiv$$

$$\sum_{i_{N-1}^+=0}^{M-1}\sum_{i_{N-1}^-=0}^{M-1} \left(\prod_{k=N-1}^{\min\{\kappa+N,\kappa+N-1\}} \tilde{\mathscr{F}}_{(N-1,k)}\big(\tilde{s}_{i_{N-1}^\pm},\, \tilde{s}_{i_k^\pm}\big) \right)$$

$$\times\, \tilde{\mathscr{S}}_{(N-1,N)}\big(\tilde{s}_{i_{N-1}^\pm},\, \tilde{s}_{i_N^\pm}\big)$$

$$\times\, r\big(\tilde{s}_{i_{N-1}^\pm},\, \ldots,\, \tilde{s}_{i_{N+\kappa-2}^\pm};\, (N-\kappa-1)\Delta t\big) \qquad (\text{E.22})$$

with the initial condition

$$r(\tilde{s}_{i_0^{\pm}}, \ldots, \tilde{s}_{i_{\kappa-1}^{\pm}}; -\kappa\Delta t) = \delta_{i_0^+,i_0^-} \quad . \tag{E.23}$$

The calculation of the discrete TCF requires the additional summation

$$\tilde{C}_{\Gamma\Omega}(N\Delta t) = \frac{1}{Z(\beta)} \sum_{i_N^+=0}^{M-1} \cdots \sum_{i_{N+\kappa-1}^+=0}^{M-1} \sum_{i_N^-=0}^{M-1} \cdots \sum_{i_{N+\kappa-1}^-=0}^{M-1} \sum_{i=0}^{M-1}$$

$$\times Z_{\mathrm{B}}(\beta) \left(\prod_{k'=N}^{N+\kappa} \prod_{k=k'}^{\min\{N+\kappa,k'+\kappa\}} \tilde{\mathscr{F}}_{(k',k)} \left(\tilde{s}_{i_{k'}^{\pm}}, \tilde{s}_{i_k^{\pm}} \right) \right) \left(\prod_{k=N}^{N+\kappa-1} \tilde{\mathscr{S}}_{(k,k+1)} \left(\tilde{s}_{i_k^{\pm}}, \tilde{s}_{i_{k+1}^{\pm}} \right) \right)$$

$$\times r(\tilde{s}_{i_N^{\pm}}, \ldots, \tilde{s}_{i_{N+\kappa-1}^{\pm}}; (N-\kappa)\Delta t) \quad . \tag{E.24}$$

With the following substitutions, the iterative scheme can be expressed in terms of complex time FBC segments $\tilde{\mathfrak{s}}^{\pm}$ with the shared end point $\tilde{s}_i$.

First, the discrete complex time influence functional takes the form

$$Z_{\mathrm{B}}(\beta) \prod_{k'=N}^{N+\kappa} \prod_{k=k'}^{\min\{N+\kappa,k'+\kappa\}} \tilde{\mathscr{F}}_{(k',k)} \left(\tilde{s}_{i_{k'}^{\pm}}, \tilde{s}_{i_k^{\pm}} \right) \xrightarrow{k' \to k'+N} Z_{\mathrm{B}}(\beta) \prod_{k'=0}^{\kappa} \prod_{k=k'}^{\kappa} \tilde{\mathscr{F}}_{(k'+N,k+N)} \left(\tilde{\mathfrak{s}}_{k'}^{\pm}, \tilde{\mathfrak{s}}_k^{\pm} \right) = \tilde{\mathscr{F}}_{(N,N+\kappa)} \left[\tilde{\mathfrak{s}}^{\pm}, \tilde{s}_i \right] \tag{E.25}$$

with

$$\tilde{\mathscr{F}}_{(k'+N,k+N)} \left(\tilde{\mathfrak{s}}_{k'}^{\pm}, \tilde{\mathfrak{s}}_k^{\pm} \right) = \exp \left\{ -\frac{1}{\hbar} \left(\eta_{k'+N,k+N}^{++} \tilde{\mathfrak{s}}_{k'}^+ \tilde{\mathfrak{s}}_k^+ + \eta_{k'+N,k+N}^{--} \tilde{\mathfrak{s}}_{k'}^- \tilde{\mathfrak{s}}_k^- \right. \right.$$
$$\left. \left. + \eta_{k'+N,k+N}^{-+} \tilde{\mathfrak{s}}_{k'}^- \tilde{\mathfrak{s}}_k^+ + \eta_{k'+N,k+N}^{+-} \tilde{\mathfrak{s}}_{k'}^+ \tilde{\mathfrak{s}}_k^- \right) \right\} \quad . \tag{E.26}$$

Second, the discrete complex time bare system part is written as

$$\prod_{k=N}^{N+\kappa-1} \tilde{\mathscr{S}}_{(k,k+1)}^{\Gamma\Omega} \left(\tilde{s}_{i_k^{\pm}}, \tilde{s}_{i_{k+1}^{\pm}} \right) \xrightarrow{k' \to k'+N} \prod_{k=0}^{\kappa-1} \tilde{\mathscr{S}}_{(k+N,k+N+1)}^{\Gamma\Omega} \left(\tilde{\mathfrak{s}}_k^{\pm}, \tilde{\mathfrak{s}}_{k+1}^{\pm} \right) = \tilde{\mathscr{S}}_{(N,N+\kappa)}^{\Gamma\Omega} \left[\tilde{\mathfrak{s}}^{\pm}, \tilde{s}_i \right] \quad , \tag{E.27}$$

where

$$\tilde{\mathscr{S}}^{\Gamma\Omega}_{(k+N,k+N+1)}\left(\tilde{\mathfrak{s}}^{\pm}_k,\,\tilde{\mathfrak{s}}^{\pm}_{k+1}\right) \equiv \begin{cases} \langle\tilde{\mathfrak{s}}^-_k|e^{-\hat{H}_{\mathrm{S}}\Delta\beta/\hbar}|\tilde{\mathfrak{s}}^-_{k+1}\rangle\langle\tilde{\mathfrak{s}}^+_{k+1}|e^{-\hat{H}_{\mathrm{S}}\Delta\beta/\hbar}|\tilde{\mathfrak{s}}^+_k\rangle, & 0 \le k+N \le \kappa-1 \\[4pt] \langle\tilde{\mathfrak{s}}^-_k|\hat{\Gamma}e^{i\hat{H}_{\mathrm{S}}\Delta t/\hbar}|\tilde{\mathfrak{s}}^-_{k+1}\rangle\langle\tilde{\mathfrak{s}}^+_{k+1}|e^{-i\hat{H}_{\mathrm{S}}\Delta t/\hbar}|\tilde{\mathfrak{s}}^+_k\rangle, & k+N=\kappa \\[4pt] \langle\tilde{\mathfrak{s}}^-_k|e^{i\hat{H}_{\mathrm{S}}\Delta t/\hbar}|\tilde{\mathfrak{s}}^-_{k+1}\rangle\langle\tilde{\mathfrak{s}}^+_{k+1}|e^{-i\hat{H}_{\mathrm{S}}\Delta t/\hbar}|\tilde{\mathfrak{s}}^+_k\rangle, & \kappa+1 \le k+N \le \kappa+N-2 \\[4pt] \langle\tilde{\mathfrak{s}}^-_k|e^{i\hat{H}_{\mathrm{S}}\Delta t/\hbar}|\tilde{s}_i\rangle\langle\tilde{s}_i|\hat{\Omega}e^{-i\hat{H}_{\mathrm{S}}\Delta t/\hbar}|\tilde{\mathfrak{s}}^+_k\rangle, & k+N=\kappa+N-1 \ , \end{cases}$$
$$\text{(E.28)}$$

Note that for any $N > \kappa$ the quantity $\tilde{\mathscr{S}}^{\Gamma\Omega}_{(N,N+\kappa)}\left[\tilde{\mathfrak{s}}^{\pm},\tilde{s}_i\right]$ consists *constantly* only of real time propagators, thus

$$\tilde{\mathscr{S}}^{\Gamma\Omega}_{(N,N+\kappa)}\left[\tilde{\mathfrak{s}}^{\pm},\tilde{s}_i\right] = \tilde{\mathscr{S}}^{\Gamma\Omega,\mathrm{re}}_{(0,\kappa)}\left[\tilde{\mathfrak{s}}^{\pm},\tilde{s}_i\right] \equiv \prod_{k=0}^{\kappa-1}\tilde{\mathscr{S}}^{\Gamma\Omega,\mathrm{re}}_{(k,k+1)}\left(\tilde{\mathfrak{s}}^{\pm}_k,\,\tilde{\mathfrak{s}}^{\pm}_{k+1}\right) \qquad\text{(E.29)}$$

with

$$\tilde{\mathscr{S}}^{\Gamma\Omega,\mathrm{re}}_{(k,k+1)}\left(\tilde{\mathfrak{s}}^{\pm}_k,\,\tilde{\mathfrak{s}}^{\pm}_{k+1}\right) \equiv \begin{cases} \langle\tilde{\mathfrak{s}}^-_k|e^{i\hat{H}_{\mathrm{S}}\Delta t/\hbar}|\tilde{\mathfrak{s}}^-_{k+1}\rangle\langle\tilde{\mathfrak{s}}^+_{k+1}|e^{-i\hat{H}_{\mathrm{S}}\Delta t/\hbar}|\tilde{\mathfrak{s}}^+_k\rangle, & 0 \le k \le \kappa-2 \\[4pt] \langle\tilde{\mathfrak{s}}^-_k|e^{i\hat{H}_{\mathrm{S}}\Delta t/\hbar}|\tilde{s}_i\rangle\langle\tilde{s}_i|\hat{\Omega}e^{-i\hat{H}_{\mathrm{S}}\Delta t/\hbar}|\tilde{\mathfrak{s}}^+_k\rangle, & k=\kappa-1 \ . \end{cases} \qquad\text{(E.30)}$$

Third, the quantity $r(\tilde{s}_{i^\pm_N},\,\ldots,\,\tilde{s}_{i^\pm_{N+\kappa-1}};\,(N-\kappa)\Delta t)$ is replaced by the multi-time TCF functional $\tilde{\mathscr{R}}\left[\tilde{\mathfrak{s}}^{\pm};(N-\kappa)\Delta t\right]$ with $\tilde{s}_{i^\pm_N} \to \tilde{\mathfrak{s}}^{\pm}_0,\ldots,\tilde{s}_{i^\pm_{N+\kappa-1}} \to \tilde{\mathfrak{s}}^{\pm}_{\kappa-1}$.

Fourth, the quantity $r(\tilde{s}_{i^\pm_{N-1}},\,\ldots,\,\tilde{s}_{i^\pm_{N+\kappa-2}};\,(N-\kappa-1)\Delta t)$ at the previous time step is substituted by $\tilde{\mathscr{R}}\left[\tilde{\mathfrak{t}}^{\pm};(N-\kappa-1)\Delta t\right]$, where $\tilde{s}_{i^\pm_{N-1}} \to \tilde{\mathfrak{t}}^{\pm}_0,\ldots,\tilde{s}_{i^\pm_{N+\kappa-2}} \to \tilde{\mathfrak{t}}^{\pm}_{\kappa-1}$. Note that $\tilde{\mathfrak{t}}^{\pm}_1 = \tilde{\mathfrak{s}}^{\pm}_0,\ldots,\tilde{\mathfrak{t}}^{\pm}_{\kappa-1} = \tilde{\mathfrak{s}}^{\pm}_{\kappa-2}$.

Fifth, the complex time lambda propagator is defined

$$\left(\prod_{k=N-1}^{\min\{\kappa+N,\kappa+N-1\}}\tilde{\mathscr{F}}_{(N-1,k)}\left(\tilde{s}_{i^\pm_{N-1}},\,\tilde{s}_{i^\pm_k}\right)\right)\tilde{\mathscr{S}}^{\Gamma\Omega}_{(N-1,N)}\left(\tilde{s}_{i^\pm_{N-1}},\,\tilde{s}_{i^\pm_N}\right) \xrightarrow{k\to k+N-1}$$

$$\tilde{\mathscr{S}}^{\Gamma\Omega}_{(N-1,N)}\left(\tilde{\mathfrak{t}}^{\pm}_0,\tilde{\mathfrak{t}}^{\pm}_1\right)\left(\prod_{k=0}^{\kappa-1}\tilde{\mathscr{F}}_{(N-1,k+N-1)}\left(\tilde{\mathfrak{t}}^{\pm}_0,\tilde{\mathfrak{t}}^{\pm}_k\right)\right)\cdot\tilde{\mathscr{F}}_{(N-1,N+\kappa-1)}\left(\tilde{\mathfrak{t}}^{\pm}_0,\tilde{\mathfrak{s}}^{\pm}_{\kappa-1}\right)$$

$$\equiv \mathscr{L}_{(N-1,N+\kappa)}\left[\tilde{\mathfrak{t}}^{\pm},\,\tilde{\mathfrak{s}}^{\pm}\right]. \quad\text{(E.31)}$$

Note that due to the constraint $\tilde{\mathfrak{s}}_0^+ = \tilde{\mathfrak{s}}_0^- = \tilde{\mathfrak{s}}_0$ the the multi-time TCF functional has the special initial condition

$$\tilde{\mathscr{R}}\left[\tilde{\mathfrak{s}}^\pm; -\kappa\Delta t\right] = \begin{cases} 1, & \tilde{\mathfrak{s}}_0^+ = \tilde{\mathfrak{s}}_0^- \\ 0, & \tilde{\mathfrak{s}}_0^+ \neq \tilde{\mathfrak{s}}_0^- \end{cases} \tag{E.32}$$

With the given substitutions, the iterative propagation of the discrete TCF can be formulated as written down in Sec. E.1.

E.2. Virtual time-dependence of memory coefficients

The memory coefficients $\eta_{k'k}^{\pm\pm}$ and $\eta_{k'k}^{\pm\mp}$ depend on the absolute value of k if $k, k' \leq \kappa$, since the real and imaginary parts of the propagation changes during the first κ iteration steps. Consequently the times τ_k in Eqs. B.16-B.20, thus the memory coefficients have to calculated accordingly. For the $\kappa + 1$-st step and all following steps the imaginary part of the complex time is fixed. It is shown in App. B.2 that coefficients like $\eta_{k'+N,k+N}^{\pm\pm}$ and $\eta_{k'+N,k+N}^{\pm\mp}$ in Eq. (E.26) depend only on $\Delta k = k - k'$ if $N > \kappa$, thus, they do not change during the iteration. These coefficients are called $\eta_{k'k}^{\pm\pm,\text{mid-fin}}$ and $\eta_{k'k}^{\pm\mp,\text{mid-fin}}$, respectively in the following. Accordingly the discrete complex time influence functional for any $N > \kappa$ reads

$$\tilde{\mathscr{F}}_{(N,N+\kappa)}\left[\tilde{\mathfrak{s}}^\pm, s_\pm\right] = \tilde{\mathscr{F}}_{(0,\kappa)}^{\text{mid-fin}}\left[\tilde{\mathfrak{s}}^\pm, s_\pm\right] \equiv \prod_{k=0}^{\kappa}\prod_{k=k'}^{\kappa} \tilde{\mathscr{F}}_{(k',k)}^{\text{mid-fin}}\left(\tilde{\mathfrak{s}}_{k'}^\pm, \tilde{\mathfrak{s}}_k^\pm\right) \quad, \tag{E.33}$$

with

$$\tilde{\mathscr{F}}_{(k',k)}^{\text{mid-fin}}\left(\tilde{\mathfrak{s}}_{k'}^\pm, \tilde{\mathfrak{s}}_k^\pm\right) = \exp\left\{ -\frac{1}{\hbar}\left(\eta_{k'k}^{++,\text{mid-fin}}\,\tilde{\mathfrak{s}}_{k'}^+\tilde{\mathfrak{s}}_k^+ + \eta_{k'k}^{--,\text{mid-fin}}\,\tilde{\mathfrak{s}}_{k'}^-\tilde{\mathfrak{s}}_k^- \right.\right.$$
$$\left.\left. +\eta_{k'k}^{-+,\text{mid-fin}}\,\tilde{\mathfrak{s}}_{k'}^-\tilde{\mathfrak{s}}_k^+ + \eta_{k'k}^{+-,\text{mid-fin}}\,\tilde{\mathfrak{s}}_{k'}^+\tilde{\mathfrak{s}}_k^- \right)\right\} \quad. \tag{E.34}$$

For the complex time lambda propagator in Eq. (E.31) the coefficients $\eta_{k'k}^{\pm\pm}$ and $\eta_{k'k}^{\pm\mp}$ in the point-to-point influence depend only on $\Delta k = k - k'$ if $N > \kappa + 1$, hence, they are also fixed within the ongoing propagation, see App. B.1. Consequently, the complex time lambda propagator itself does not depend on the absolute propagation time. The memory coefficients

for any $N > \kappa + 1$ are labeled by $\eta_{k'k}^{\pm\pm,\mathrm{mid}}$ and $\eta_{k'k}^{\pm\mp,\mathrm{mid}}$ and

$$
\mathscr{L}_{(N-1,N+\kappa)}\left[\tilde{\mathfrak{r}}^{\pm},\,\tilde{\mathfrak{s}}^{\pm}\right] = \mathscr{L}_{(0,\kappa)}^{\mathrm{mid}}\left[\tilde{\mathfrak{r}}^{\pm},\,\tilde{\mathfrak{s}}^{\pm}\right] \equiv \tilde{\mathscr{S}}_{(0,1)}^{\mathrm{re}}\left(\tilde{\mathfrak{r}}_0^{\pm},\tilde{\mathfrak{r}}_1^{\pm}\right) \prod_{k=0}^{\kappa-1} \tilde{\mathscr{F}}_{(0,k)}^{\mathrm{mid}}\left(\tilde{\mathfrak{r}}_0^{\pm},\tilde{\mathfrak{r}}_k^{\pm}\right) \cdot \tilde{\mathscr{F}}_{(0,\kappa)}^{\mathrm{mid}}\left(\tilde{\mathfrak{r}}_0^{\pm},\tilde{\mathfrak{s}}_{\kappa-1}^{\pm}\right) \;,
$$

(E.35)

with

$$
\tilde{\mathscr{F}}_{(k',k)}^{\mathrm{mid}}\left(\tilde{\mathfrak{s}}_{k'}^{\pm},\,\tilde{\mathfrak{s}}_k^{\pm}\right) = \exp\left\{-\frac{1}{\hbar}\left(\eta_{k'k}^{++,\mathrm{mid}}\,\tilde{\mathfrak{s}}_{k'}^+\tilde{\mathfrak{s}}_k^+ + \eta_{k'k}^{--,\mathrm{mid}}\,\tilde{\mathfrak{s}}_{k'}^-\tilde{\mathfrak{s}}_k^-\right.\right.
$$
$$
\left.\left. + \eta_{k'k}^{-+,\mathrm{mid}}\,\tilde{\mathfrak{s}}_{k'}^-\tilde{\mathfrak{s}}_k^+ + \eta_{k'k}^{+-,\mathrm{mid}}\,\tilde{\mathfrak{s}}_{k'}^+\tilde{\mathfrak{s}}_k^-\right)\right\}\;.
$$

(E.36)

Note that since $N > \kappa$ the complex time bare system part consists only of real time propagators as it was stated in the previous section. For any $N \leq \kappa + 1$ the complex time memory coefficients have to be calculated via the general expressions given in App. B.2. Due to the presented features of the complex time memory coefficients, all parts of the discrete PI apart from $\tilde{\mathscr{R}}\left[\tilde{\mathfrak{s}}^{\pm}; (N-\kappa)\Delta t\right]$ are fixed if $N > \kappa + 1$.

E.3. Path filtering

As it was derived in the previous sections, the TCF can be propagated for arbitrary long times by summing over a constant set of $M^{2\kappa}$ path segments. In this section it will be shown that in analogy the RDM propagation it is not necessary to sum over all possible FBCs, thus, the number of arithmetic operations can be significantly reduced.

According to Eq. (4.108) the absolute value of the TCF for any $N > \kappa$ can be estimated via the triangular inequality as

$$
\left|\tilde{C}_{\Gamma\Omega}(N\Delta t)\right| \;\leq\; \frac{1}{Z(\beta)}\sum_{i=0}^{M-1}\sum_{\tilde{\mathfrak{s}}^{\pm}\in\mathbb{P}_{\kappa,M}}\left|\tilde{\mathscr{F}}_{(0,\kappa)}^{\mathrm{mid\text{-}fin}}\left[\tilde{\mathfrak{s}}^{\pm},\tilde{s}_i\right]\tilde{\mathscr{S}}_{(0,\kappa)}^{\Gamma\Omega,\mathrm{re}}\left[\tilde{\mathfrak{s}}^{\pm},\tilde{s}_i\right]\tilde{\mathscr{R}}\left[\tilde{\mathfrak{s}}^{\pm};(N-\kappa)\Delta t\right]\right| \text{(E.37)}
$$

$$
\leq\; |\mathcal{C}|\sum_{i=0}^{M-1}\sum_{\tilde{\mathfrak{s}}^{\pm}\in\mathbb{P}_{\kappa,M}}\left|\left(\prod_{k'=0}^{\kappa-1}\prod_{k=k'}^{\kappa-1}\tilde{\mathscr{F}}_{(k',k)}^{\mathrm{mid\text{-}fin}}\left(\tilde{\mathfrak{s}}_{k'}^{\pm},\tilde{\mathfrak{s}}_k^{\pm}\right)\right)\prod_{k=0}^{\kappa-2}\tilde{\mathscr{S}}_{(k,k+1)}^{\Gamma\Omega,\mathrm{re}}\left(\tilde{\mathfrak{s}}_k^{\pm},\tilde{\mathfrak{s}}_{k+1}^{\pm}\right)\right| \text{(E.38)}
$$

where

$$\mathcal{C} \equiv \max_{\tilde{\mathfrak{s}}^\pm \in \mathbb{P}_{\kappa,M}} \left\{ \tilde{\tilde{\mathcal{R}}} \left[\tilde{\mathfrak{s}}^\pm; (N-\kappa)\Delta t \right] \left(\prod_{k'=0}^{\kappa} \tilde{\mathcal{F}}_{(k',\kappa)}^{\text{mid-fin}} \left(\tilde{\mathfrak{s}}_{k'}^\pm, \tilde{s}_i \right) \right) \tilde{\mathscr{S}}_{(\kappa-1,\kappa)}^{\Gamma\Omega,\text{re}} \left(\tilde{\mathfrak{s}}_{\kappa-1}^\pm, \tilde{s}_i \right) \right\} \qquad (E.39)$$

Note that $\mathcal{C}$ is defined such that the time-dependent $\tilde{\tilde{\mathcal{R}}} \left[\tilde{\mathfrak{s}}^\pm; (N-\kappa)\Delta t \right]$ and the shared end points $\tilde{s}_i$ do not occur in the sum in Eq. (E.38), thus the summands are equal for any N and any shared end point. The summand for particular $\tilde{\mathfrak{s}}^\pm$ is now defined as its *complex time path weight*

$$\mathcal{W}_{\kappa-1} \left[\tilde{\mathfrak{s}}^\pm \right] \equiv \left| \left(\prod_{k'=0}^{\kappa-1} \prod_{k=k'}^{\kappa-1} \tilde{\mathcal{F}}_{(k',k)}^{\text{mid-fin}} \left(\tilde{\mathfrak{s}}_{k'}^\pm, \tilde{\mathfrak{s}}_k^\pm \right) \right) \prod_{k=0}^{\kappa-2} \tilde{\mathscr{S}}_{(k,k+1)}^{\Gamma\Omega,\text{re}} \left(\tilde{\mathfrak{s}}_k^\pm, \tilde{\mathfrak{s}}_{k+1}^\pm \right) \right| \quad . \qquad (E.40)$$

Recapitulating the arguments given in Sec. 4.1.6, the set in Eq. (4.108) can be substituted by the *filtered* subset

$$\mathbb{P}_{\kappa,M}^\theta \equiv \left\{ \tilde{\mathfrak{s}}^\pm \in \mathbb{P}_{\kappa,M} \ \big| \ \mathcal{W}_{\kappa-1} \left[\tilde{\mathfrak{s}}^\pm \right] > \theta \right\} \qquad (E.41)$$

without changing the propagation of the TCF crucially for a given *threshold* θ, where the actual value of θ serves as a convergence parameter. The subset $\mathbb{P}_{\kappa,M} \left[\tilde{\mathfrak{s}}^\pm \right]$ appearing in Eq. (4.107) is filtered accordingly

$$\mathbb{P}_{\kappa,M}^\theta \left[\tilde{\mathfrak{s}}^\pm \right] \equiv \left\{ \tilde{\mathfrak{t}}^\pm \in \mathbb{P}_{\kappa,M}^\theta \ \big| \ \tilde{\mathfrak{t}}_k^\pm = \tilde{\mathfrak{s}}_{k-1}^\pm, \ k=1,\ldots,\kappa-1 \right\} \ , \quad \tilde{\mathfrak{s}}^\pm \in \mathbb{P}_{\kappa,M}^\theta \ . \qquad (E.42)$$

Bibliography

[1] Max Planck and Karl Ernst Ludwig. Zur theorie des gesetzes der energieverteilung im normalspectrum. *Verhandl. Dtsc. Phys. Ges.*, 2:237 pp., 1900.

[2] C Davisson and LH Germer. Diffraction of electrons by a crystal of nickel. *Phys. Rev.*, 3, 1927.

[3] W Heisenberg. Über quantentheoretische Umdeutung kinematischer und mechanischer Beziehungen. *Orig. Sci. Pap. Wissenschaftliche . . .*, 1925.

[4] E Schrödinger. Quantisierung als Eigenwertproblem I. *Annalen der physik*, 1926.

[5] E Wigner. On the quantum correction for thermodynamic equilibrium. *Physical Review*, 40:749, 1932.

[6] Hermann Weyl. *The theory of groups and quantum mechanics*. Courier Dover Publications, 1950.

[7] RP Feynman. Space-time approach to non-relativistic quantum mechanics. *Rev. Mod. Phys.*, 64(2), 1948.

[8] D. Marx and J. Hutter. *Ab Initio Molecular Dynamics: Basic Theory and Advanced Methods*. Cambridge University Press, 2009.

[9] Miguel Angel Sepúlveda and Frank Grossmann. Time-dependent semiclassical mechanics. *Advances in Chemical Physics, Volume 96*, pages 191–304, 1996.

[10] David Chandler and P. G. Wolynes. Exploiting the isomorphism between quantum theory and classical statistical mechanics of polyatomic fluids. *J. Chem. Phys.*, 74(7):4078, 1981.

[11] Jianshu Cao and Gregory a. Voth. A new perspective on quantum time correlation functions. *J. Chem. Phys.*, 99(12):10070, 1993.

Bibliography

[12] Ian R Craig and David E Manolopoulos. Quantum statistics and classical mechanics: real time correlation functions from ring polymer molecular dynamics. *J. Chem. Phys.*, 121(8):3368–73, August 2004.

[13] Alexander Witt, Sergei D Ivanov, Motoyuki Shiga, Harald Forbert, and Dominik Marx. On the applicability of centroid and ring polymer path integral molecular dynamics for vibrational spectroscopy. *J. Chem. Phys.*, 130(19):194510, May 2009.

[14] Sergei D Ivanov, Alexander Witt, Motoyuki Shiga, and Dominik Marx. Communications: On artificial frequency shifts in infrared spectra obtained from centroid molecular dynamics: Quantum liquid water. *J. Chem. Phys.*, 132(3):031101, January 2010.

[15] Francesco Paesani and Gregory a Voth. A quantitative assessment of the accuracy of centroid molecular dynamics for the calculation of the infrared spectrum of liquid water. *J. Chem. Phys.*, 132(1):014105, January 2010.

[16] J.L. Skinner. Vibrational line shapes and spectral diffusion in fluids. *Mol. Phys.*, 106(16-18):2245–2253, August 2008.

[17] Edward Harder, Joel D Eaves, Andrei Tokmakoff, and B J Berne. Polarizable molecules in the vibrational spectroscopy of water Vibrational Spectroscopy from Computer Simulations. (11), 2005.

[18] R P Feynman and F L Vernon. The Theory of a General a Linear Quantum Dissipative System System Interacting with. *Ann. Phys. (N. Y).*, 24:118–173, 1963.

[19] Robert Zwanzig. *Nonequilibrium statistical mechanics*. Oxford University Press, 2001.

[20] S. Mukamel. *Principles of Nonlinear Optical Spectroscopy*. Oxford University Press, 1995.

[21] Ko Okumura and Yoshitaka Tanimura. Femtosecond two-dimensional spectroscopy from anharmonic vibrational modes of molecules in the condensed phase. *The Journal of chemical physics*, 107(7):2267–2283, 1997.

[22] D. Thirumalai and B.J. Berne. Path integral methods for simulating electronic spectra. *Chemical Physics Letters*, 116:471–473, 1985.

Bibliography

[23] N Makri. Effective non-oscillatory propagator for Feynman path integration in real time. *Chem. Phys. Lett.*, 1989.

[24] Nancy Makri. Improved Feynman propagators on a grid and non-adiabatic corrections within the path integral framework. *Chem. Phys. Lett.*, 193(5):435–445, June 1992.

[25] DE Makarov and N Makri. Tunneling dynamics in dissipative curve-crossing problems. *Phys. Rev. A*, 1993.

[26] Nancy Makri and Dmitrii E. Makarov. Tensor propagator for iterative quantum time evolution of reduced density matrices. I. Theory. *J. Chem. Phys.*, 102(11):4611, 1995.

[27] Nancy Makri and Dmitrii E. Makarov. Tensor propagator for iterative quantum time evolution of reduced density matrices. II. Numerical methodology. *J. Chem. Phys.*, 102(11):4611, 1995.

[28] Eunji Sim and Nancy Makri. Filtered propagator functional for iterative dynamics of quantum dissipative systems. *Comput. Phys. Commun.*, 99(2-3):335–354, January 1997.

[29] Jiushu Shao and Nancy Makri. Iterative path integral calculation of quantum correlation functions for dissipative systems. *Chem. Phys.*, 268(1-3):1–10, June 2001.

[30] Jiushu Shao and Nancy Makri. Iterative path integral formulation of equilibrium correlation functions for quantum dissipative systems. *J. Chem. Phys.*, 116(2):507, 2002.

[31] Roberto Lambert and Nancy Makri. Memory propagator matrix for long-time dissipative charge transfer dynamics. *Mol. Phys.*, 110(15-16):1967–1975, August 2012.

[32] Nancy Makri. Molecular Physics : An International Journal at the Interface Between Chemistry and Physics Path integral renormalization for quantum dissipative dynamics with multiple timescales. *Molecular Physics*, (June):37–41, 2012.

[33] Roberto Lambert and Nancy Makri. Quantum-classical path integral. I. Classical memory and weak quantum nonlocality. *J. Chem. Phys.*, 137(22):22A552, December 2012.

[34] Roberto Lambert and Nancy Makri. Quantum-classical path integral. II. Numerical methodology. *J. Chem. Phys.*, 137(22):22A553, December 2012.

Bibliography

[35] V. May and O. Kühn. *Charge and Energy Transfer Dynamics in Molecular Systems.* Wiley-VCH, 2011.

[36] R. Ramírez, T. López-Ciudad, P. Kumar P, and D. Marx. Quantum corrections to classical time-correlation functions: hydrogen bonding and anharmonic floppy modes. *J. Chem. Phys.*, 121:3973, 2004.

[37] Mark E Tuckerman. *Path Integration via Molecular Dynamics*, volume 10. 2002.

[38] Alexander N Drozdov, Peter Talkner, and I Introduction. Path integrals for Fokker-Planck dynamics with singular diffusion: Accurate factorization for the time evolution operator. *J. Chem. Phys.*, 109(6):2080–2091, 1998.

[39] Fabian Gottwald. Vibrational spectroscopy via generalized langevin dynamics: Applicability and beyond. Master's thesis, University Rostock, 2014.

[40] Hao Liu, Lili Zhu, Shuming Bai, and Qiang Shi. Reduced quantum dynamics with arbitrary bath spectral densities: hierarchical equations of motion based on several different bath decomposition schemes. *J. Chem. Phys.*, 140(13):134106, April 2014.

[41] Yoshitaka Tanimura and Ryogo Kubo. Time evolution of a quantum system in contact with a nearly gaussian-markoffian noise bath. *Journal of the Physical Society of Japan*, 58(1):101–114, 1989.

[42] Yoshitaka Tanimura. Stochastic liouville, langevin, fokker–planck, and master equation approaches to quantum dissipative systems. *Journal of the Physical Society of Japan*, 75(8), 2006.

[43] Rui-Xue Xu and YiJing Yan. Dynamics of quantum dissipation systems interacting with bosonic canonical bath: Hierarchical equations of motion approach. *Physical Review E*, 75(3):031107, 2007.

[44] Richard Currier. In 2013 the amount of data generated worldwide will reach four zettabytes, June 2013.

Acknowledgments

Selbstständigkeitserklärung

Hiermit erkläre ich, dass ich die vorliegende Arbeit selbstständig und ohne fremde Hilfe angefertigt habe. Ich versichere, dass ich keine weiteren als die im Literaturverzeichnis angegebenen Quellen verwendet und die den genutzten Werken wörtlich oder inhaltlich entnommenen Stellen als solche kenntlich gemacht habe.

Rostock, 10.10.2014

Sven Karsten